

UNIVERSITY OF CALGARY

Interactions between Reservoir Simulations of Heavy Oil and
Viscoelastic Seismic Modeling

by

Hossein Aghabarati

A THESIS

SUBMITTED TO THE FACULTY OF GRADUATE STUDIES
IN PARTIAL FULFILMENT OF THE REQUIREMENTS FOR THE
DEGREE OF DOCTOR OF PHILOSOPHY

DEPARTMENT OF GEOSCIENCE

CALGARY, ALBERTA

SEPTEMBER 2012

© Hossein Aghabarati 2012



UNIVERSITY OF
CALGARY

The author of this thesis has granted the University of Calgary a non-exclusive license to reproduce and distribute copies of this thesis to users of the University of Calgary Archives.

Copyright remains with the author.

Theses and dissertations available in the University of Calgary Institutional Repository are solely for the purpose of private study and research. They may not be copied or reproduced, except as permitted by copyright laws, without written authority of the copyright owner. Any commercial use or re-publication is strictly prohibited.

The original Partial Copyright License attesting to these terms and signed by the author of this thesis may be found in the original print version of the thesis, held by the University of Calgary Archives.

Please contact the University of Calgary Archives for further information:

E-mail: uarc@ucalgary.ca

Telephone: (403) 220-7271

Website: <http://archives.ucalgary.ca>

Abstract

When seismic waves pass through a porous medium saturated with heavy oil and gas they experience attenuation. This attenuation is related to the coexistence of fluids with significantly different bulk moduli. White's patchy saturation model was found to be a suitable constitutive model to estimate the velocity dispersion and attenuation of seismic waves in heavy oil reservoirs. The attenuation predicted from the White's model depends on rock and fluid properties such as saturation, patch size (bubble size), modulus and mobility of liquid phase. A feasibility analysis of viscoelastic forward modeling was performed to illustrate that the propagation of seismic waves was sensitive to the patchy saturation reservoir heterogeneity as predicted by White's attenuation theory.

Modeling of fluid flow including the process of gas bubbles coming out of solution (patch creation) was completed for a Canadian heavy oil reservoir. The results were then used to estimate White's attenuation parameters. The accuracy of the flow simulation was ensured through a history matching process. Obtaining a decent history match leads to a high confidence level in the estimation of in situ properties. White's attenuation model was considered a criterion to indicate the portion of frequency content of repeated seismic data which is affected by saturation heterogeneity. Therefore analysis was focused on this frequency portion which contains information about the depletion in the reservoir. This new processing method developed in this study leads to a better understanding and interpretation of time lapsed data for this type of Canadian heavy oil reservoir. This method helps for mapping the possible bypass reservoir for future infill drilling or possible Enhanced Oil Recovery (EOR) opportunities.

Preface

Reliable sources of energy are an imperative part of sustaining the fast pace of population growth and industrial expansion in the twenty-first century. Fossil fuels are still a major component of the world energy. Therefore it is becoming more important to develop optimized depletion methods to extract the limited amount of the oil and gas reserves on the earth. An important part of this task is to develop better monitoring techniques for optimization and evaluation of reservoir depletion methods.

The focus of this research was to develop a new method to transform the information obtained from reservoir simulation of heavy oil reservoir such as saturation of different phases, pressure, and temperature changes into seismic modeling. The major parts of this process are to understand the main mechanism involved in the production of heavy oil and their impact on seismic wave propagation.

In primary production of the heavy oil reservoirs solution gas drive mechanisms and the creation of foamy oil has been known to be the key components of heavy oil production. This research proposed a new method which could be used to obtain a more accurate image of reservoir depletion state through time-lapse seismology and reservoir simulation.

This imaging technique was done by considering White's attenuation model as a constitutive model that connects the reservoir simulation data to seismic wave propagation in heavy oil reservoir. The results of the case study presented in this thesis confirm the application of this method in real field cases.

Acknowledgements

It has been a great privilege to spend several years of my life in the Departments of Geoscience and Chemical & Petroleum Engineering at the University of Calgary. I am very thankful to the faculty members and staff for their contribution to my knowledge through my course and research work over this time.

At first I would like to thank my advisor, Dr. Larry Lines. He patiently provided the vision, encouragement and support necessary for me during the doctoral program and completion of my dissertation. Dr. Lines has been a very strong and supportive adviser to me throughout my program, and he has always given me great freedom to pursue independent work. Special thanks to my committee, Dr. Gary Margrave, and Dr. Brij Maini for their support, guidance and helpful suggestions.

I am also very thankful to Professor Peter Moczo and Dr. Joseph Kristek for their contribution to the finite difference viscoelastic modeling section of my thesis. I thank them for their hospitality during my visit to Comenius University, Bratislava in Slovakia.

I want to thank CHORUS manager Ms. Joan Embleton and industry sponsors of CHORUS for generous software donation, financial support and the seismic data for this research. I would like to acknowledge Mr. Hassan Khaniani and Mr. Amir Shamsa for their contribution and technical discussion during the completion of my thesis.

I should also mention the companies who sponsored my graduate studies, Devon Canada and Suncor Energy for their financial support.

Lastly I wish to thank my parents and my family. Their love provided my inspiration and was my driving force.

Dedication

To my love and my family

Table of Contents

Approval Page.....	ii
Abstract.....	iii
Preface	iv
Acknowledgements.....	v
Dedication.....	vi
Table of Contents	vii
List of Tables	ix
List of Figures and Illustrations	x
Epigraph*	xvi
CHAPTER ONE: INTRODUCTION.....	1
1.1 Waves In Porous Medium.....	1
1.2 Thesis structure	6
CHAPTER TWO: BIOT THEORY BACKGROUND	8
2.1 Basis of Biot Theory	11
2.1.1 Various Scales involved in wave propagation in porous medium	11
2.2 Assumptions of Biot Theory.....	14
2.3 The Solution of Biot Theory	15
2.4 Numerical Examples of Biot Theory	19
CHAPTER THREE: WHITE - DUTTA ODE´ MODEL FOR VELOCITY DISPERSION AND ATTENUATION OF PATCHY SATURATION.....	24
3.1 Literature review.....	24
3.2 White Model	26
3.3 Sensitivity Analysis on White Theory Inputs	31
3.3.1 Static Parameters	31
3.3.2 Dynamic Parameters.....	32
CHAPTER FOUR: VISCOELASTIC SEISMIC MODELING.....	63
4.1 Rheological Models of Heavy Oil	63
4.2 Wave Propagation in Viscoelastic Medium.....	65
4.3 The Concept of Memory Variable	71
4.4 Forward Modeling	73
4.4.1 Forward Modeling Inputs	74
4.4.2 Forward Modeling Results	77
4.4.3 Discussion.....	88
CHAPTER FIVE: CASE STUDY OF INTERACTION BETWEEN RESERVOIR SIMULATION AND VISCOELASTIC SEISMIC.....	90
5.1 Case study of Primate Field	92
5.2 CHOPS Background.....	94
5.3 Primate Field Geological Model.....	96

5.4 Reservoir Simulation	99
5.5 History Matching	100
5.5.1 Fluid Modeling	101
5.5.2 Rock Properties	107
5.6 History Match Results:	108
5.7 White Attenuation Model	111
5.8 Time-Lapse Seismology	114
5.9 Seismic and Well Logs Tie	115
5.10 Design of Band Pass Filters	117
5.11 Discussion of Time-Lapse Results	119
 CHAPTER SIX: CONCLUSIONS.....	 124
6.1 Suggestions for Future Research on This Topic.....	127
 REFERENCES	 129

List of Tables

Table 2-1 Biot's theory assumption and validations.....	14
Table 2-2 Input parameter used to create a numerical example using the Biot theory.....	21
Table 3-1 White model of gas inclusion White (1975).....	33
Table 3-2 Dynamic parameters used in the sensitivity analysis of White's theory, continued.....	34
Table 3-3 Dynamic parameters used in the sensitivity analysis of White's theory	35
Table 5-1 Properties of the pseudo components used for fluid modeling of Primate field	102
Table 5-2 Comparison between modeled and measured data of Primate oil field	104
Table 5-3 Summary of reservoir properties used as input for attenuation model.....	111
Table 5-4 Input Parameters of White theory for Primate field	112
Table 5-5 Specifications of the band pass filters used to separate the low and high frequency data.....	118

List of Figures and Illustrations

Figure 2-1 Schematic of a wave propagation in porous medium (Schanz 2002)	9
Figure 2-2 Schematic of the three waves predicted by the Biot's theory (Schanz 2002). 10	
Figure 2-3 Comparison of Sam's et al. (1997) field data of attenuation versus frequency, with modeled data from the viscosity-based damping of the Biot theory Vogelaar & Smeulders (2005)	20
Figure 2-4 Comparison of the two saturation models fast P wave velocity the Biot theory does not predict significant dispersion in seismic frequencies (10 to 100 Hz).....	22
Figure 2-5 Comparison of the attenuation of fast P wave predicted by the Biot theory... 23	
Figure 3-1 White model of gas inclusion, White (1975)	27
Figure 3-2 Gas Bulk Moduli sensitivity results	37
Figure 3-3 Liquid bulk moduli sensitivity results.....	38
Figure 3-4 Gas density sensitivity results	43
Figure 3-5 Liquid density sensitivity analyses.....	44
Figure 3-6 Gas viscosity sensitivity analyses	48
Figure 3-7 Liquid viscosity sensitivity analyses.....	49
Figure 3-8 Gas Permeability sensitivity analyses	51
Figure 3-9 Liquid permeability sensitivity analyses.....	52
Figure 3-10 Diffusion limited vs. general growth: gradual decline in pressure. Kumar et al (2001)	56
Figure 3-11 Bubble growth model presented by Wong & Maini (2005)	56
Figure 3-12 Relationships between (a) dimensionless equilibrium time T versus bubble density number n; (b) gas saturation versus n, Wong (2006)	58
Figure 3-13 Evolution of solute concentration in liquid for bubble density $n = 6$	59
Figure 3-14 Gas saturation sensitivity analyses.....	61

Figure 3-15 Gas bubble size sensitivity analysis	62
Figure 4-1 Zener body, J. Kristek and P. Moczo (2006)	64
Figure 4-2 Relaxation response of a viscoelastic rod to a unit step strain input.....	67
Figure 4-3 schematic of the geological model.....	75
Figure 4-4 Attenuation model used by 3rd standard linear solid.....	77
Figure 4-5 Time response of MODEL1 initial simulation of initial survey	78
Figure 4-6 Time response of MODEL1 simulation of monitor survey	79
Figure 4-7 Time response of MODEL2 simulation of initial survey.....	79
Figure 4-8 Time response of MODEL2 simulation of monitor survey	80
Figure 4-9 Gabor transform of MODEL1 initial survey simulation.....	82
Figure 4-10 Gabor transform of MODEL1 monitor survey simulation	82
Figure 4-11 Gabor transform of MODEL2 initial survey simulation.....	83
Figure 4-12 Gabor transform of MODEL2 monitor survey simulation	83
Figure 4-13 Frequency depth analysis of MODEL1 initial survey simulation.....	84
Figure 4-14 Frequency depth analysis of MODEL1 monitor survey simulation	85
Figure 4-15 Frequency depth analysis of MODEL2 initial survey simulation.....	85
Figure 4-16 Frequency depth analysis of MODEL2 monitor survey	86
Figure 4-17 Difference due to the change in the attenuation (production related) in MODEL1	87
Figure 4-18 Difference due to the change in the attenuation (production related) in MODEL2	88
Figure 5-1 Primate Field (Equal Energy website)	92
Figure 5-2 Stratigraphic correlation chart of Saskatchewan (Saskatchewan energy recourse website)	93
Figure 5-3 Well logs and facies model picked used to create the primate model	96

Figure 5-4 Cross plot of porosity versus gamma distribution after neural network analysis.....	97
Figure 5-5 Variogram of the sand facies.....	98
Figure 5-6 3D view of effective porosity map created using wireline logs and geological interpretations.....	98
Figure 5-7 Equation of State Match to the dead oil viscosity data.....	103
Figure 5-8 Liquid density of Primate Oil.....	105
Figure 5-9 Vapour (gas) density of primate oil	105
Figure 5-10 Liquid viscosity of Primate oil.....	106
Figure 5-11 Vapour viscosity of Primate Oil.....	106
Figure 5-12 relative permeability of oil water system.....	107
Figure 5-13 relative permeability of liquid gas system	108
Figure 5-14 Results of history match of cumulative production of Primate field	109
Figure 5-15 Results of history match of rates of Primate field.....	109
Figure 5-16 Ternary diagram of the saturations of different phases.....	110
Figure 5-17 Pressure distribution of the model after production.....	110
Figure 5-18 Attenuation model of Primate field for 2009 seismic survey	113
Figure 5-19 Wavelet extracted from 2004 seismic survey	115
Figure 5-20 sample of synthetic seismogram and seismic tie.....	116
Figure 5-21 Correlation between synthetic seismogram and seismic data across the Primate field.....	116
Figure 5-22 Amplitude spectrum of two seismic surveys of Primate field	117
Figure 5-23 Amplitude spectrum of low frequency volumes	118
Figure 5-24 Amplitude spectrum of high frequency volumes	119
Figure 5-25 Amplitude difference of low frequency seismic volumes (2009 - 2004)....	120
Figure 5-26 Amplitude difference of high frequency seismic volumes (2009 - 2004) ..	120

Figure 5-27 Shaping filter used in the workflow of low frequency seismic.....	121
Figure 5-28 Amplitude envelope of difference between low frequency volumes after applying 4D corrections	122
Figure 5-29 Amplitude envelope of difference between high frequency volumes after applying 4D corrections	123

List of Symbols, Abbreviations and Nomenclature

Symbol	Definition
ω_{AC}	<i>Acentric factor of the substance</i>
ω	<i>Angular frequency</i>
α	<i>Aspect ratio</i>
*	<i>Convolution symbol</i>
P_c	<i>Critical pressure of the substance</i>
T_c	<i>Critical temperature of the substance</i>
λ_d	<i>Diffusion length</i>
δ	<i>Dirac function</i>
K_d	<i>Dry bulk moduli</i>
Ω_a	<i>Equation Of State constant</i>
Ω_b	<i>Equation Of State constant</i>
K_f	<i>Fluid bulk moduli</i>
ρ_f	<i>Fluid density</i>
p	<i>Fluid pressure</i>
$\varepsilon_{i j}$	<i>Fluid strain</i>
ρ_g	<i>Gas density</i>
h	<i>Gird spacing</i>
K_s	<i>Grain bulk moduli</i>
$\theta(t)$	<i>Heaviside function</i>
Z	<i>incompressibility coefficient</i>
ρ_m	<i>Matrix density</i>
V max	<i>Maximum velocity of the model</i>
V min	<i>Minimum velocity of the model</i>
V	<i>Molar volume</i>
Mw	<i>Molecular weight</i>
κ	<i>Permeability of the medium</i>
ϕ	<i>Porosity of the medium</i>
Q	<i>Quality factor</i>
R	<i>Radius of bubble</i>
R	<i>Radius of bubble</i>
T_r	<i>Reduced temperature T/Tc</i>
M_R	<i>Relaxed stress corresponding to M(t)</i>
K_{sat}	<i>Saturate bulk moduli</i>
a	<i>Shape factor</i>
μ	<i>Shear moduli</i>
$e_{i j}$	<i>Solid strain</i>

Symbol	Definition
ρ_{dg}	<i>Solute concentration at radius R</i>
ρ_{dg}	<i>Solute concentration at radius R</i>
D	<i>Solute diffusion coefficients</i>
τ_{ϵ}	<i>Strain relaxation time</i>
$\sigma(t)$	<i>Stress</i>
$\psi(t)$	<i>Stress relaxation function</i>
τ_{σ}	<i>Stress relaxation time</i>
$M(t)$	<i>Stress response to the Dirac δ</i>
T	<i>Temperature</i>
$\dot{\epsilon}(t)$	<i>Time derivative of strain</i>
Δt	<i>Time step used for simulating</i>
R	<i>Universal gas constant</i>
η	<i>Viscosity of the fluid</i>
p_v	<i>Vapour pressure of a substance at 70% of the critical temperature.</i>
K_w	<i>Woods bulk moduli</i>

Epigraph*

“Life is like riding a bicycle. To keep your balance, you must keep moving.”

— *Albert Einstein*



* Walter Issacson, 2007, “Einstein: His Life and Universe”, Publisher Simons & Schuster, 1st Edition, page viii

CHAPTER ONE: INTRODUCTION

1.1 Waves In Porous Media

Understanding the process of seismic wave transmission in porous medium is an important part of subsurface imaging and reservoir characterization. There are many applied/engineering research articles devoted to address this problem and the theory for a satisfactory explanation of wave propagation in porous materials. Lab tests and field studies by different researchers such as Johnson (1994) have shown that a major cause of attenuation in porous media is wave-induced fluid flow, which occurs at different frequencies.

In order to create the synthetic seismograms or evaluate the seismic response one has to first understand the existing link and relationship between the heterogeneities and the seismic response. The source of these heterogeneities are either existing at initial in situ conditions or they could be created as the conditions change due to production or injection of fluids into/ out of reservoirs.

In a porous medium saturated with a single fluid Bourbie et al. (1987) showed that frequency dependent attenuation is significant when the frequency of the wave is comparable with critical frequency ω_c predicted by Biot characteristic frequency.

$$\omega_c = \frac{\eta\phi}{\kappa\rho_f} \quad (1.1)$$

where

η = viscosity of the fluid [Pa.sec]

ϕ = porosity of the medium [Fraction]

κ = permeability of the medium [m²]

ρ_f = fluid density [Kg/m³]

If we consider a case where the frequencies of interest are much lower than ω_c the dynamic effects can then be ignored and the Gassmann theory is a valid assumption. Based on the Gassmann theory the bulk moduli of a saturated rock (K^{satG}) can be calculated using the following relationships.

$$K^{satG} = K_d + \alpha_G^2 M \quad (1.2)$$

$$\alpha_G = 1 - \frac{K_d}{K_s} \quad (1.3)$$

$$M = \frac{1}{\frac{(\alpha_G - \phi)}{K_s} + \frac{\phi}{K_f}} \quad (1.4)$$

where:

K_d = dry bulk moduli [kPa]

K_f = fluid bulk moduli [kPa]

K_s = grain bulk moduli [kPa]

φ = porosity of the medium [fraction]

ρ_f = fluid density [kg/m³]

α_G is a dimensionless number and usually referred as the “*Biot factor*”. A basic and important assumption of the Gassman theory is that the pressure equilibrium is achieved instantly. This means that at low frequency the propagation of the wave induced pressure change is insignificant compared to the diffusion length.

Fluid motion in a porous medium is governed by the conservation of mass, momentum, and energy. For slightly compressible fluid the diffusion equation is

$$\varphi \rho_f c_t \frac{\partial p}{\partial t} = \nabla \cdot \left(\frac{\rho_f}{\mu} \kappa (\nabla p - \rho g \nabla z) \right) + q \quad (1.5)$$

φ = porosity of medium [fraction]

ρ = fluid density [kg/m³]

c_t = total system compressibility [kpa⁻¹]

p = pore pressure [Pascal]

κ = effective permeability [m²]

μ = viscosity of fluid [Pascal.sec]

g = gravity acceleration coefficient [m/s²]

(∇z) = elevation changes [m]

q = fluid flow [m²/s]

However, the existence of more than one fluid in the porous medium leads to presence of finer scale heterogeneities which happens in relatively smaller scales. Norris, (1993) showed that the distribution of pressure is governed by the diffusion equation with the diffusion length λ_d .

$$\lambda_d = \left(\frac{\kappa N}{\omega \eta} \right)^{1/2} \quad (1.6)$$

Here ω is the angular frequency and N is estimated based on the ratio of the dry rock and saturated rock P wave moduli.

$$N = \frac{ML}{H} \quad (1.7)$$

M is previously defined in equation 1.4 and L and H are defined below.

$$L = K_m + \frac{4}{3}\mu \quad (1.8)$$

$$H = K_{sat} + \frac{4}{3}\mu \quad (1.9)$$

K_{sat} is the saturated bulk moduli and the μ is the shear modulus which is considered to be the same for both dry and saturated cases.

When there is more than one fluid saturating the rock (heterogeneity due to change in saturation) there will be a greater internal attenuation created. If we consider the heterogeneity to be characterized with a respective length d , at low frequencies d is

much smaller than the λ_d , Mavko et al. (1998) showed that under these conditions the fluid bulk moduli can be estimated using Wood's averaging method

$$K_w = \frac{1}{\frac{s_1}{K_{f1}} + \frac{s_2}{K_{f2}}} \quad (1.10)$$

Where $s_1 s_2$ are the saturations of different fluids and $K_{f1} K_{f2}$ are the bulk moduli of different fluids. Although there is heterogeneity existing in this case due to the fact that the changes are locally significant and globally insignificant it is referred as *homogenous* case.

On the other hand, in cases where the heterogeneity length d is much larger than diffusion length λ_d , the communication between saturation pockets is very small. This means that there is no communication readily between the pockets of saturation. This case is usually known as *patchy saturation*. Mavko et al., (1998) showed that in this case the fluid saturated bulk moduli can be estimated using the Hill averaging method for high frequencies. Hill (1963) showed that when all of the phases or constituents in a composite have the same shear modulus (μ), the effective P-wave modulus K_e , can be calculated using the following equation.

$$\frac{1}{\left(K_e + \frac{4}{3}\mu_e\right)} = \sum_{i=1}^n \frac{x_i}{\left(K_i + \frac{4}{3}\mu_i\right)} \quad (1.11)$$

Here K_i are the bulk moduli of each heterogeneity and x_i is its volume fraction. Although the P wave moduli in both patchy and homogenous cases are a real number, they are valid at two sides of the frequency spectrum. Johnson (2001) developed a more general theory for elastic properties of rock containing regular distribution of pockets of two fluids assuming that the bulk modulus must obey Gassmann theory at low frequencies and at high frequencies must also obey causality constraints. The fact that the two moduli at high and low frequencies are not the same, the causality constraint lead to the dispersion and makes the P wave moduli a complex number therefore the attenuation needs to be a function of frequency.

1.2 Thesis structure

In this thesis the objective is to develop a technique for estimating the reservoir rock properties using the frequency dependent attenuation relationship resulting from seismic wave propagation in porous media. A new method was proposed in this study which involves updating the rock physics properties using reservoir simulation.

Chapter 2 presents the background of the Biot theory and its application and limitation in estimating the attenuation in real cases. The limitations of the Biot's theory were then outlined and compared with literature data.

In Chapter 3 the details of White patchy saturation model is described. A sensitivity analysis is then carried out to understand the impact of the input parameters on dispersion outcome.

Chapter 4 focuses on viscoelastic modeling. The first part of this chapter presents the rheological model of heavy oil reservoir using Standard Linear Solid model. Then the theory of viscoelastic modeling is briefly explained. Using a peer reviewed viscoelastic computer code; the sensitivity analysis is then carried out to quantify the seismic response by varying quality factor in a heterogeneous 1D model.

Chapter 5 summarizes a case study of applying the new workflow on a typical Canadian heavy oil reservoir. At first the results of the reservoir simulation is presented. Then using White's attenuation model and reservoir simulation results the target frequencies which contains changes related to the production are estimated. And finally time-lapse seismic results are presented using the new workflow.

Chapter 6 outlines the conclusion of this thesis and a series of recommendations are provided for future research on this topic.

CHAPTER TWO: BIOT THEORY BACKGROUND

The theory of poroelasticity was first introduced by Biot (1962). The Biot theory can be used to describe the acoustic properties of an elastic isotropic porous solid fully-saturated with a compressible Newtonian fluid. The theory assumes that anelastic effects arise from viscous interaction between a fluid and a solid. Biot predicted the existence of three bulk waves: two compressional waves and one shear wave as wave propagated through a poroelastic medium. Biot arrived at his equations by coupling the motion between the fluid and the solid matrix. In Biot's expressions the existence of attenuation is due to the flow of fluids within non-connecting pores initiated by elastic waves.

The Biot theory takes into account frequency variations, and allows for relative motion between fluid and rock framework. This theory predicts the existence of a so-called slow wave in addition to the shear wave and the compressional or fast wave. The slow wave arises when the fluid and the skeleton move 180° out-of-phase with each other. The input parameters of the theory can be estimated on a given sample by independent measurements.

During the last five decades, understanding of the attenuation of Biot's waves has been an interesting part of the research in rock physics. The Biot's waves have been observed and therefore suggested that there must be a relation between the attenuation on the wave frequency and the diffusion process of the reservoir fluid. The success of the theory in predicting the dispersion and the attenuation of the fast compressional, slow

compressional, and shear modes has been demonstrated in a number of relevant experiments Johnson, (1994).

Consider a porous medium as it is shown in Figure 2-1 when a wave passes through such a medium based on the Biot theory there are 3 types of waves generated as per followings;

- 1) Fast P wave: both solids and fluid are in phase and no change in the wave propagation direction
- 2) Shear wave: no fractional change in the volume is generated due to the fact that the volume has to be conserved
- 3) Slow P wave: generated in the opposite direction of the initial wave propagation

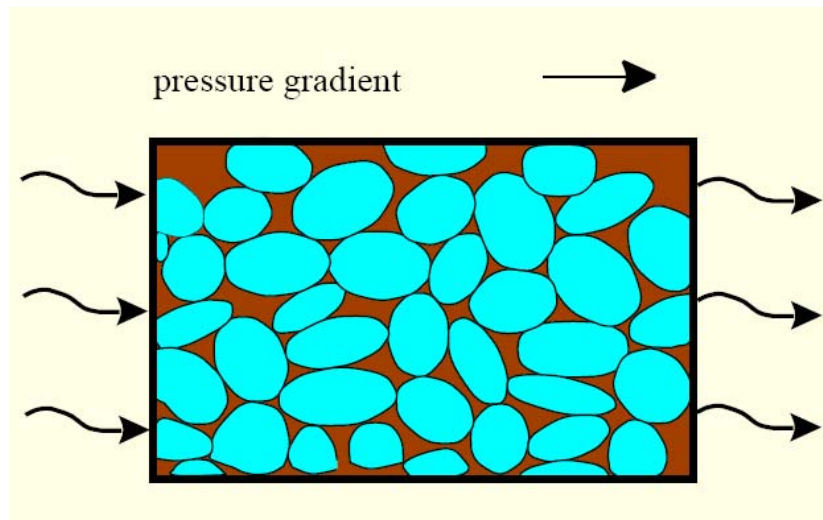


Figure 2-1 Schematic of a wave propagation in porous medium (Schanz 2002)

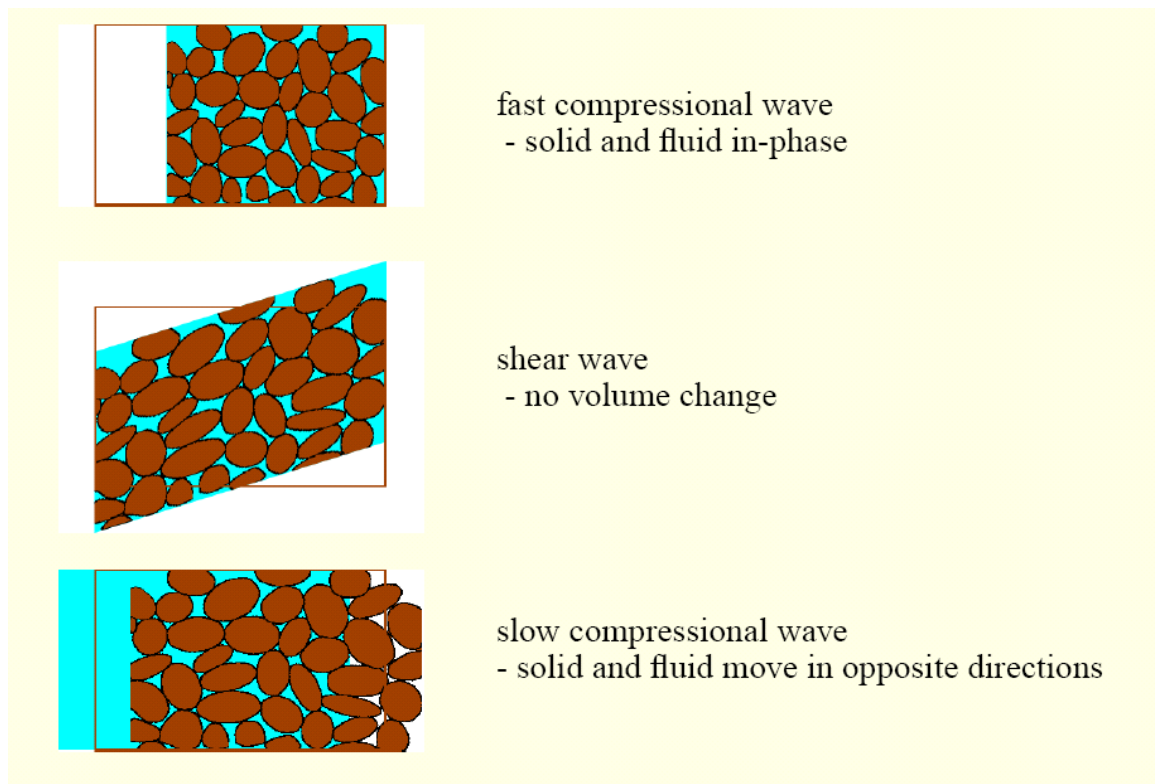


Figure 2-2 Schematic of the three waves predicted by the Biot's theory (Schanz 2002)

Biot developed the formulas to predict the velocity of these three waves as they go through the porous medium. In the next part a brief overview of how this theory was initially developed is presented.

2.1 Basis of Biot Theory

There are three fundamental equations which are the backbone of Biot theory. The first equation relates the stress and strain and is known as the constitutive relations. The second equation is the equation of motion, which relates the net force acting on a given volume element to the mass times acceleration. Lastly the dynamic version of Darcy's law is used to incorporate the pressure diffusion in the medium as a result of wave propagation. For derivations of the Biot theory see Stoll (1977). In this thesis the focus is on the results of Biot theory when it is used for application in the exploration and monitoring through seismic studies.

2.1.1 Various Scale involved in wave propagation in porous medium

A fundamental point of heterogeneous systems is the difference of macroscale behaviour compared to meso- or microscale. The equations and models which are developed for the macroscale are not necessarily well-correlated by equations of the meso- or microscale. In some simple physics cases like electrical conduction and linear elasticity, the equations describing macroscale behave similar to the microscale. However, in complex systems, such as fluid flow in porous media, two sets of equations govern different scales. The fluid flow of the microscale behaviour is well-described by

Navier-Stokes' equations for liquid in the pores while the macroscale behaviour is described by Darcy's equation.

The scales involved in understanding of the wave propagation in porous medium are ranging from sub millimetres (fluid flow with respect to grain size of the rock) to tens of meters (seismic wavelength). Passing waves through a porous medium creates pressure difference. The pressure difference causes flow until eventually the porous medium reaches the equilibrium in a diffusive environment. When dealing with diffusion processes the diffusion length plays an important role in time required to achieve equilibrium. Pride et al. (2003 a and b) describe the three scales which need to be considered when dealing with wave propagation in porous medium. One has to consider an average volume for seismic theory which the properties inside this arbitrary volume is constant when considering the different scales.

1. Macro or wavelength-scale where there is equilibration between the peaks and troughs of a P-wave that were allowed for by the Biot's theory (1962). Here there is only one pressure gradient to consider in the porous medium. The average volume dimensions are much smaller than the wavelength.
2. Microscopic flow mechanism or "*squirt flow*" Mavko and Nur, (1975, 1979) O'Connell and Budiansky (1977); Dvorkin et al. (1995) which is based on the fact that any broken grain contacts or microcracks in the grains more compliant than the main part of the pore space. This leads to the fact that when a compressional

wave squeezes the material, there is a non equilibrium condition existing between fluid-pressure response in the microcracks and in the main pores. When the medium is equilibrating, the fluid flows from the microcracks to the main pore spaces. The microscopic squirt flow is used to explain the ultrasonic attenuation data. Here there is more than one pressure gradient coexisting in the medium. In this case the average volume is much bigger than the wavelength. This scale applies to large seismic frequencies (kHz and above) and it is a topic of BISQ theory.

3. The mesoscopic scale is somewhere between the macroscopic and microscopic scales. The flow at mesoscopic scales happens due to heterogeneity of the porous-continuum properties within each averaging volume. Heterogeneity is rather a general phrase which can be interpreted as layering, saturation changes, and change in the mobility and permeability. White (1975) was the first one who modeled the wave-induced fluid flow by identical mesoscopic scale spherical gas-filled inclusions in porous media. Some of the assumptions used by White (1975) were removed by Dutta and Odé (1979a, b) who decoupled the wave equations of Biot's theory and solved the problem of a radially oscillating gas pocket in porous rocks.

2.2 Assumptions of Biot Theory

Table 2-1 is the list of the key assumptions of Biot theory and the possible limitations in real world of application.

Assumption	Reality
The matrix is homogeneous	Most reservoirs are not homogenous and different production rock facies exist in the reservoir
The matrix is isotropic	In highly laminated reservoir or dominant fractures system the isotropic assumption is not valid
Small size of the pores compared to both rock elements and the wavelength	This assumption is valid given the particle size of the rock /pore space are at a much lower scale than seismic wave lengths
Rock is fully saturated with a single phase Newtonian fluid	In most reservoirs , the reservoir rocks are saturated with at least two fluids water and hydrocarbons such as oil or gas, however for dry gas reservoirs with no active bottom water this assumption is valid.
Darcy law assumption	For typical frequency of a seismic wave this is a valid assumption
Constant temperature	The fluid flow properties and seismic velocity and density are temperature dependent. Except for thermal methods, this is a valid assumption,

Table 2-1 Biot's theory assumption and validations

2.3 The Solution of Biot Theory

The poroelastic coefficients (P, Q, and R) are required to write the two fundamental equations of the Biot theory. These coefficients depend on the matrix bulk and shear (K_m) moduli, fluid (K_f) modulus and solid bulk moduli (K_s) and the porosity of the porous medium (ϕ) .

$$\gamma = \frac{1 - K_m}{K_s} \quad (2.1)$$

$$K' = K_f (\gamma - \phi) \quad (2.2)$$

$$\phi' = \phi + \frac{K'}{K_s} \quad (2.3)$$

$$P = \frac{\phi K_m + (1 - \phi)K'}{\phi'} + \frac{4}{3}\mu \quad (2.4)$$

$$Q = \frac{\phi K'}{\phi'} \quad (2.5)$$

$$R = \frac{\phi^2 K_f}{\phi'} \quad (2.6)$$

In a fluid saturated homogeneous poroelastic rock the total stress τ_{ij} and pore fluid pressure p in terms of the solid and fluid strains, e_{ij} and \mathcal{E}_{ij} , are related as per following equation of Biot theory.

$$\tau_{ij} = [(P + Q - 2\mu) e_{kk} + (Q + R)\varepsilon_{kk}] \delta_{ij} + 2\mu e_{ij} \quad (2.7)$$

$$-\varphi p = Q e_{kk} + R \varepsilon_{kk} \quad (2.8)$$

The porosity is φ that is the ratio between the void volumes to the bulk volume.

The shear modulus of the matrix is μ .

As presented by (Biot, 1962; Stoll, 1977; Berryman, 1980a), the solution is frequency dependent and it is obtained by developing the dispersion relation which can be written as per following equations:

$$\begin{vmatrix} H/V_p^2 - \rho & \rho_{f_l} - C/V_p^2 \\ C/V_p^2 - \rho_f & q - M/V_p^2 \end{vmatrix} = 0 \quad (2.9)$$

$$\begin{vmatrix} \rho - \mu_f/V_s^2 & \rho_f \\ \rho_f & q \end{vmatrix} = 0 \quad (2.10)$$

The solution is calculated by defining the roots of above equation.

$$\frac{1}{V_p^2} = \frac{-(Hq + M\rho - 2C\rho_f) \pm \sqrt{(Hq + M\rho - 2C\rho_f)^2 - 4(C^2 - MH)(\rho_f^2 - q\rho)}}{2(C^2 - MH)} \quad (2.11)$$

$$\frac{1}{V_s^2} = \frac{qp - \rho_f^2}{q\mu_f} \quad (2.12)$$

$$H = K_m + \frac{4}{3}\mu + \frac{(K_s - K_m)^2}{(D - K_m)} \quad (2.13)$$

$$C = \frac{(K_s - K_m)K_s}{(D - K_m)} \quad (2.14)$$

$$M = \frac{K_s^2}{(D - K_m)} \quad (2.15)$$

$$D = K_s \left[1 + \varphi \left(\frac{K_s}{K_m} - 1 \right) \right] \quad (2.16)$$

$$\rho = (1 - \varphi)\rho_m + \varphi \rho_f \quad (2.17)$$

$$q = \frac{\alpha\rho_f}{\varphi} - \frac{i\eta F(\zeta)}{w\kappa} \quad (2.18)$$

where:

η = Fluid viscosity [Pascal.sec]

w = Angular frequency [Hz]

κ = Permeability [m^2]

$F(\zeta)$ = Viscodynamic operator

$$F(\zeta) = \frac{1}{4} \left(\frac{\zeta T(\zeta)}{1 + \frac{2i T(\zeta)}{\zeta}} \right) \quad (2.19)$$

$$T(\zeta) = \frac{e^{i3\pi/4} J_1(\zeta e^{-i\pi/4})}{J_0(\zeta e^{i\pi/4})} \quad (2.20)$$

$$\zeta = \left(\frac{\omega a^2 \rho_f}{\eta} \right)^{1/2} \quad (2.21)$$

In the above equation 2.21 a (the aspect ratio), is related to the dimension and shape of the pores and is usually determined by conduction experimental measurements.

In equation 2.20 J_0 and J_1 is the first and second kind Bessel functions of ζ .

2.4 Numerical Examples of Biot Theory

Biot theory results tend to underestimate the attenuation when compared to the field data. Sams et al. (1997) made a very important contribution in understanding of frequency effects on seismic attenuation. They conducted a sequence of seismic experiments on saturated sedimentary rocks (a finely layered sequence of limestones, sandstones, siltstones and mudstones) using four boreholes drilled to 250–280 m depth at the Imperial College test site in the north east of England. They acquired many data sets at widely different frequencies:

1. VSP experiments (30–280 Hz)
2. Cross-hole experiments (200–2300 Hz)
3. Sonic logging (8–24 KHz)
4. Laboratory measurements (0.3–0.9MHz)

Using classic definition by Knopoff (1964) the seismic quality factor Q is defined as

$$\frac{2\pi}{Q} = \frac{\Delta E}{E} \quad (2.22)$$

This definition is borrowed from electrical circuit theory. ΔE is the energy loss over one cycle and E the total energy. Following this simple equation attenuation is simply the reverse of Q . Here the assumption is that Q is not depending on the frequency. In Chapter 4 a more rigorous definition of Q is presented using the equations of viscoelastic wave propagation.

The results of Sam's work were compared with Biot Theory by Vogelaar and Smeulders (2005). Figure 2-3 presents the results of this study. As it is shown in this figure the Biot's predicted attenuation is one order of magnitude less than the real measurements from Sam's work. It should be mentioned that the attenuation of seismic wave is not just due to fluid flow resulted from seismic wave propagation. When wave is passing through the earth there is continues exchange between the kinetic energy (velocity) and potential energy (displacement). This exchange is not perfectly elastic and therefore there is energy being converted to heat and permanent movements of rock particles. This energy loss is usually referred as "*intrinsic attenuation*".

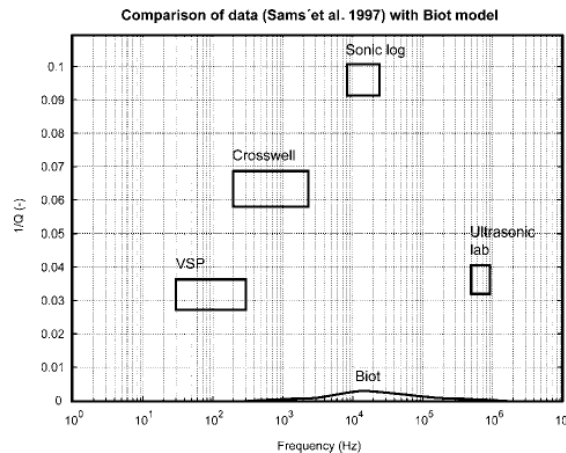


Figure 2-3 Comparison of Sam's et al. (1997) field data of attenuation versus frequency, with modeled data from the viscosity-based damping of the Biot theory Vogelaar & Smeulders (2005)

Using MATLAB Bessel functions a code was developed to calculate the Biot theory response. The code was used for to create a numerical example to estimate the response of Biot theory for wave propagation in a typical unconsolidated sandstone reservoir. Table 2-2 summarizes the input parameters used to calculate the fast and slow

compressional wave and the shear wave using the Biot theory. The frequencies of this study ranges from 10 Hz to 10,000 Hz. The Biot attenuation was estimated for model 1, where it is 100% saturated with brine. The same calculation was done for model 2 which is 100% gas saturated.

Parameter	Values	Unit
Dry bulk moduli (K_m)	7.6E+09	Pascal
Dry shear moduli (μ_m)	4.5E+09	Pascal
Solid bulk moduli (K_s)	37E+09	Pascal
Solid shear moduli (μ_s)	44E+09	Pascal
Fluid bulk moduli (K_f)	2E+09	Pascal
Water , Gas	1E+05	
Grain density (ρ_s)	2650	Kg/m ³
Fluid density (ρ_f)	1,000	Kg/m ³
Water Gas	20	
Porosity (φ)	0.35	fraction
Viscosity (η)	1,	Pascal.sec
Water, Gas	0.0002	
Effective permeability (κ)	2E-12	m ²
Aspect ratio (α)	3	
Shape factor (a)	0.15	

Table 2-2 Input parameter used to create a numerical example using the Biot theory

The following Figures 2-4 and 2-5 present the fast P wave velocity and the attenuation predicted by Biot theory. Similar results which were predicted by Voegelaar et al. (2005) were obtained in this study. The first conclusion is that the response of Biot theory does not show peak attenuation in seismic frequency between 10 Hz to 200 Hz. The other observation is that the gas saturated case is showing a higher attenuation and lower P wave velocity which is expected based on the fact the overall density of the medium is smaller and also gas had lower bulk moduli. The results of this modeling confirms the observation by Vogelaar (2005) and therefore it is obvious that by only using the Biot theory is not possible to estimate the attenuation in the seismic frequency range.

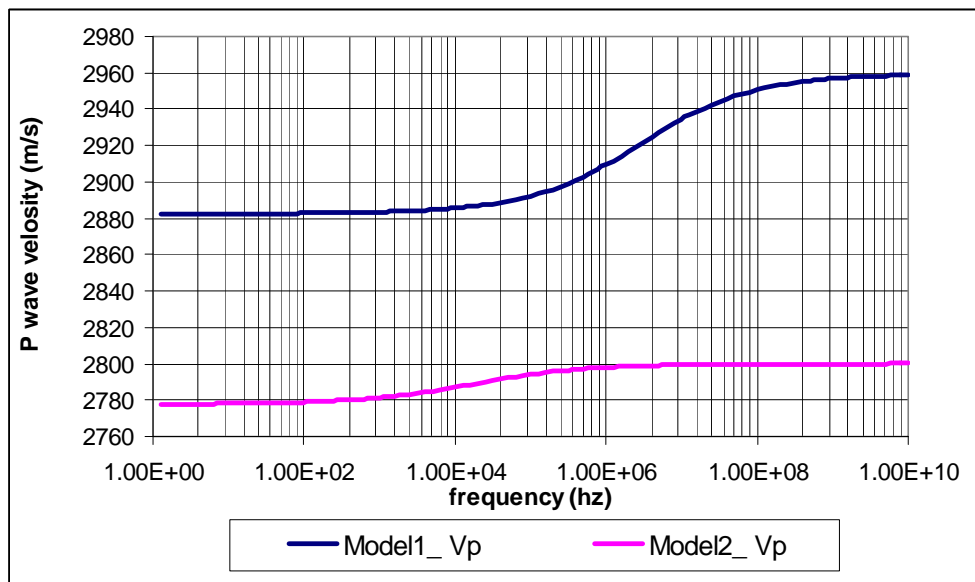


Figure 2-4 Comparison of the two saturation models fast P wave velocity the Biot theory does not predict significant dispersion in seismic frequencies (10 to 100 Hz)

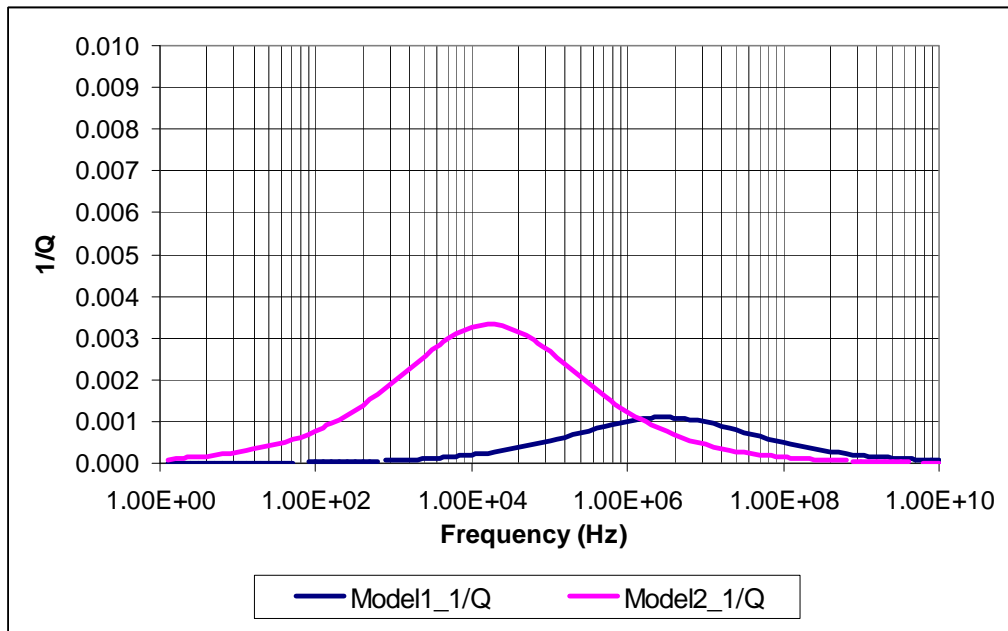


Figure 2-5 Comparison of the attenuation of fast P wave predicted by the Biot theory

CHAPTER THREE: WHITE - DUTTA ODE' MODEL FOR VELOCITY DISPERSION AND ATTENUATION OF PATCHY SATURATION

3.1 Literature review

White (1975) was the first to model the wave-induced fluid flow by considering spherical gas-filled inclusions in porous media. Figure 3-1 presents the schematics of his saturation model which is called patchy saturation model. Dutta and Odé (1979a, b) obtained more rigorous solutions for the same spherical geometry by solving a boundary-value problem involving Biot's poroelastic field equations.

White's idea of enhanced attenuation in the presence of small volume fractions of gas in the pore fluid has been experimentally confirmed by Murphy (1982). The presence of a local fluid flow due to the un-equilibrated pore pressures among patches of the two fluids creates attenuation and dispersion of seismic waves traveling through the rock.

Dutta and Seriff (1979) modified White's equations in the case of spherical gas-filled patches, bringing the results into good agreement with the more exact calculations of Dutta and Odé (1979a, b). This modification made the results to be similar to the expected Gassmann-Wood velocity at very low frequencies. In addition Dutta and Seriff (1979) also compare the results obtained using three different geometries of the patches. They concluded that the geometry configuration has a minimal effect on the magnitude of attenuation.

In more recent studies by Johnson (2001); Müller and Gurevich, (2004a, b) developed another generalization of the White model for patches of arbitrary shape. Besides the usual parameters of Biot theory, the new proposed models have geometrical parameters such as the specific surface area and the size of the patches. The two papers by Johnson (2001) and Müller and Gurevich (2004b) compare attenuation and dispersion predictions obtained from the White (1975) model to those generated from a 3D numerical model with any type of random in-homogeneity. They find that, even if the attenuation peak for the random model is broader and smaller in amplitude than that of the White periodic model, the frequency dependence of attenuation and velocity are very similar. This means that, qualitatively, the effects of geometry are not as important.

Carcione et al. (2003) performed a series of numerical-modeling experiments based on Biot's equations of poroelasticity and White's model. They considered regularly distributed spherical gas inclusions and they demonstrated that the attenuation and velocity dispersion measurements can be explained by the combined effect of mesoscopic scale inhomogeneities and energy transfer between wave modes. Cadoret et al. (1995) conducted a physical experiment that showed with the help of a computerized tomography CT scans; it is possible to map the fluid distribution and saturation changes happening in rocks. Fractal models, such as the von Kármán correlation function, calibrated by the CT scans, were used by Helle et al. (2003). More recently, Lebedev et al. (2009) conducted a very interesting test where they simultaneously measured the P-wave velocity and rock sample saturation changes using X-ray computer tomography

(CT) imaging. The test was conducted for a water imbibition case and the results were consistent with theoretical predictions and numerical simulations.

From the literature review it is concluded that, in spite of the simple derivation and assumptions, the White model has been validated and found to be accurate for establishing the attenuation relationship of patchy saturation cases.

3.2 White Model

The patchy saturation case was described first by White considering an outer and inner spherical shape. The inner sphere is the gas saturated medium and the outer sphere is usually the water saturated (or the second phase). If the inner and outer spheres have radii of a and b respectively it can be shown by simply using the volume formula of spherical shape the gas saturation is a^3/b^3 . However the model is based on cubes with length of l . Therefore, the outer radius b is simply

$$b = \left(\frac{l^3}{\left(\frac{4}{3}\pi\right)} \right)^{1/3} \quad (3.1)$$

A fundamental assumption is that the gas saturation pockets are acting separately and they are not connected. Therefore the maximum value of the inner circle is $\pi/6$ or 52% gas saturation. A number higher than this saturation leads to bubbles collapsing into each other which make the assumption of derivation invalid. This is an important point which has to be considered when using this theory. Figure 3-1 presents the schematic of the White model as it was presented in his original paper.

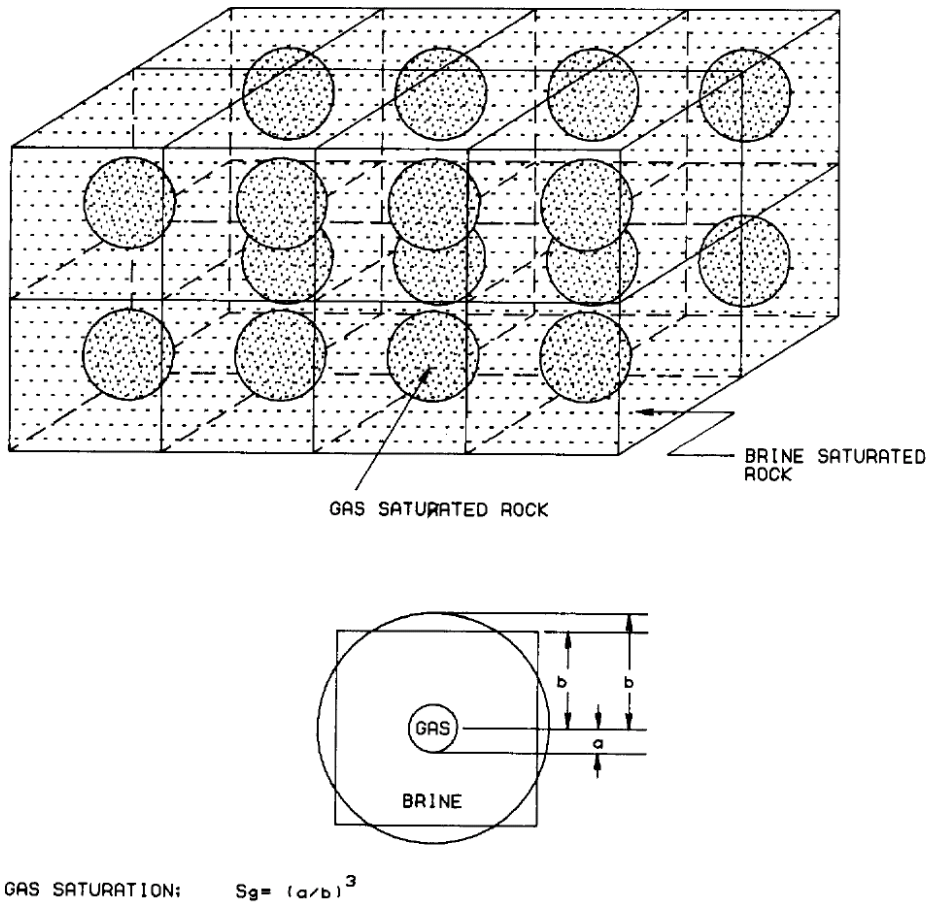


Figure 3-1 White model of gas inclusion, White (1975)

The White theory was developed based on the principle that the displacement in the outer sphere will create a pressure acting on the inside sphere. The pressure difference creates a fluid flow across the boundary which is calculated by

$$v = \frac{P_0(R_1 - R_2)}{(Z_1 + Z_2)} \quad (3.2)$$

Where P_0 is the impressed pressure applied as wave is passing through the element. White named R_1 and R_2 the constants of proportionality. With the following expression, they can be derived following the concept of pressure creation due to dilatation.

$$R_1 = \frac{K_1 - K_{dry1}}{1 - \frac{K_{dry1}}{K_{01}}} \frac{3k_2 + 4\mu_2}{K_2(3K_1 + 4\mu_2) + 4\mu_2(K_1 - K_2)S_g} \quad (3.3)$$

$$R_2 = \frac{K_2 - K_{dry2}}{1 - \frac{K_{dry2}}{K_{02}}} \frac{3k_1 + 4\mu_1}{K_2(3K_1 + 4\mu_2) + 4\mu_2(K_1 - K_2)S_g} \quad (3.4)$$

R_1 is always greater than R_2 because the bulk modulus of the liquid is usually several orders of magnitude greater than that of gas. Z_1 and Z_2 are the acoustic impedance of each medium and they can be derived based on the relative velocities of each phase based on Darcy's Law.

$$Z_1 = \frac{\eta_1 a}{\kappa_1} \left[\frac{1 - \exp(2\alpha_1 a)}{(\alpha_1 a - 1) + (\alpha_1 a + 1) \exp(-2\alpha_1 a)} \right] \quad (3.5)$$

$$Z_2 = -\frac{\eta_2 a}{\kappa_2} \left[\frac{(\alpha_2 b + 1) + (\alpha_2 b - 1) \exp(2\alpha_2(b - a))}{(\alpha_2 b + 1)(\alpha_2 a - 1) - (\alpha_2 b - 1)(\alpha_2 a + 1) \exp(2\alpha_2(b - a))} \right] \quad (3.6)$$

$$\alpha_j = \left(\frac{i\omega\eta_j}{\kappa_j K_{Ej}} \right)^{1/2} \quad j = 1, 2 \quad (3.7)$$

$$K_{Ej} = \left[1 - \frac{K_{fj}(1 - \frac{K_j}{K_{0j}})(1 - \frac{K_{dryj}}{K_{0j}})}{\phi K_j (1 - \frac{K_{fj}}{K_{0j}})} \right] K_{Aj} \quad j = 1, 2 \quad (3.8)$$

$$K_{Aj} = \frac{1}{\left(\frac{\phi}{K_{fj}} + \frac{1 - \phi}{K_{0j}} - \frac{K_{dryj}}{K_{0j}^2} \right)} \quad , j = 1, 2 \quad (3.9)$$

$$Q_j = \frac{(1 - \frac{K_{dryj}}{K_{0j}}) K_{Aj}}{K_j} \quad , j = 1, 2 \quad (3.10)$$

The important point which has not been addressed by White's initial paper is the fact that due to the presence of more than one phase, the permeability of each medium has to be the effective permeability rather than absolute permeability. Absolute permeability of a porous medium is measured using single phase Darcy's Law. Effective permeability of each phase (liquid or gas) is the products of absolute permeability and relative permeability. Relative permeability is usually determined by performing a core-flood and measuring the flow rate of each phase as saturation is changing during core-flood.

If we consider D_0 to be the relative dilation when there is no flow happening between the spheres, the pressure change is

$$P_0 = -K_\infty D_0 \quad (3.11)$$

Where K_∞ happens when dealing with really high frequency case.

$$K_\infty = \frac{k_2(3K_1 + 4\mu_2) + 4\mu_2(K_1 - K_2)S_g}{(3K_1 + 4\mu_2) - 3(K_1 - K_2)S_g} \quad (3.12)$$

On the other hand when there is flow the sum of the pressure from the outside P_0 and the pressure which is converted to flow ΔP_0 is equal to the compliance times the dilation.

$$P_0 + \Delta P_0 = -K^* D_0 \quad (3.13)$$

Where the pressure loss due to the flow is calculated from

$$\Delta P_0 = K^* W P_0 \quad (3.14)$$

$$W = \frac{3 a^2 (R_1 - R_2)(-Q_1 - Q_2)}{b^3 i \omega (Z_1 + Z_2)} \quad (3.15)$$

Therefore the following expression can be calculated for the complex moduli.

$$K^* = \frac{K_\infty}{1 - K_\infty W} = K_r^* + iK_i^* \quad (3.16)$$

Equation 3.16 is used to calculate the attenuation based on the ratio between the imaginary and real part of bulk moduli. The derivation is explained in more details in chapter 4 based on the theory of viscoelasticity.

As it is explained by White, the shear modulus of a patchy saturated case is the same as dry shear moduli which is similar to the assumption of Gassmann theory.

3.3 Sensitivity Analysis on White Theory Inputs

Before using White theory in monitoring a hydrocarbon reservoir one needs to understand the sensitivity of different input parameters on the results. This will help to evaluate the uncertainty in the results and also helps to identify the most controlling parameters.

In this study the input parameters of White's model are divided into static and dynamic properties. This classification is done to differentiate between the rock properties which are not fluid dependent and fluid dependent properties. The static parameters are the purely rock depending properties which are considered to be constant. For example the bulk moduli and shear moduli of the grains. However the fluid dependent parameters such as saturation and fluid properties are the dynamic properties. These properties depend on the state of depletion of the hydrocarbon reservoir which could change during production.

3.3.1 Static Parameters

Using the literature data the static parameters (rock properties) were estimated for an unconsolidated sandstone reservoir. Although in reality the static parameters are not always constant and they can vary spatially, however in contrast with the dynamic parameters one could consider them to have fixed values. The static properties are listed below:

- Dry bulk moduli of frame = 6.0E+9 Pascal
- Dry shear moduli of frame = 5.0E+9 Pascal
- Grain bulk moduli (quartz) = 35.0E+9 Pascal

- Grain shear moduli (quartz) = 45.0E+9 Pascal
- Grain density = 2600 kg/m³
- Porosity = 0.30

3.3.2 Dynamic Parameters

For reservoir monitoring the main objective is to understand the impact of the saturation and fluid acoustic properties on the seismic response. Therefore the sensitivity analysis was performed on the dynamic parameters. Below is the list of the dynamic parameters of White theory.

- | | |
|----------------------|---------------------------------|
| • Gas bulk moduli | • Liquid viscosity |
| • Liquid bulk moduli | • Gas effective permeability |
| • Gas density | • Liquid effective permeability |
| • Liquid density | • Gas saturation |
| • Gas viscosity | • Gas bubble size |

Table 3-1 presents the default values which were used in this analysis for dynamic properties. These values were obtained using the knowledge of the reservoir fluid (heavy oil) and the saturations were estimated for a typical heavy oil reservoir condition at its initial states.

Parameter	Value
Gas Bulk Moduli (Pascal)	1E+6
Liquid Bulk Moduli (Pascal)	2E+9
Gas Density (kg/m ³)	80
Liquid Density (kg/m ³)	950
Gas Viscosity (Pa.sec)	0.0000001
Liquid Viscosity (Pa.sec)	0.5
Gas effective permeability (m ²)	0.000001E-12
Liquid effective permeability (m ²)	0.1 1E-12
Gas saturation (fraction)	0.1
Gas bubble size (m)	0.001

Table 3-1 White model of gas inclusion White (1975)

The following table present the input parameters used for sensitivity analysis of the White theory on the dynamic properties. In order to run any given sensitivity analysis the rest of the parameters were set at the default values presented in Table 3-1.

Parametric study was done by changing one parameter at a time. The range of sensitivity was decided based on the range of possible change during production and also uncertainty associated with the given parameter. The input parameters are summarized in Table 3-2 and 3-3.

Parameter	Unit	1	2	3	4	5
Gas Bulk Moduli	Pascal	5.00E+05	1.00E+06	1.50E+06	2.00E+06	2.50E+06
Liquid Bulk Moduli	Pascal	2.00E+08	4.00E+08	6.00E+08	8.00E+08	1.00E+09
Gas Density	kg/m ³	4.50E+01	6.00E+01	7.50E+01	9.00E+01	1.05E+02
Liquid Density	kg/m ³	7.70E+02	7.90E+02	8.10E+02	8.30E+02	8.50E+02
Gas Viscosity	Pascal.sec	5.00E-06	1.00E-05	1.50E-05	2.00E-05	2.50E-05
Liquid Viscosity	Pascal.sec	1.00E-01	2.00E-01	3.00E-01	4.00E-01	5.00E-01
Gas effective permeability	m ²	1.00E-16	2.00E-16	3.00E-16	4.00E-16	5.00E-16
Gas effective permeability	m ²	5.00E-14	1.00E-13	1.50E-13	2.00E-13	2.50E-13
Gas saturation	fraction	3. 0E-02	4.00E-02	5.00E-02	6.00E-01	7.00E-01
Gas bubble size	m	1.00E-04	2.00E-04	3.00E-04	4.00E-04	5.00E-04

Table 3-2 Dynamic parameters used in the sensitivity analysis of White's theory, continued

Parameter	Unit	6	7	8	9	10
Gas Bulk Moduli	Pascal	3.00E+06	3.50E+06	4.00E+06	4.50E+06	5.00E+06
Liquid Bulk Moduli	Pascal	1.20E+09	1.40E+09	1.60E+09	1.80E+09	2.00E+09
Gas Density	kg/m ³	1.20E+02	1.35E+02	1.50E+02	1.65E+02	1.80E+02
Liquid Density	kg/m ³	8.70E+02	8.90E+02	9.10E+02	9.30E+02	9.50E+02
Gas Viscosity	Pascal.sec	3.00E-05	3.50E-05	4.00E-05	4.50E-05	5.00E-05
Liquid Viscosity	Pascal.sec	6.00E-01	7.00E-01	8.00E-01	9.00E-01	1.00E+00
Gas effective permeability	m ²	6.00E-16	7.00E-16	8.00E-16	9.00E-16	1.00E-15
Gas effective permeability	m ²	3.00E-13	3.50E-13	4.00E-13	4.50E-13	5.00E-13
Gas saturation	fraction	8.00E-01	9.00E-01	1.00E-01	1.10E-01	1.20E-01
Gas bubble size	m	6.00E-04	7.00E-04	8.00E-04	9.00E-04	1.00E-03

Table 3-3 Dynamic parameters used in the sensitivity analysis of White's theory

3.3.2.1 Effect of gas and liquid bulk moduli

Gas bulk moduli depend on the pressure, composition and temperature. For this sensitivity analysis gas bulk moduli was varied linearly from $5E+05$ Pascal to $5E+06$ Pascal linearly in 10 steps. The results are presented in Figure 3-2. These results show that the attenuation and the velocity dispersion are not significantly depending on the gas bulk moduli.

On the other hand the liquid bulk moduli seem to play an important role in the attenuation. Liquid bulk moduli are related to the type of liquid, pressure, and temperature of the system. Water is a relatively incompressible fluid, whereas oil can be a compressible fluid deepening on its Gas Oil Ratio (GOR) and composition.

Figure 3-3 presents the results of the sensitivity analysis. The liquid bulk modulus was linearly varied from $2E+08$ kPa to $2E+09$ kPa in ten steps. As liquid bulk moduli were increased both the maximum attenuation and the peak frequency increased toward higher frequencies. The P wave velocity dispersion is also increased for higher liquid bulk moduli.

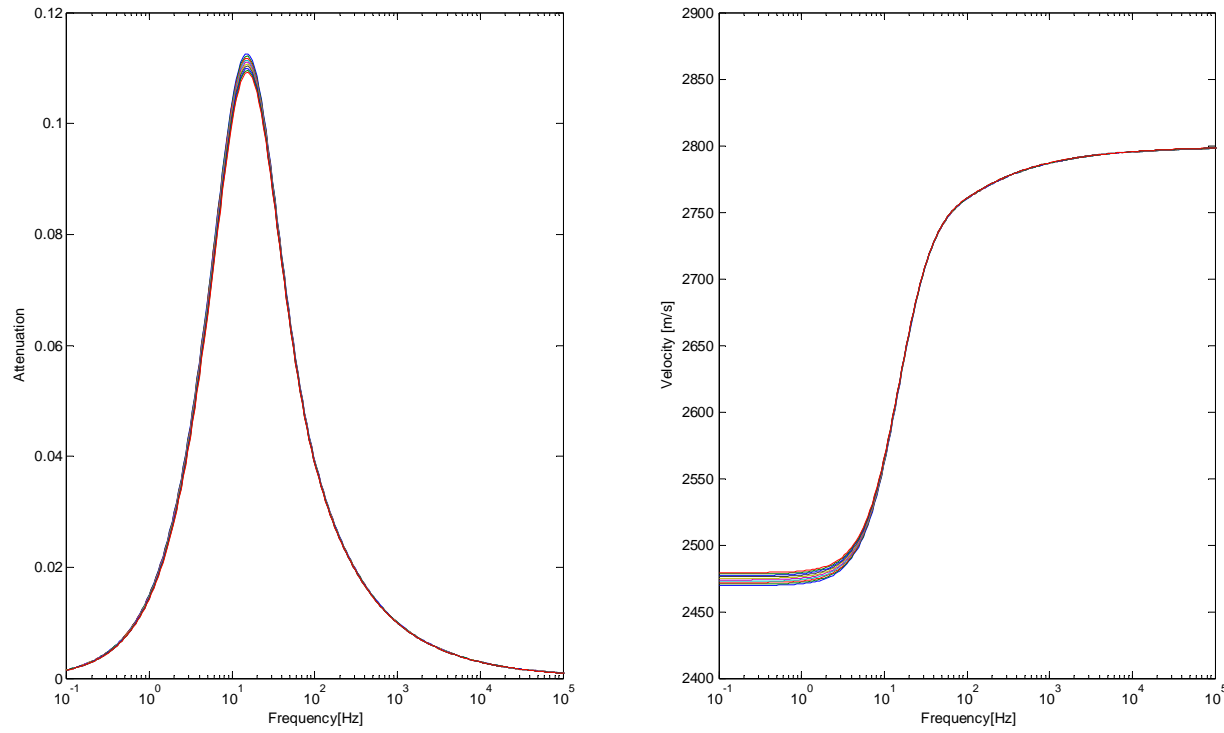


Figure 3-2 Gas Bulk Moduli sensitivity results

Parameter	unit	1	2	3	4	5	6	7	8	9	10
Gas Bulk Moduli	Pascal	5.00E+05	1.00E+06	1.50E+06	2.00E+06	2.50E+06	3.00E+06	3.50E+06	4.00E+06	4.50E+06	5.00E+06

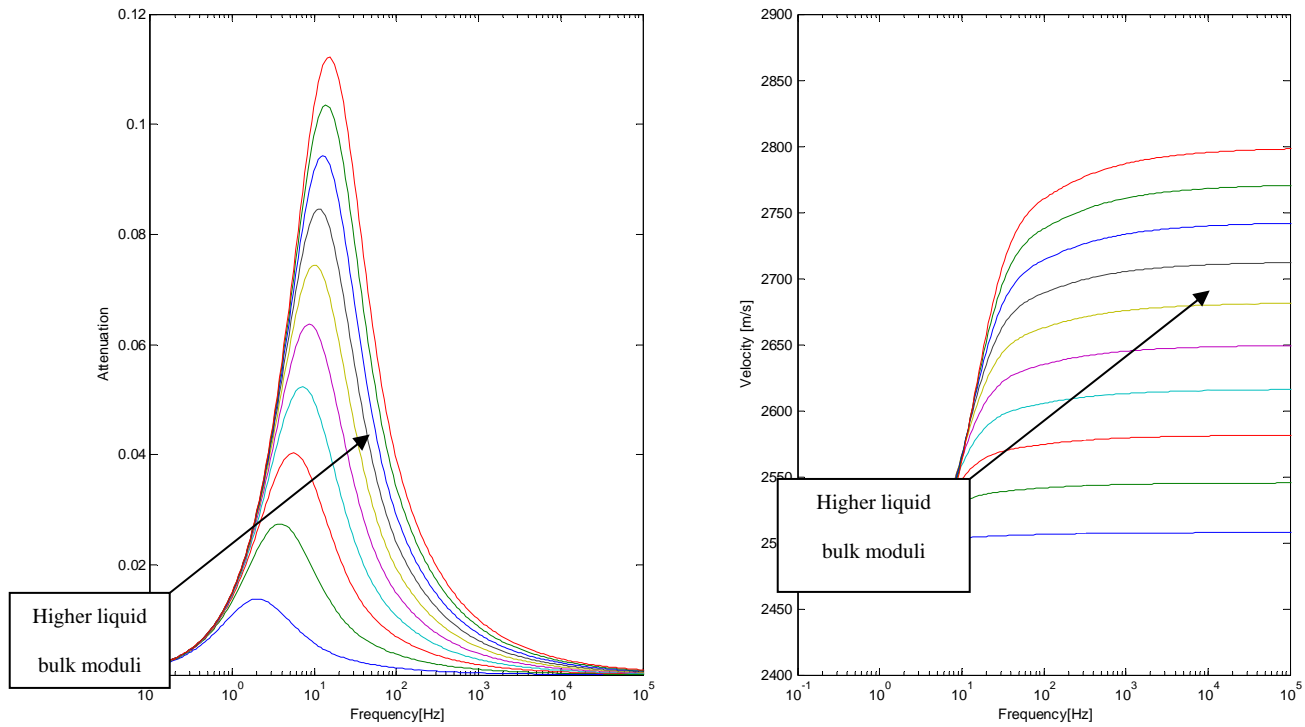


Figure 3-3 Liquid bulk moduli sensitivity results

Parameter	unit	1	2	3	4	5	6	7	8	9	10
Liquid Bulk Moduli	Pascal	2.00E+08	4.00E+08	6.00E+08	8.00E+08	1.00E+09	1.20E+09	1.40E+09	1.60E+09	1.80E+09	2.00E+09

3.3.2.2 Effect of gas and liquid density

Similar to the bulk moduli, gas and liquid densities also depend on the reservoir fluid composition, pressure and temperature. In order to investigate the gas and liquid density effect on patchy saturation model sensitivity analysis was performed. It is very important to understand the reservoir fluid properties and their phase behaviour with respect to changes during the production.

An Equation Of State (EOS) is an analytical expression relating the pressure (P) to the temperature (T) and the volume (V). The best known and the simplest example of an equation of state is the ideal gas law. As a common practice of industry in this thesis the fluid model was created using the Peng-Robinson EOS. Peng and Robinson (1976) conducted a comprehensive study on the behaviour of naturally occurring hydrocarbon systems. The main improvement they added was the ability of their equation of state to predict liquid densities and other fluid properties particularly in the vicinity of the critical region. Peng and Robinson proposed the following expression:

$$P = \frac{RT}{V - b} - \frac{a\alpha}{V(V + b) + b(V - b)} \quad (3. 17)$$

$$a = \Omega_a \frac{R^2 T_c^2}{P_c}$$

$$b = \Omega_b \frac{RT_c}{P_c}$$

$$\alpha = [1 + m(1 - \sqrt{T_r})]^2$$

$$m = 0.3796 + 1.54226\omega_{AC} - 0.2699\omega_{AC}^2$$

$$\omega_{AC} = -\log\left(\frac{p_v}{P_c}\right)_{T=0.7T_c} - 1$$

where:

P = Pressure [kPa]

V = Molar volume [m³/mol]

R = Universal gas constant 8.31451 E-3 kPa m³ K⁻¹ mol⁻¹

T = Temperature [K]

Ω_a = constant 0.45724

Ω_b = constant 0.07780

P_c = Critical pressure of the substance [kPa]

T_c = Critical temperature of the substance [K]

T_r = Reduced temperature T/T_c

ω_{AC} = Acentric factor of the substance initially introduced by Pitzer (1955) to quantify

the nonsphericity of a substance

p_v = Vapour pressure of a substance at 70% of the critical temperature.

Peng and Robinson (1978) proposed the following modified expression for m that is recommended for heavier components with acentric values $\omega_{AC} > 0.49$:

where:

$$m = 0.379642 + 1.48503\omega_{AC} - 0.1644\omega_{AC}^2 + 0.016667\omega_{AC}^3$$

Peng Robinson equation of state can be written in a cubic format resulting :

$$z^3 - z^2(1 - b) + Z(a - 3b^2 - 2b) - (ab - b^2 - b^3) = 0 \quad (3. 18)$$

By solving the above cubic equation the smallest root is the liquid phase z value and the largest root is the gas phase z factor. After calculation of the Z factors of the gas and liquid phases density can be calculated using the following equation:

$$\rho = \frac{PM_w}{ZRT} \quad (3. 19)$$

P is the pressure, Z is the incompressibility coefficient of liquid or gas calculated from equation of state, T is the temperature of the system in Kelvin, R is the universal constant and M_w is the molecular weight.

When dealing with more than one component in the gas and liquid phase mixing rules is used to estimate the molecular weight of the mixture in different phases bases on the mole fractions of each phase. The mixing rule is calculated by taking a weighting average of the molecular weight using the mole fractions.

As shown in Figure 3-4 by changing gas density from 4 kg/m^3 to 18 kg/m^3 in ten linear steps no significant change was observed on the results of the attenuation and the P wave velocity at different frequencies. The sensitivity analysis of liquid density shows that the liquid density does not have a significant effect on the attenuation. However as shown in Figure 3-5 by changing the liquid density from 770 kg/m^3 to 950 kg/m^3 (in 10 linear steps), the velocity is changing linearly. Heavy oil reservoirs have densities as high as 850 kg/m^3 . For bitumen type reservoirs density can be higher than 1000 kg/m^3 .

The effect of both liquid and gas density on the P wave velocity and attenuation of a patchy saturation system is not significant. This is due to the fact that the density is a linear scaling factor and does not affect the frequency dependency of attenuation and velocity predicted by Whites theory.

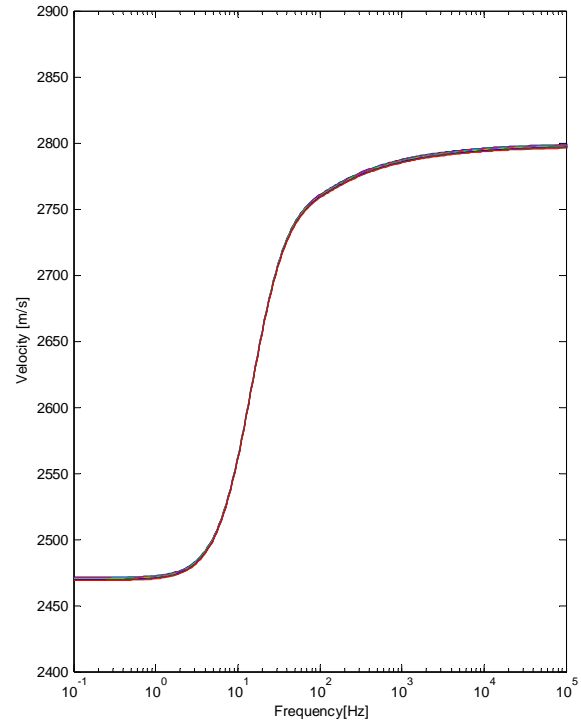
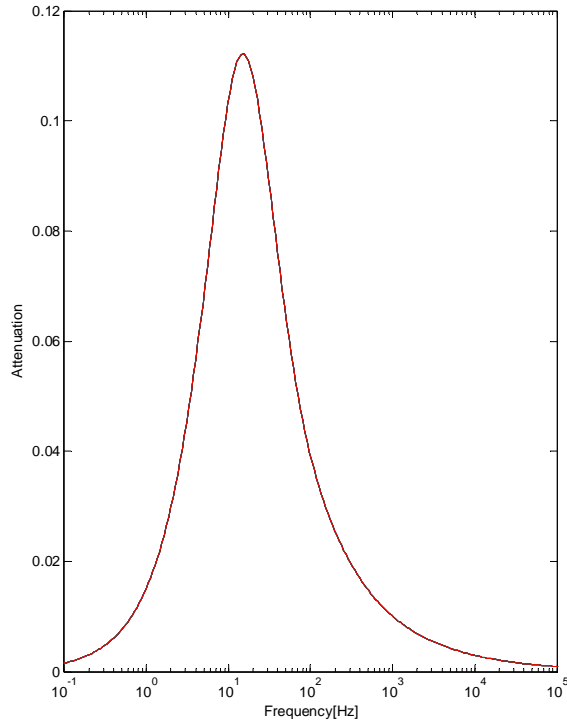


Figure 3-4 Gas density sensitivity results

Parameter	unit	1	2	3	4	5	6	7	8	9	10
Gas Density	kg/m ³	4.50E+01	6.00E+01	7.50E+01	9.00E+01	1.05E+02	1.20E+02	1.35E+02	1.50E+02	1.65E+02	1.80E+02

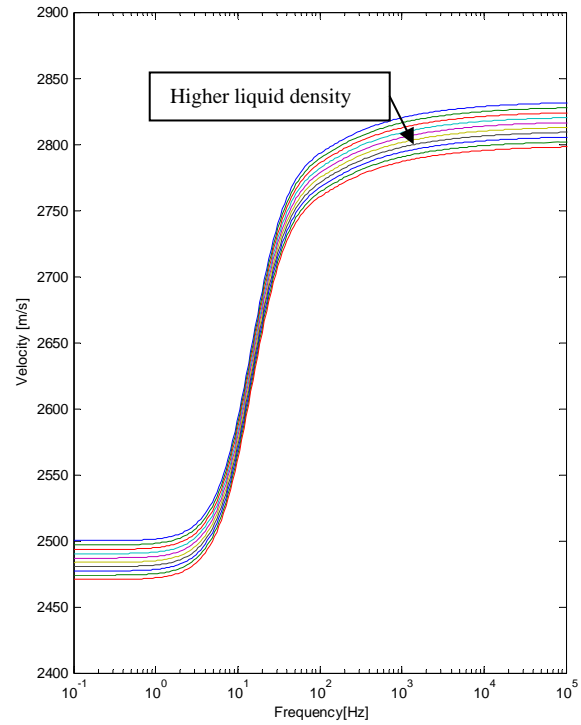
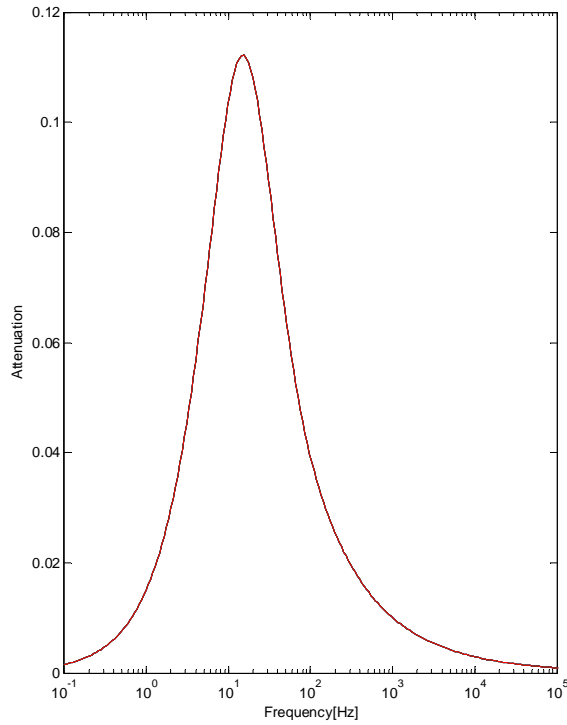


Figure 3-5 Liquid density sensitivity analyses

Parameter	unit	1	2	3	4	5	6	7	8	9	10
Liquid Density	kg/m ³	7.70E+02	7.90E+02	8.10E+02	8.30E+02	8.50E+02	8.70E+02	8.90E+02	9.10E+02	9.30E+02	9.50E+02

3.3.2.3 Effect of gas and liquid viscosity

Viscosity of a given fluid is simply its internal friction to flow. Gas viscosity is mostly estimated using known correlations such as Carr-Kobayashi-Burrows (1954) correlation and the Lee-Gonzalez-Eakin (1966) method. Gas viscosity is a function of pressure, temperature and the composition of the gas. Using Lee et al.(1966) method the gas viscosity can be calculated using the following equations.

$$\mu_g = 10^{-4} K \exp\left(X \left(\frac{\rho_g}{62.4}\right) Y\right) \quad (3. 20)$$

where

$$K = \frac{(9.4 + 0.02M_w)T^{1.5}}{209 + 19M_w + T}$$

$$X = 3.5 + \frac{986}{T} + 0.01M_w$$

$$Y = 2.4 - 0.2X$$

ρ_g is gas density at reservoir condition [lb/ft³] and T [R] is the reservoir temperature and Mw is the molecular weight of the gas mixture.

The liquid viscosity of oil which has to be used in estimating the P wave velocity and attenuation is the in situ viscosity. Depending on the initial reservoir pressure and depletion path one might be dealing with saturated oil viscosity or under-saturated oil viscosity. If the reservoir pressure is kept above bubble point pressure of the mixture, the under-saturated system exists and if the reservoir pressure is below bubble point pressure the system is saturated. Oil viscosity decreases as more gas is being dissolved in the oil.

However, after reaching the bubble point pressure no more gas would be dissolved therefore, with increase in the pressure oil viscosity slightly increases.

Pederson et al (1984) presented a new method for calculating the viscosity of the heavy oil that has been very successful in predicting lab measurement data. According to Pedersen et al. (1984) the problems associated with representing poly-disperse mixtures (such as heavy crude oils) are associated with the computation of average molar masses. Their results indicated that larger molecules should make a greater contribution to viscosity than the smaller ones. This is done by using corresponding states to calculate the viscosity of a component or mixture, knowing the viscosity of a reference substance at the same condition of reduced pressure and temperature. Pederson's equation can be simplified to

$$\frac{\mu_{mix}(P, T)}{\mu_0(P_0, T_0)} = \left(\frac{T_{c,mix}}{T_{c,0}} \right)^{\frac{1}{6}} \left(\frac{P_{c,mix}}{P_{c,0}} \right)^{\frac{2}{3}} \left(\frac{MW_{mix}}{MW_0} \right)^{\frac{1}{2}} \left(\frac{\alpha_{mix}}{\alpha_0} \right) \quad (3. 21)$$

$$T_{c,mix} = \sum_{n=1}^n x_i T_{c,i}$$

$$P_{c,mix} = \sum_{n=1}^n x_i P_{c,i}$$

$$MW_{mix} = b_1 (MW_w^{b_2} - MW_n^{b_2}) + MW_n$$

$$\alpha = 1 + b_3 \rho_r^{b_4} MW^{b_5}$$

where :

μ = viscosity [cp]

T_c = critical temperature [k]

P_c = critical pressure [k]

MW = molecular weight [gr/mol]

ρ = density [kg/m³]

b_1, b_2, b_3, b_4, b_5 = constants could be used as matching parameters

The subscript *mix* refers to the mixture properties and subscript *0* is the reference properties. The reference condition is referred to the methane (c1). MW_w is the weight fraction average molecular weight and MW_n is the mole fraction averaged molecular weight. α is called “*rotational coupling coefficient*” .

The results of the sensitivity analysis of the gas and liquid (oil) viscosity are presented in Figures 3-6 and 3-7. Gas viscosity does not seem to have a big impact on the P wave velocity and its attenuation. However the liquid (oil) viscosity has a very significant impact on the results. As liquid (oil) viscosity increases the frequency at which maximum attenuation occurring decreases. In the sensitivity analysis liquid/oil viscosity was varied from 0.1 Pa.sec (100 cp) to 1 Pa.sec (1000cp) in ten linear steps. The peak frequency has moved almost one order of magnitude over this range of change from 100 Hz to 10Hz. This is a very important point to consider while estimating attenuation over seismic frequency of heavy oil.

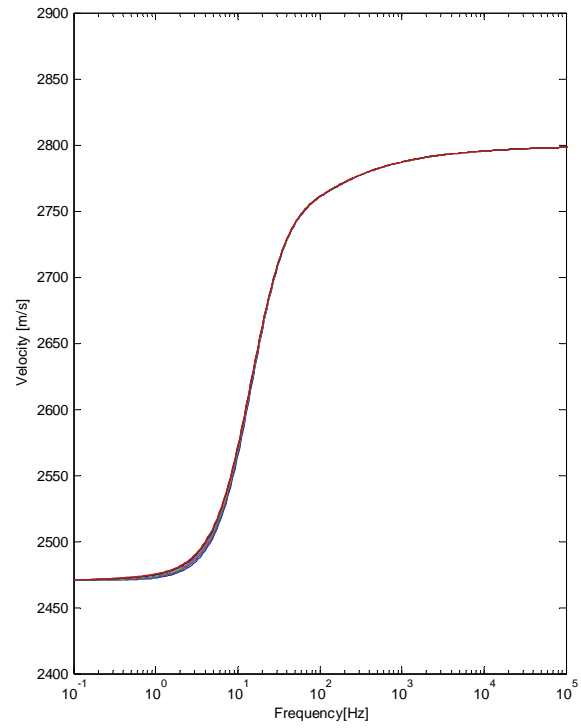
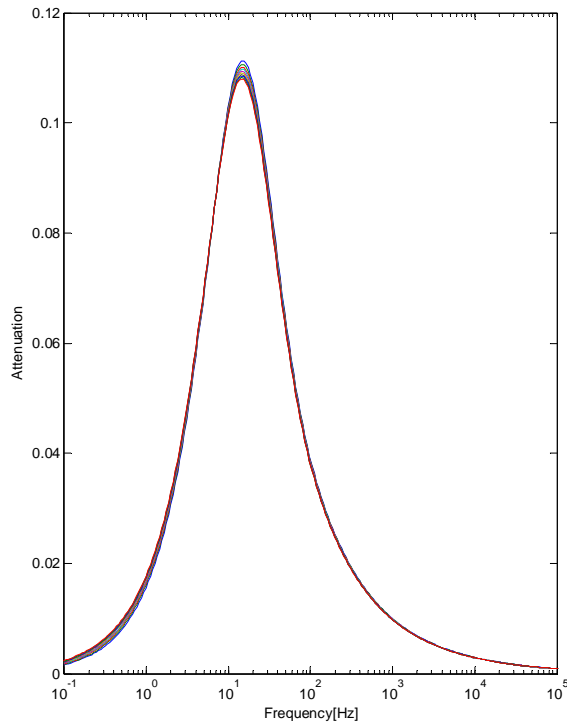


Figure 3-6 Gas viscosity sensitivity analyses

Parameter	unit	1	2	3	4	5	6	7	8	9	10
Gas Viscosity	Pascal.sec	5.00E-06	1.00E-05	1.50E-05	2.00E-05	2.50E-05	3.00E-05	3.50E-05	4.00E-05	4.50E-05	5.00E-05

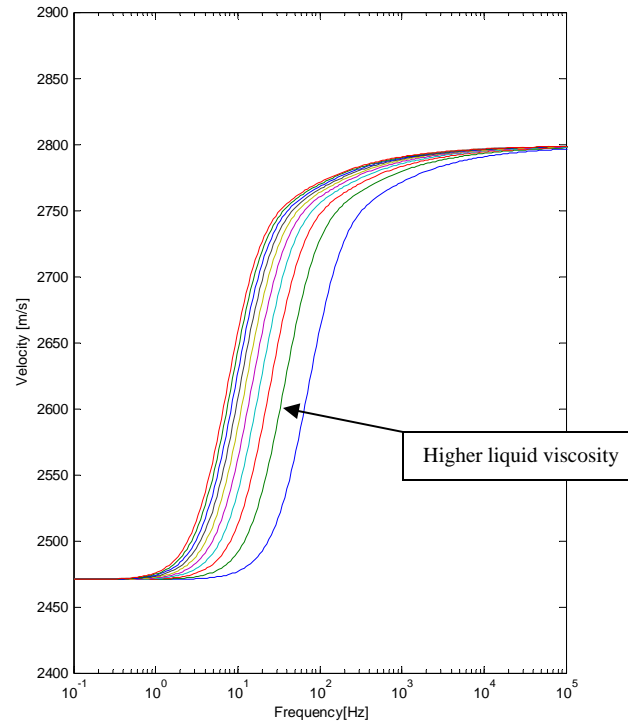
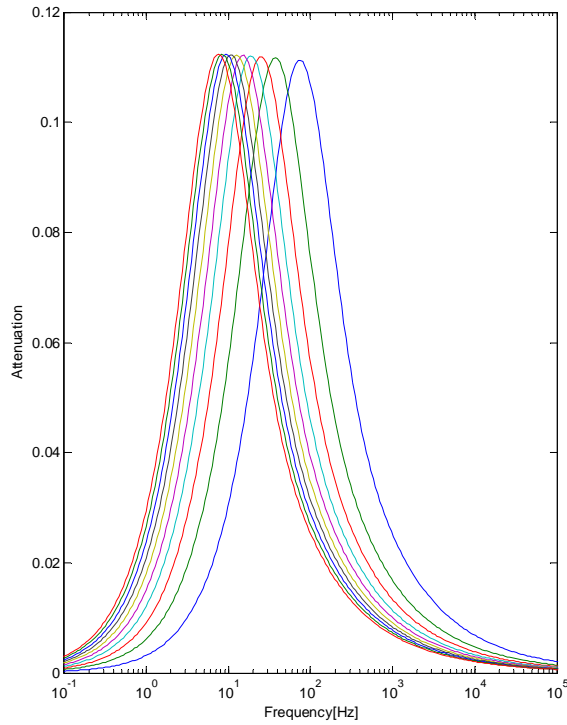


Figure 3-7 Liquid viscosity sensitivity analyses

Parameter	unit	1	2	3	4	5	6	7	8	9	10
Liquid Viscosity	Pascal.sec	1.00E-01	2.00E-01	3.00E-01	4.00E-01	5.00E-01	6.00E-01	7.00E-01	8.00E-01	9.00E-01	1.00E+00

3.3.2.4 Effect of Gas and Liquid Permeability

Permeability of a porous medium is one of the most important parameters in flow modeling. Permeability is the ability of the porous medium to flow. When cores are available one can estimate the absolute permeability of a porous medium using Darcy's Law. This is done by flowing air through clean core and measuring the flow rate and the pressure drop across the core plug. However when more than one phase exists the effective permeability of each phase is estimated by multiplying the relative permeability (number between 0 to 1) to the absolute permeability. The in situ effective permeability can be also measured by a flow and build-up analysis. Pressure Transient Analysis (PTA) is usually done through type curve matching and bottomhole pressure history matching.

There are few parameters such as grain size, sorting, compaction level and shale content which control the permeability. However there is no single best method for estimating permeability. Core permeability values tend to be higher than the well test driven permeability numbers as they do not represent the actual in-situ reservoir conditions such as compaction. The relative permeability is explained in more detail in the history matching section of Chapter 5.

Figures 3-8, and 3-9 present the impact of effective permeability of gas and liquid on the P wave attenuation and velocity at different frequencies respectively. Gas permeability does not impact the velocity. However the liquid permeability seems to have a very significant impact on the velocity. In this analysis the permeability was increased from $5E-14$ (50 mD) to $5E-13(m^{-2})$ (500 mD) in ten linear steps. The peak frequency increased from 100 Hz to 1000 Hz.

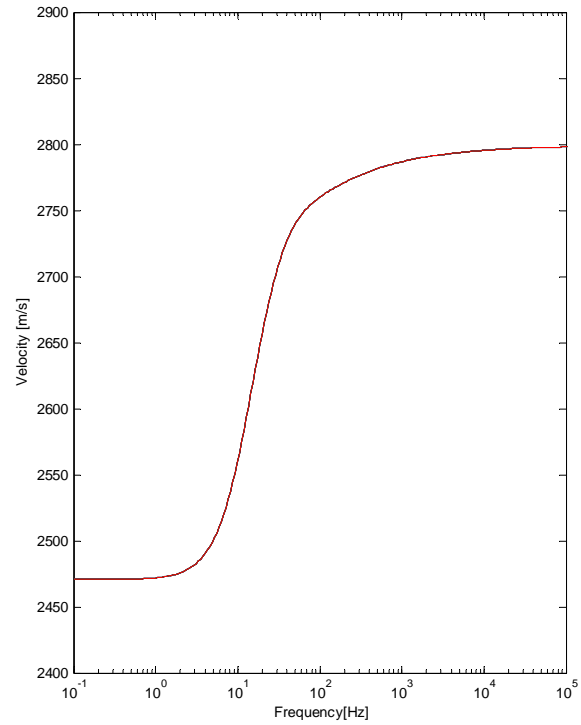
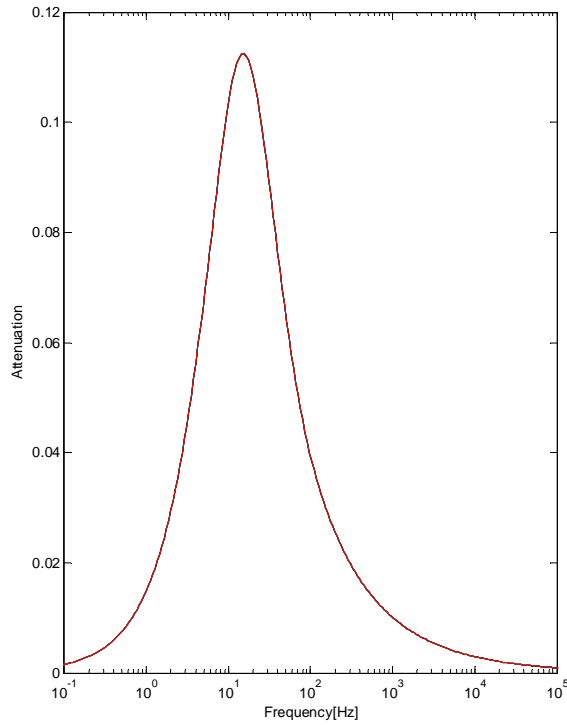


Figure 3-8 Gas Permeability sensitivity analyses

Parameter	unit	1	2	3	4	5	6	7	8	9	10
Gas effective permeability	²	1.00E-16	2.00E-16	3.00E-16	4.00E-16	5.00E-16	6.00E-16	7.00E-16	8.00E-16	9.00E-16	1.00E-15

m

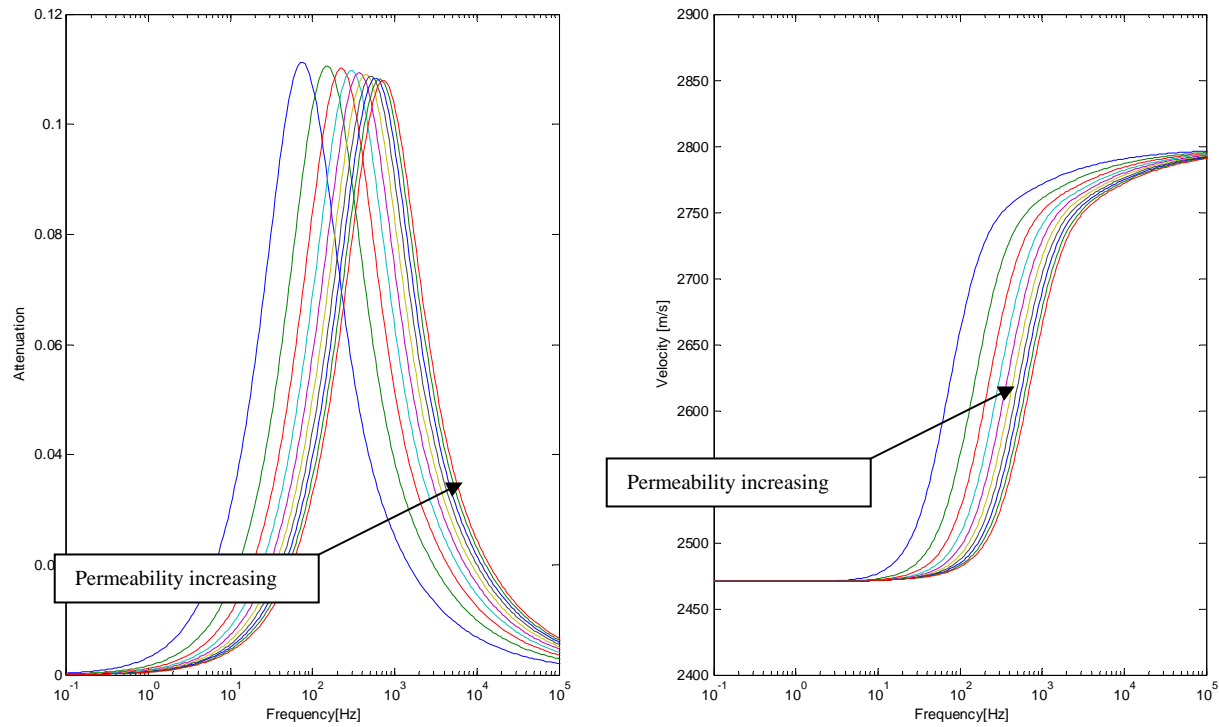


Figure 3-9 Liquid permeability sensitivity analyses

Parameter	unit	1	2	3	4	5	6	7	8	9	10
liquid effective permeability	1/m ²	5.00E-14	1.00E-13	1.50E-13	2.00E-13	2.50E-13	3.00E-13	3.50E-13	4.00E-13	4.50E-13	5.00E-13

3.3.2.5 Effect of Gas Saturation and Bubble Size

In order to use patchy saturation theory the gas saturation should be low enough that gas bubbles are still presented in the porous medium. If gas bubbles form a continuous phase the assumption of patchy saturation is not honoured. To understand the impact of gas saturation on the P wave attenuation and velocity the sensitivity analysis was done by changing gas saturation from 0.03 to 0.12 linearly. The theoretical limit of gas saturation based on the geometry explained in Figure 3-1 is about 52%.

The value of gas saturation at which gas phase starts to move and form a continuous phase moving toward the wellbore in the reservoir is usually referred as “*critical gas saturation*”. Critical gas saturation depends on the rock properties such as pore throat sizes (capillary forces) and also the rheology of the oil.

Under primary depletion of a reservoir as pressure is drawn down in the producing wells the reservoir pressure starts to decline. When the reservoir pressure goes below the bubble point, pressure gas bubbles start to form. In conventional oil reservoirs the critical gas saturation is usually under 5% and the time for forming a continuous gas phase is relatively short (few months). However in heavy oil reservoirs the critical gas saturation can be higher and it is usually controlled by foamy oil behaviour.

Due to the presence of gas (methane) when heavy oil goes under a rapid depressurization it forms “foamy oil” Maini (1996) described the “foamy oil” as a major mechanism for producing cold heavy production in Canada which is governed by a

solution gas drive. The presence of the foam or suspended gas phase has been observed on wellhead samples. Foam has been seen on the production vessels and pipes even a few hours after the production at lowered surface pressure conditions. The mechanism of foamy oil formation is an important part to understand the rock physics of White's patchy saturation theory.

The simplest explanation of the formation of foamy oil was given by Mastmann et al. (2001). The study summarizes the foamy oil formation to be related to the existence of a pseudo bubble point pressure. In conventional oil with relatively low viscosity the bubble point pressure is defined as the pressure at which, at the reservoir temperature, the first small bubbles of free gas evolve from solution in the oil and nucleate as a distinct free gas phase. Because the viscosity of the conventional oil is relatively low, these small bubbles will coalesce with each other and form larger bubbles and then form a continuous gas phase rapidly. In foamy oil reservoirs, the time for the small gas bubbles to form a continuous gas phase is substantially longer. Therefore there are gas bubbles presented in the oil and they flow with same Darcy velocity to the production well. The point for the foamy oil formation occurs when the bubbles of free gas can finally start to escape from solution as a distinct free gas phase. This is known as the pseudo bubble point. Maini (1996) identifies this critical saturation as a percolation limit, other researcher like Pooladi-Darvish and Firoozabadi (1997) identify this even by visual observation of bubbles in a viewing window in the lab experiment. The goal here is to define two key parameters that are required for the White's theory, which are gas saturation and the bubble sizes.

In summary the solution gas drive process can be described in three steps:

1. As pressure drops in the producing wells gas nucleation occurs. This process is related to the release of the dissolved light components into a free gas phase happens when pressure goes below the bubble point pressure of the light hydrocarbon.
2. Bubble growth: corresponding to mass transfer by molecular diffusion of the dissolved light components to the free gas phase. Until equilibrium concentration is reached, the liquid is always supersaturated and the system tends to the equilibrium state by transfer to the gas phase of the dissolved light components. As the pressure disturbance reaches the boundaries and the reservoir pressure is depleting, the gas bubbles starts to grow.
3. The last stage is the gas mobilization: Above a given gas saturation, called critical gas saturation S_{gc} , the gas phase forms a continuous phase and will be produced preferentially. This is due to the higher mobility of gas phase in comparison with liquid phase.

The two major mechanism involved in the bubble growth rate are the diffusion mechanism and the pressure depletion. Kumar et al. (2001) concluded that the effect of diffusion is the major mechanism in the rate of bubble growth. Figure 3-10 presents the results of study which was conducted and it clearly illustrates that the diffusion is the major mechanism.

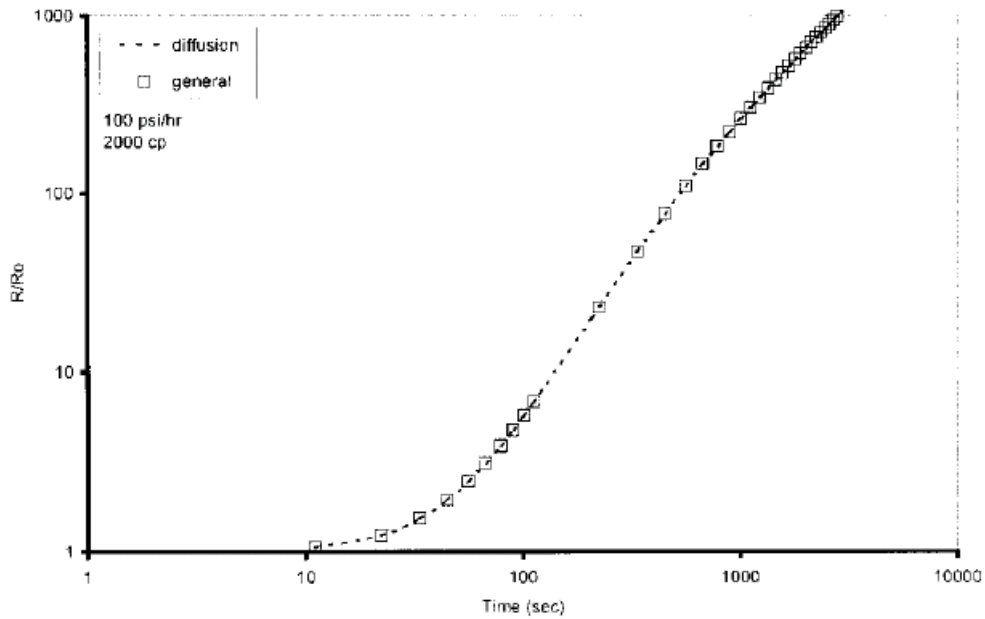


Figure 3-10 Diffusion limited vs. general growth: gradual decline in pressure. Kumar et al (2001)

Wong and Maini (2005) presented a model for estimating the size of gas bubbles in the foamy oil systems. In this model the effect of diffusion is being considered.

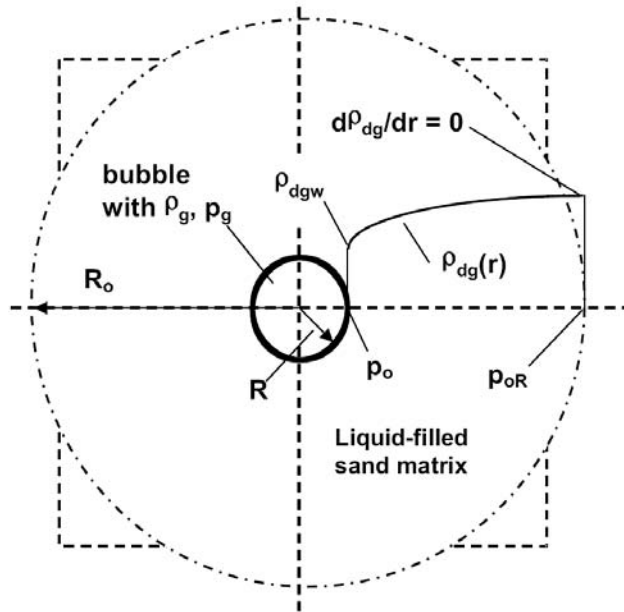


Figure 3-11 Bubble growth model presented by Wong & Maini (2005)

The Wong model is based on the radial mass diffusion of the super saturated liquid phase into the bubbles. Figure 3-11 presents the bubble growth model as presented by Wong. The mass diffusion of light hydrocarbons into the bubble is governed by:

$$D \left[\frac{\partial^2 \rho_{dg}}{\partial r^2} + \frac{2}{r} \frac{\partial \rho_{dg}}{\partial r} \right] - \left(\frac{R}{r} \right)^2 \left[\frac{\partial \rho_{dg}}{\partial r} \frac{dR}{dt} \right] = \frac{\partial \rho_{dg}}{\partial t} \quad (3. 22)$$

where:

D= solute diffusion coefficients

ρ_{dg} = is the solute concentration at radius r

R= radius of the bubble

By relating mass flux at the surface of bubble to the rate of bubble growth Wong related the mass transfer of dissolved gas to the free gas. Then by combining Henry's Law with ideal gas law the final derivation was completed. Before reviewing the results of Wong the following normalized parameters need to be defined:

$$\text{Normalized time: } T = \frac{\varphi D t}{a_i^2} \quad (3. 23)$$

Here φ is the porosity and a_i is the initial size of the bubble. Wong did not use any specific number for the initial bubble radius. However based on the gas saturation they developed a curve for number of bubble versus gas saturation and normalized time.

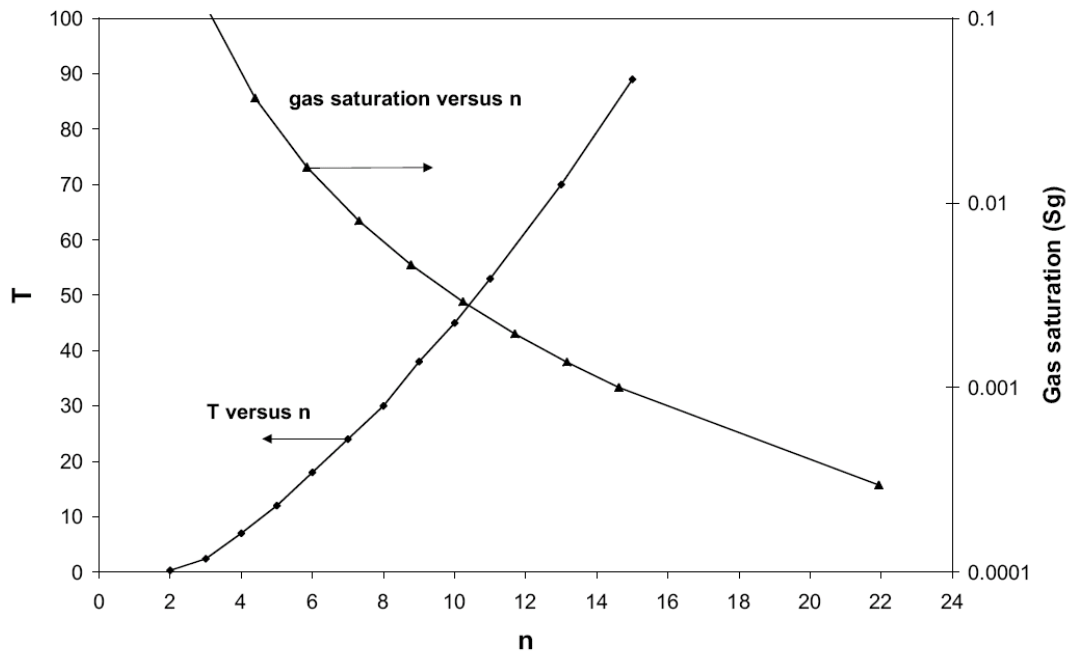


Figure 3-12 Relationships between (a) dimensionless equilibrium time T versus bubble density number n ; (b) gas saturation versus n , Wong (2006)

Wong defined the normalized solute concentration:

$$\text{Normalized solute concentration: } \rho = \frac{\rho_{dg} - \rho_{dg,i}}{\rho_{dge} - \rho_{dg,i}} \quad (3.24)$$

where:

ρ_{dg} = is the solute concentration in liquid phase a time t

$\rho_{dg,i}$ = initial solute concentration at the bubble surface in the beginning of the gas

exclusion

ρ_{dge} = final equilibrium solute concentration at the end of gas exsolution

The normalized parameter ρ varies between zero to 1 and it represents how far the bubble is compared to the equilibrium from the point of view of solute concentration.

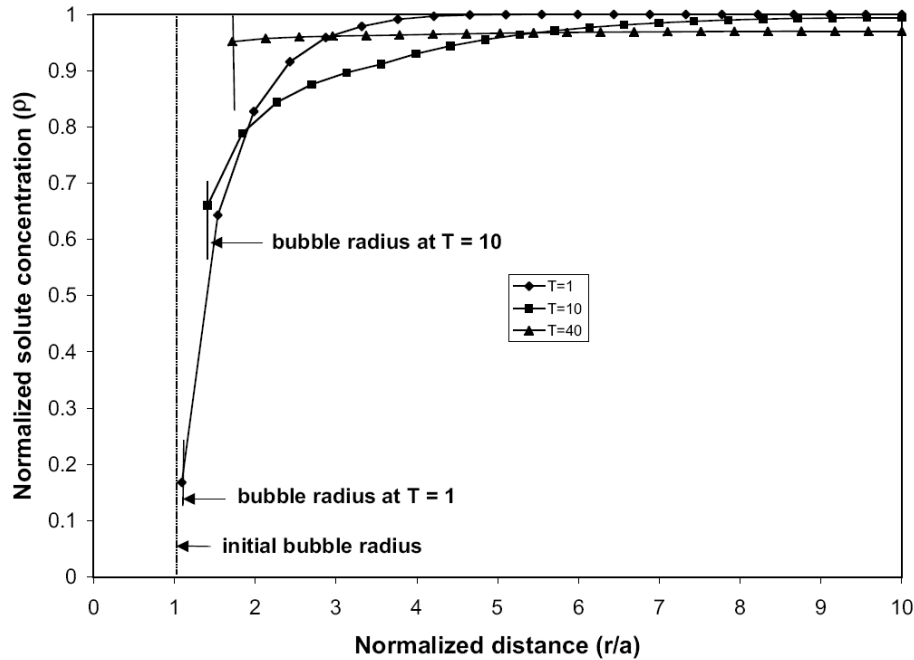


Figure 3-13 Evolution of solute concentration in liquid for bubble density $n = 6$

If we assume that in a given unit of volume the presence of 6 bubbles, based on the work by Wong at time after T passes values of 40, the change in the bubble radius is not very significant. If considering the initial size of the bubble to be 0.0005m and $D = 1E-10$ (m^2/s) and porosity of 31%, the time of equilibrium is about 3.7 years. The maximum size of bubble will be 1 mm after 3.7 years.

The results of the sensitivity analysis to understand the impact of gas saturation and bubble size are presented in Figures 3-14 and 3-15, respectively. The gas saturation was varied from 0.03 to 0.12 in ten linear steps. The sensitivity analysis shows that lower gas saturation has higher attenuation. However for high frequencies the impact on

velocity is less for low gas saturation cases. Examination of Figure 3-14 suggests that the peak frequency of attenuation is moving to higher frequencies as gas saturation increases.

The bubble size sensitivity analysis results are presented in Figure 3-15. Bubble size was varied from $1.0\text{E-}4$ m to $1.0\text{E-}3$ m to understand the impact on the results on P wave velocity and attenuation at different frequencies. As illustrated by Figure 3-15 as bubble size grows the peak frequency decreases. For small size of bubble the attenuation happens at high frequencies (~ 1000 Hz), which is not within the seismic frequency range. However for higher bubble size the peak frequency is in the seismic frequency range (10 to 100 Hz). The bubble size does not have an impact on the magnitude of the attenuation.

In summary the review of White's theory presented in this chapter confirms that it can be used for properly estimating the seismic response of a patchy saturation system such as the foamy oil case that has been observed during cold heavy oil production.

The parametric study (sensitivity analysis) of the input parameters of White's theory suggests that it is imperative to have proper knowledge on the uncertainty of the liquid and gas properties. The sensitivity showed that the major controlling parameters are the liquid properties such as density, bulk moduli, permeability and viscosity. The gas saturation and bubble size also have a major impact on the response of White's patchy saturation model.

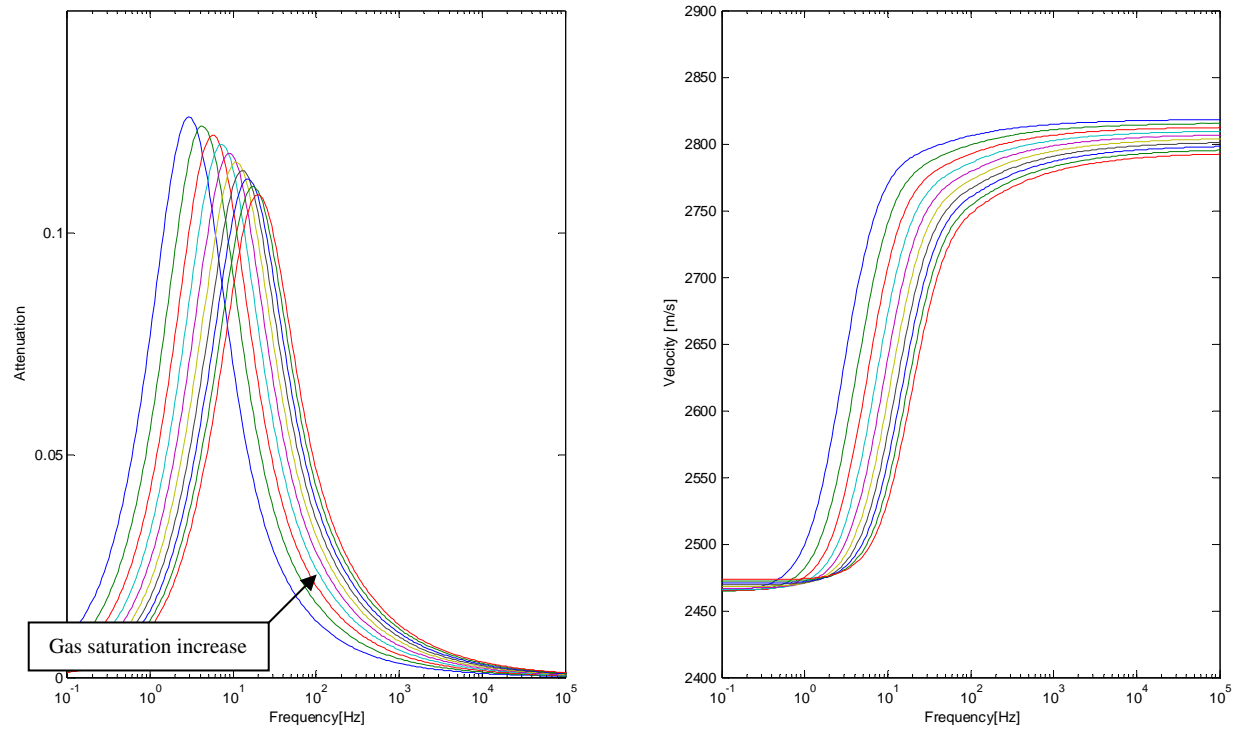


Figure 3-14 Gas saturation sensitivity analyses

Parameter	unit	1	2	3	4	5	6	7	8	9	10
Gas saturation	fraction	3.0E-02	4.00E-02	5.00E-02	6.00E-01	7.00E-01	8.00E-01	9.00E-01	1.00E-01	1.10E-01	1.20E-01

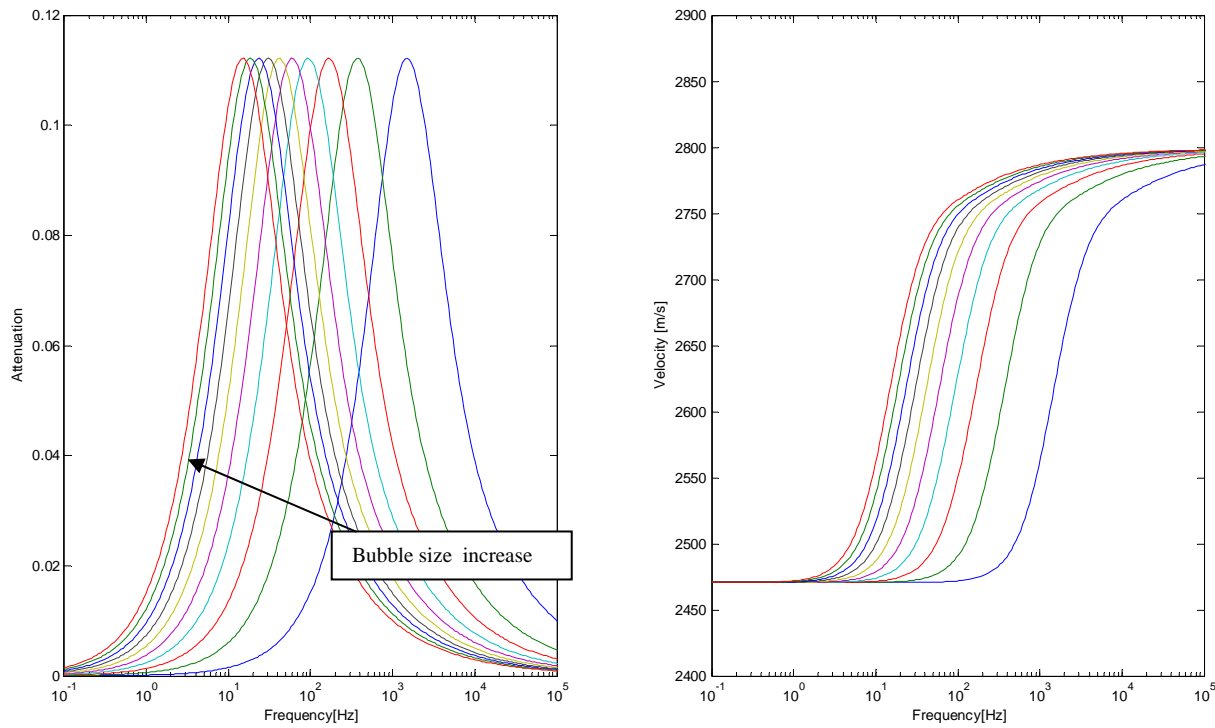


Figure 3-15 Gas bubble size sensitivity analysis

Parameter	unit	1	2	3	4	5	6	7	8	9	10
Gas bubble size	m	1.00E-04	2.00E-04	3.00E-04	4.00E-04	5.00E-04	6.00E-04	7.00E-04	8.00E-04	9.00E-04	1.00E-03

CHAPTER FOUR: VISCOELASTIC SEISMIC MODELING

The objective of this chapter is to describe a method to quantify the response of seismic data to reservoir changes during heavy oil production which is not just based on velocity and density changes. Based on Chapter 3 of this thesis it is clear that the response of a heavy oil reservoir with patchy gas saturation to the seismic wave is not an elastic response. The first section of this chapter is focused on introducing a constitutive model which can be used to honour the response of heavy oil reservoir with patchy gas saturation. Then the basics of viscoelasticity are explained followed by forward modeling results. The forward modeling is aimed to show the possibility of using attenuation based monitoring program to understand response of heavy oil to seismic wave.

4.1 Rheological Models of Heavy Oil

The two extremes of material behaviour are described by a linear elastic body and a linear viscous body. For a linear elastic body the response of a medium (strain) is instantaneous and proportional to the stress with a constant known as its compliance. The symbol for this type material is a spring. However for the linear viscous case the stress is proportional to strain rate. In this medium an application of a stress yields non-instantaneous and linearly increasing deformation. When the load is removed this does not lead to removal of deformation; therefore, viscous materials have an extreme strain memory. The symbol for this type material is a dashpot.

In the real world, materials are between these two extreme cases. Therefore the stress-strain relation depends on time and they remember their past strain history. The behaviour of most materials is approximated using viscoelastic models. A viscoelastic material is any material that dissipates energy when subjected to stress or strain. Based on the second law of thermodynamics, all materials are considered to be viscoelastic. However the level at which material dissipates energy determines how far they can be from the perfect elastic case.

The Zener body (Standard Linear Solid) is the most popular and general model which has been used to describe the heavy oil behaviour Vasheghani (2011). Figure 4.1 presents the two possible representations of Zener bodies.

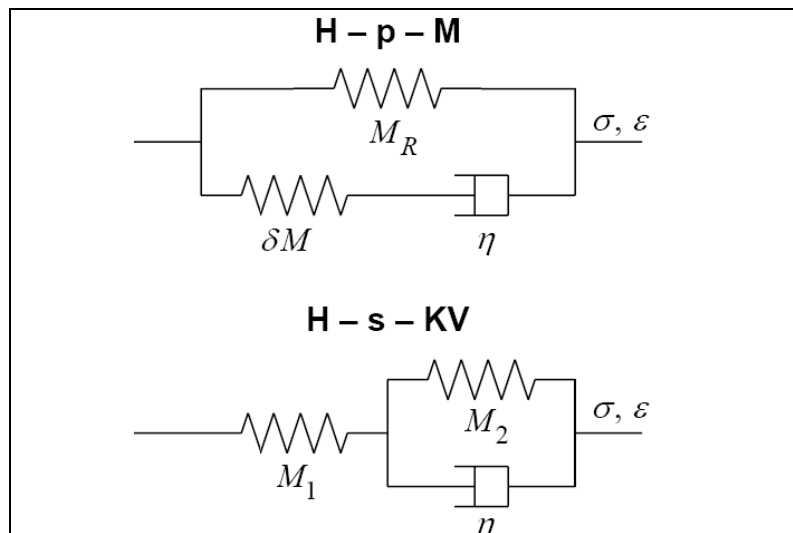


Figure 4-1 Zener body, J. Kristek and P. Moczo (2006)

The two possible way of explaining the Zener body are:

1. A Hooke body (spring) connected in parallel with a Maxwell body (H – p – M or a spring in series with a dashpot) as shown in Figure 4.1 upper set.
2. Hooke body connected in series with Kelvin-Voigt body (H – s – KV, or spring and a dashpot in parallel). Figure 4.1 lower set.

When applying the unit-step strain instantaneously, i.e., the un-relaxed, stress will be given by the sum of moduli of the two elastic springs, $M_U = M_R + \delta M$. This will also trigger the dashpot to start to grow from zero. This would gradually release stress of the spring connected to the Maxwell or Kelvin-Voigt body. Moczo (2003) showed that the two representations of Zener body are equivalent to each other and they are eventually produce similar response for SLS model.

4.2 Wave Propagation in Viscoelastic Medium

For a linear isotropic viscoelastic material the stress-strain relation is described with the help of two major principles:

- The Boltzmann Superposition Principle
- The Causality Principle

As per following equation 4.1

$$\sigma(t) = \int_{-\infty}^t \psi(t - \tau) \dot{\epsilon}(\tau) d\tau \quad (4. 1)$$

where:

$\sigma(t)$ = stress [Pascal]

$\dot{\varepsilon}(t)$ = time derivative of strain [m/s]

$\psi(t)$ = stress relaxation function [kg/s]

This equation suggests that the stress at a given time t is determined by the entire history of the strain until time t . The upper integration limit ensures causality. Mathematically, this integral is called the hereditary integral which represents a time convolution of the relaxation function and strain rate. Since $\psi(t)$ is the stress response to a unit step function in strain, its time derivative.

$$M(t) = \dot{\psi}(t) \quad (4.2)$$

$M(t)$ is the stress response to the Dirac δ -function in strain. Now using (*) as convolution symbol and the properties of convolution (switching the derivative) equation 4.1 can be written as:

$$\sigma(t) = M(t) * \varepsilon(t) \quad (4.3)$$

One can understand this by considering the time domain response of a slender mass-less viscoelastic rod (silk thread) to a unit step strain. Due to assumption that there is no mass involved therefore the inertial effects is neglected, based on the second law of

thermodynamics the response, $M(t)$ for $t > 0$, has to monotonically decrease with time to a value greater than zero.

The shape of the decaying stress curve is general. $M(t)$ is referred to Dirac δ - function or relaxation function. The initial response, M_u , is elastic with an asymptotic decay to either zero or some offset value M_R . M_u and M_R are the infinite and zero frequency moduli respectively. If M_R is zero the material is defined to be a fluid; otherwise it is a solid.

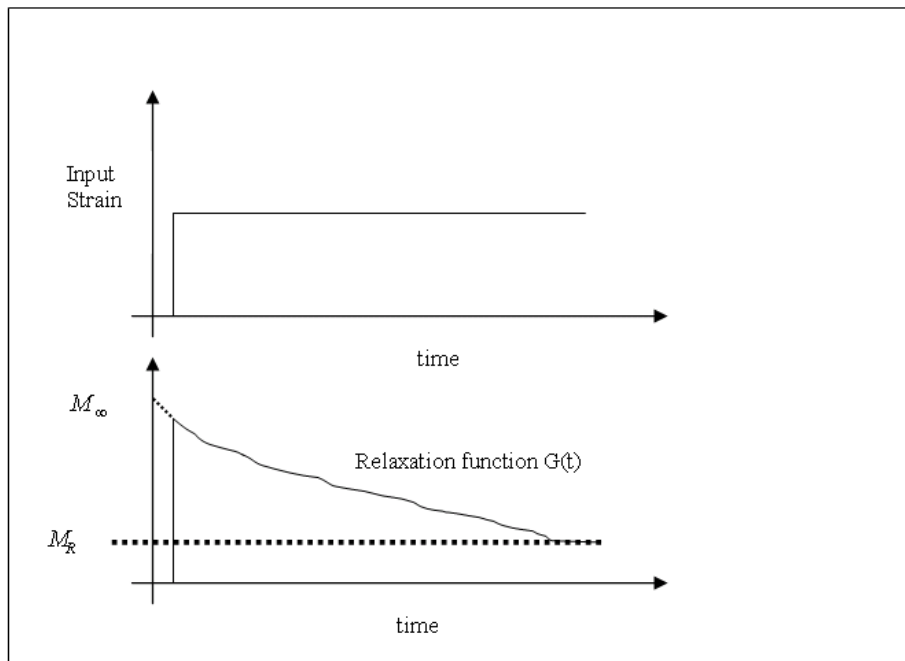


Figure 4-2 Relaxation response of a viscoelastic rod to a unit step strain input

Blanch et al. (1993) showed that Standard Linear Solid (SLS) could be used as a general mechanical viscoelastic model. An array of SLS has the stress relaxation function:

$$M(t) = M_R \left(1 - \sum_{l=1}^l \left(1 - \frac{\tau_{el}}{\tau_{\sigma l}} \right) e^{-\frac{t}{\tau_{\sigma l}}} \right) \theta(t) \quad (4.4)$$

Where:

$M(t)$ = Stress relaxation function [kg/sec²]

$\theta(t)$ = Heaviside function, [1/sec]

M_R = the relaxed stress corresponding to $M(t)$ [kg/sec]

τ_{el} = strain relaxation time [sec]

$\tau_{\sigma l}$ = stress relaxation time [sec]

For the 1st SLS M_R is related to the elastic modulus M_u Liu et al. (1976).

$$M_U = \frac{M_R}{\left(1 - \sum_{l=1}^l \left(\frac{\tau_{el} - \tau_{\sigma l}}{\tau_{\sigma l}} \right) \right)} \quad (4.5)$$

$M_U = \mu$ for S waves, and $M_U = \lambda + 2\mu$ for P waves Aki and Richards (1980).

The complex stress modulus $M(\omega)$ is defined as the Fourier transform of the stress relaxation function. Viscoelasticity is quantified by inverse of loss factor Q. The quality factor Q is defined as:

$$Q(\omega) = \frac{\text{Re}[M(\omega)]}{\text{Im}[M(\omega)]} \quad (4.6)$$

The steel Q factor is about 1000 and typical value for rocks ranges from 20 to 300. By using equations 4.6 and 4.4 the quality factor for a SLS can be defined as:

$$Q(\omega) = \frac{1 - L + \sum_{l=1}^L \frac{1 + \omega^2 \tau_{\epsilon l} \tau_{\sigma l}}{1 + \omega^2 \tau_{\sigma l}}}{\sum_{l=1}^L \frac{\omega(\tau_{\epsilon l} - \tau_{\sigma l})}{1 + \omega^2 \tau_{\sigma l}}} \quad (4.7)$$

Blanch et al. (1995) proposed the τ method for the viscoelastic modeling. The τ method is based on the simple observation that the level of attenuation caused by a SLS can be determined by a dimensionless (frequency scale independent) variable τ as:

$$\tau = \frac{\tau_{\epsilon l}}{\tau_{\sigma l}} - 1 = \frac{\tau_{\epsilon l} - \tau_{\sigma l}}{\tau_{\sigma l}} \quad (4.8)$$

Using this definition for 1st SLS equation 4.7 can be written as:

$$Q^{-1} = \frac{\omega^2 \tau_{\sigma l} \tau}{1 + \omega^2 \tau_{\sigma l}^2 (1 + \tau)} \quad (4.9)$$

Therefore the velocity will be:

$$C_{(\omega)}^2 = \frac{M_U}{\rho} \left(1 + \left(\frac{M_U}{M_R} - 1 \right) \frac{1}{1 + \omega^2 \tau_{\sigma l}^2} \right)^{-1} \quad (4.10)$$

Assuming that τ is very small the $1 + \tau = 1$ for an array of SLS equation 4.7 can be written as:

$$Q^{-1} = \sum_{l=1}^L \frac{\omega \tau_{\sigma l} \tau}{1 + \omega^2 \tau_{\sigma l}^2} \quad (4.11)$$

Equation 4.11 shows that Q^{-1} is a linear function of τ , therefore an approximation of Q^{-1} can be done using least squared method over any specified frequency range. This is done by minimizing over τ .

$$J = \int_{\omega_a}^{\omega_b} (Q^{-1}(\omega, \tau, \tau_l) - Q_0^{-1})^2 d\omega \quad (4.12)$$

The next step is to set J to zero and then solving for τ . The solution is obtained by setting the derivative of J with respect to τ to zero.

$$\frac{dJ}{d\tau} = 2 \int_{\omega_a}^{\omega_b} [Q^{-1}(\omega, \tau, \tau_l) - Q_0^{-1}] \frac{d[Q^{-1}(\omega, \tau, \tau)]}{d\tau} d\omega = 0 \quad (4.13)$$

Solving for τ leads to:

$$\tau = \frac{1}{Q_0} \frac{\sum_{l=1}^L I_{0l}}{\sum_{l=1}^L I_{1l} + 2 \sum_{l=1}^{L-1} \sum_{k=l+1}^L I_{2kl}} \quad (4.14)$$

Where:

$$I_{0l} = \frac{1}{2\tau_{\sigma l}} \left[\log(1 + \omega^2 \tau_{\sigma l}^2) \right]_{\omega_a}^{\omega_b} \quad (4.15)$$

$$I_{1l} = \frac{1}{2\tau_{\sigma l}} \left[\arctan(\omega \tau_{\sigma l}) - \frac{\omega \tau_{\sigma l}}{1 + \omega^2 \tau_{\sigma l}^2} \right]_{\omega_a}^{\omega_b} \quad (4.16)$$

$$I_{2lk} = \frac{\tau_{\sigma l} \tau_{\sigma k}}{\tau_{\sigma k}^2 - \tau_{\sigma l}^2} \left[\frac{\arctan(\omega \tau_{\sigma l})}{\tau_{\sigma l}} - \frac{\arctan(\omega \tau_{\sigma k})}{\tau_{\sigma k}} \right]_{\omega_a}^{\omega_b} \quad (4.17)$$

$$\tau_{\sigma l} = \frac{1}{\omega_l} \quad (4.18)$$

4.3 The Concept of Memory Variable

The memory variable method is a mathematical method to eliminate the computationally costly convolution appearing in the viscoelastic constitutive equation. The method was first presented by Carcione et al. (1988). The following derivation presented here was offered by Blanch et al. (1995).

Taking the time derivative from Equation 4.1 yields:

$$\frac{\partial \sigma(t)}{\partial t} = \frac{\partial(M(t))}{\partial t} * \frac{\partial \varepsilon(t)}{\partial t} \quad (4.19)$$

$\frac{\partial \varepsilon(t)}{\partial t}$ is the velocity and assuming the SLS behaviours (a series of exponential decays)

to represent the M(t) leads to:

$$\sigma_t = \left[\left(M_R + \sum_{i=1}^L M_i e^{\frac{-t}{\tau_i}} \right) \cdot \delta(t) + \sum_{l=1}^L \left(\frac{1}{\tau_l} M_l e^{\frac{-t}{\tau_l}} \right) \cdot \theta(t) \right] * u_x \quad (4.20)$$

Now by defining L memory variable

$$r_l = \left[\frac{1}{\tau_l} M_l e^{\frac{-t}{\tau_l}} \cdot \theta(t) \right] * u_x \quad (4.21)$$

Considering the definition of un-relaxed moduli for a SLS with l relaxation function

$$M_U = M_R + \sum_{l=1}^L M_l \quad (4.22)$$

Equation 4.20 can be written as:

$$\sigma_t = M_U u_x + \sum_{l=1}^L r_l \quad (4.23)$$

In the next step in order to remove the convolution from Equation 4.21 its time derivative is first calculated.

$$r_{l,t} = \left[\frac{-1}{\tau_l} \left(\frac{1}{\tau_l} M_l e^{\frac{-t}{\tau_l}} \right) \cdot \theta(t) + \left(\frac{1}{\tau_l} \left(\frac{1}{\tau_l} M_l e^{\frac{-t}{\tau_l}} \right) \cdot \delta(t) \right) \right] + *u_x \quad (4.24)$$

Then by substituting equation 4.22 into 4.24 leads to:

$$r_{l,t} = \frac{-r_l}{\tau_l} + \frac{M_l}{\tau_l} *u_x \quad (4.25)$$

Therefore the equations of a viscoelastic medium will be summarized in L+2 equations which are:

$$\begin{aligned} \sigma_t &= M_U u_x + \sum_{l=1}^L r_l \\ u_t &= \frac{1}{\rho} \sigma_x \\ r_{l,t} &= \frac{-r_l}{\tau_l} + \frac{M_l}{\tau_l} *u_x \end{aligned} \quad (4.26)$$

The memory variables are continuous corrections made to the propagation of waves in an elastic medium with moduli of M_U . At initial conditions all memory variables are set to zero. The memory variable equation tracks the rate at which the infinite frequency elastic response should be corrected due to the collective effect of past loads and of any new loads (occurring in the past time steps).

The second term of the memory variable equation $\frac{M_l}{\tau_l} * u_x$ takes into account any new strain loads which are represented by $u_x = \varepsilon_t$ and scaled by M_l (which is the share of the new load associated with that particular memory variable). The first term on the right side tracks the rate of relaxation of both new and past loads associated with a particular memory variable. Therefore the history of load is accounted for and the new load is also considered in the memory variable equation.

4.4 Forward Modeling

Forward modeling is a common way of quantifying the impact of reservoir changes on the seismic response. The seismic response of earth has been successfully modeled using viscoelastic finite difference methods by Kristek and Moczo (2003). The FD method is popular due to relatively simple way of programming and its capability in handling 3D simulation by honouring the realistic complicated earth models.

A condensed description of the finite difference method is that the operators of the differential equation governing the physical system at a given point will be approximated by a weighted sum of the field variables at that point and at judiciously selected surrounding points. This process involves discretization of the partial derivatives in both time and space. The discretization is done by replacing the time and space derivatives with their approximation based on Taylor series.

The finite-difference method starts by introducing a representative grid-point method. In the grid-point methods a computational domain is covered by a space-time grid and each function is represented by its values at grid points. When dealing with attenuating medium the properties which need to be defined are:

1. P wave velocity
2. S wave velocity
3. Density
4. P wave attenuation and
5. S wave attenuation.

When seismic waves pass through a rock containing heavy oil the response of the medium to the given strain is not instantaneous and it has a gradual decrease of stress. This concept is the basis of using viscoelastic modeling to understand the response of seismic wave. Using the 1D viscoelastic model presented by Gandomi and Takenaka (2007) the response of seismic wave was modeled. This model was used and optimized in order to illustrate the response of the viscoelastic model.

4.4.1 Forward Modeling Inputs

Figure 4-3 presents the geological model used to verify the concept of modeling response of heavy oil reservoir. The model has five layers in total. The reservoir layer is from 700 m to 800 m. The velocities and densities are presented in Figure 4.3. Our goal here is to demonstrate the seismic response to changes in the reservoir layer.

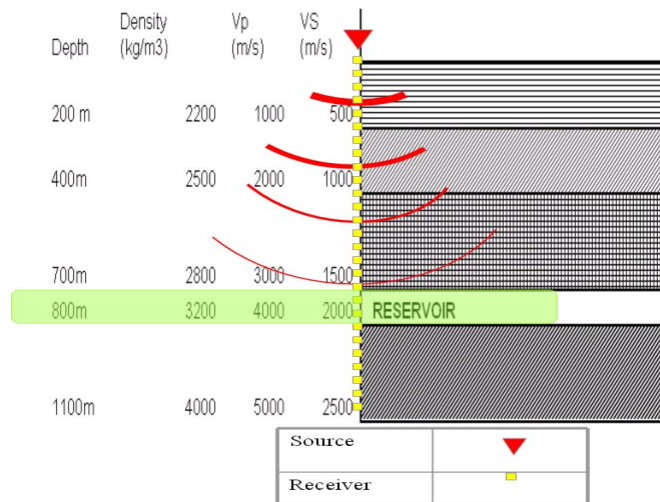


Figure 4-3 schematic of the geological model

In order to prevent the grid dispersion and accurate modeling the time steps and grid size were calculated using the following equations offered by J. Kristek and P. Moczo (2003):

$$h \leq \frac{V \min}{6f} \quad (4.26)$$

$$\Delta t \leq \frac{6h}{7V \max} \quad (4.27)$$

Where:

$V \min$ = Minimum velocity of the model (m/s)

$V \max$ = Maximum velocity of the model (m/s)

h = Special grid size (m)

Δt = Time step used for modeling (s)

f = Maximum frequency of model (Hz)

An absorbing boundary condition as per Cerjan (1985) with first-order one-way wave-equation techniques of Clayton and Engquist (1977) was used to model the non-reflecting boundary (base of the model). The free surface is modeled using Tanaka & Takenaka (2005) method. A total number of 50 receivers were set with 20 m spacing from the surface. The source is modeled to be a Ricker wavelet with central frequency of 150 Hz.

In order to model the attenuation a 3rd order SLS was used. The frequency range of constant Q was selected to be from 5Hz to 50Hz. outside this frequency range there is no attenuation considered. The reference velocity of the model at which the velocities are considered is 50Hz. Figure 4-4 presents the constant Q which was estimated using 3rd order standard linear solid model. The number of relaxation times (order of SLS) can create limitations for the memory usage and run time of the model. After a sensitivity analysis 3rd order SLS was considered to be the optimum number for this study. As it is presented in Figure 4-4, the viscoelastic model will apply the attenuation by multiplying the superposition curve (red curve on Figure 4-4) values by the attenuation value that was set for Q_p and Q_s of each given layer in the input file.

In viscoelastic modeling the attenuation model is based on the understanding of frequency dispersion of the medium. One method is to create an attenuation model based on measurement at different frequencies. In this study, the attenuation function is the connection between the White's patchy saturation theory and the viscoelastic forward

modeling. Therefore the frequency band was estimated based on the patchy saturation model which was explained in Chapter 3 as initial default case presented in Table 3.1.

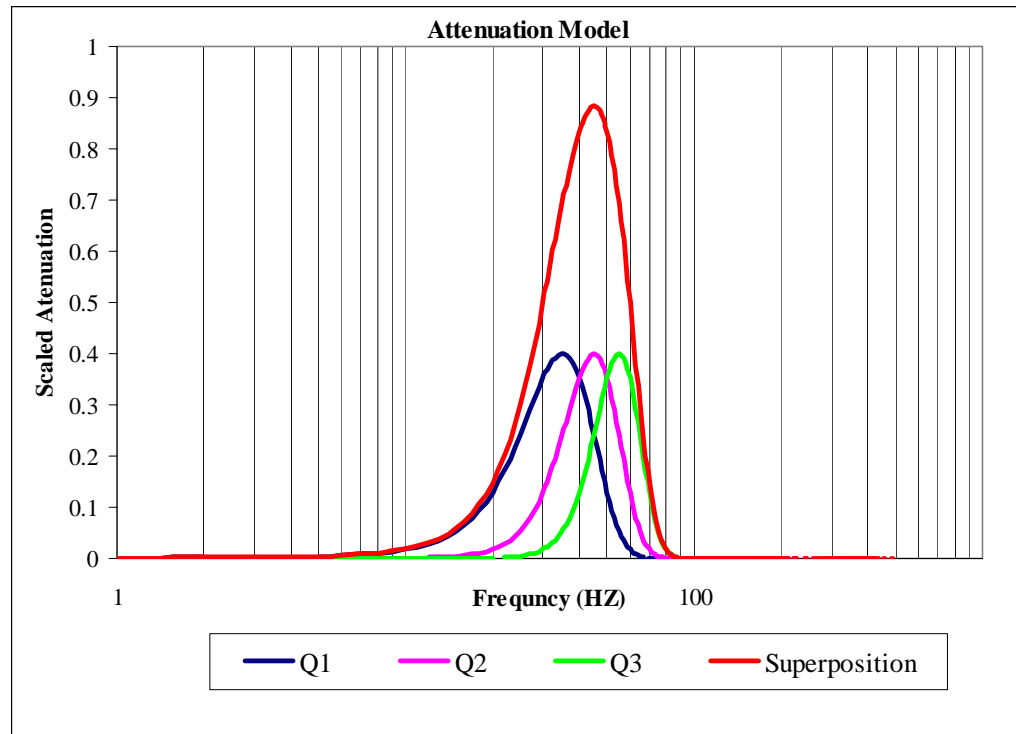


Figure 4-4 Attenuation model used by 3rd standard linear solid

4.4.2 Forward Modeling Results

The subject of this part of chapter 4 is to find and answer for this question: “Given the model description in figure 4-2 can one see sensible changes in the model response by changing in the attenuation part of viscoelastic model only?”

In order to quantify the answer to this question, two cases were considered

- Elastic case (MODEL1): In this case t first the simulation was run for initial survey by setting the Q_p and Q_s of all layers to 1000 and 500 respectively.

Then due to production, the reservoir layer Q_p and Q_s were changed to 40 and 20 respectively to simulate the monitor case results.

- The realistic case (MODEL2): In this case for initial survey simulation, the attenuation values for Q_p and Q_s are set to 100 and 50 for all layers respectively. The Q_p and Q_s of the reservoir layer are then modified to 40 and 20 to simulate the monitor case.

The time response of the four cases presented above are presented in the following figures 4-5 to 4-8.

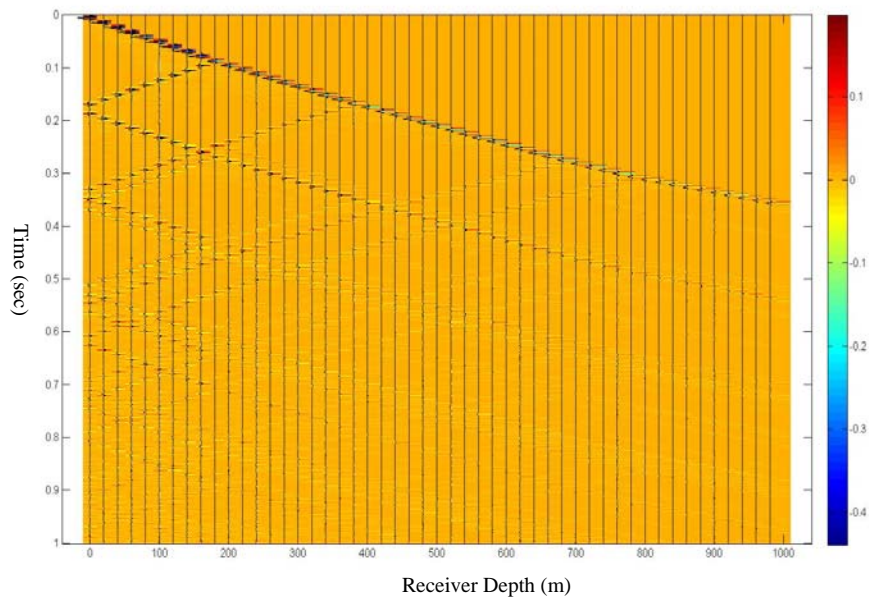


Figure 4-5 Time response of MODEL1 initial simulation of initial survey

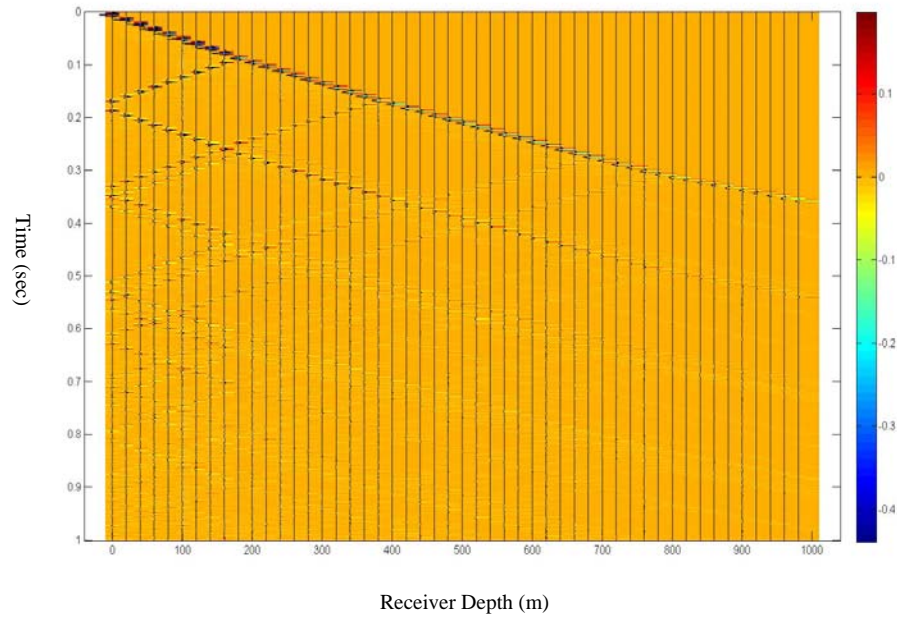


Figure 4-6 Time response of MODEL1 simulation of monitor survey

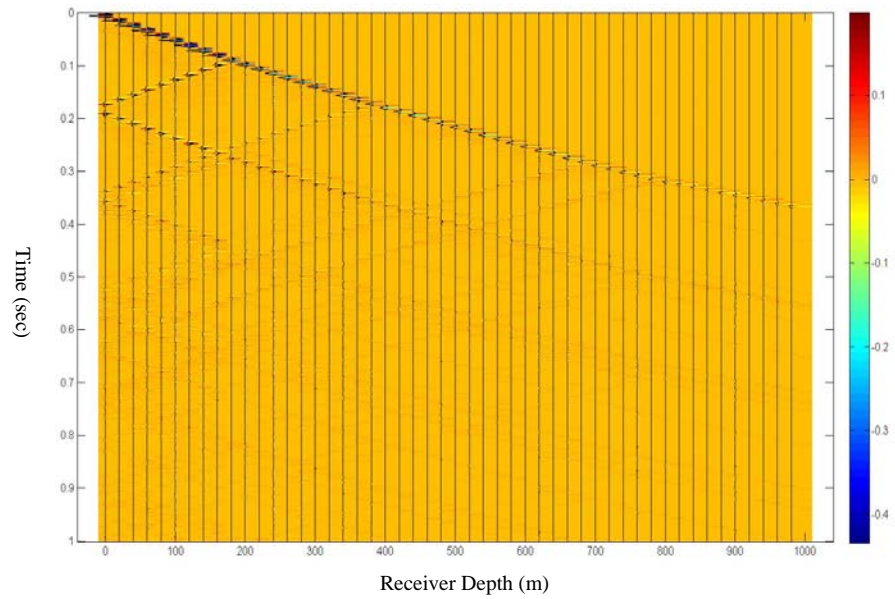


Figure 4-7 Time response of MODEL2 simulation of initial survey

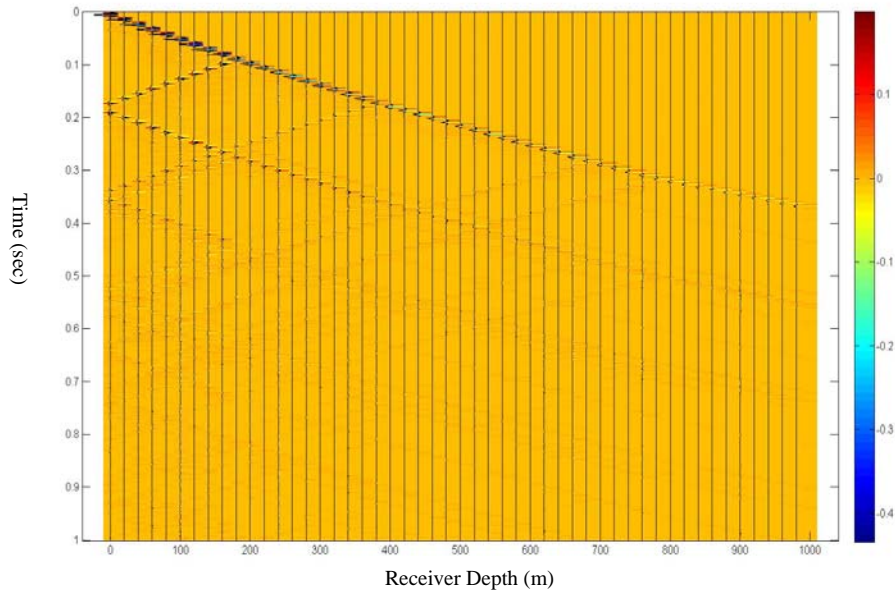


Figure 4-8 Time response of MODEL2 simulation of monitor survey

Examining Figures 4-4 to 4-8 suggest that quantifying the changes in the time domain is not trivial task without further processing. However, the following observations can be concluded from these plots:

1. In the high attenuation case (MODEL2), the velocity model of the viscoelastic model is not the same as with the elastic case due to velocity dispersion, therefore the times at which the wave front arrives at each receiver is not the same in MODEL1 and MODEL2. Subtracting MODEL1 from MODEL2 did not provide meaningful results.
2. In MODEL 1 in spite the very low attenuation the amplitude decreases as wave travels through the earth. This is due to the fact that model has to honour the energy loss due to reflection from surface and also from each layer.

Processing the data in frequency domain will provide a better way of assessing the seismic response. To evaluate the energy of the wave as it travels through the model using Gabor transform or wave front attenuation technique. Lamoureux et.al (2004) presents the following steps to estimate the Gabor transform of signal $s(\cdot)$:

- Define a Gaussian window length
- Define a temporal window
- Based on the length of the input signal and the window length shift the Gaussian window by the value of temporal window until the entire signal is covered [$\omega_\tau(\cdot)$]
- Multiple Gaussian windows by the input signal at each step
- Calculate the FFT of signal

Mathematically the above steps can be written as Equation 4.28.

$$G(\tau, \omega) = FFT\{\omega_\tau(\cdot)s(\cdot)\}(\omega). \quad (4.28)$$

Using “*fgabor*” function from CREWES toolbox and setting the Gaussian window to 5 millisecond and temporal shift to 4 millisecond Gabor transform of the time response of the wavefield recorded at the first top receiver (20m depth) was calculated. The Gabor transform can be thought of as a frequency response of the wave field as it travels through layers in time. The results of this analysis are presented in Figures 4-9 to 4-12. Examination of this plot shows the loss of energy in the case with high attenuation for both MODEL1 and MODEL2.

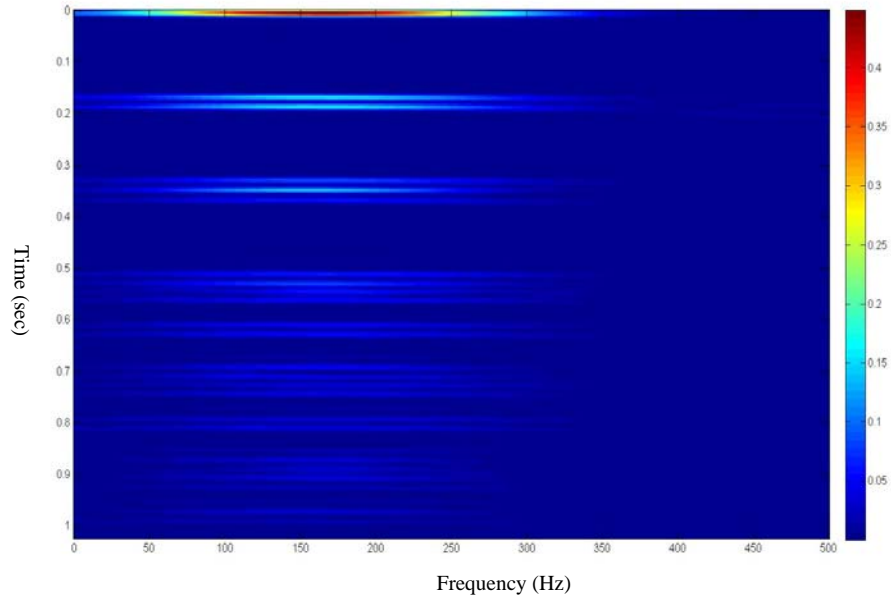


Figure 4-9 Gabor transform of MODEL1 initial survey simulation

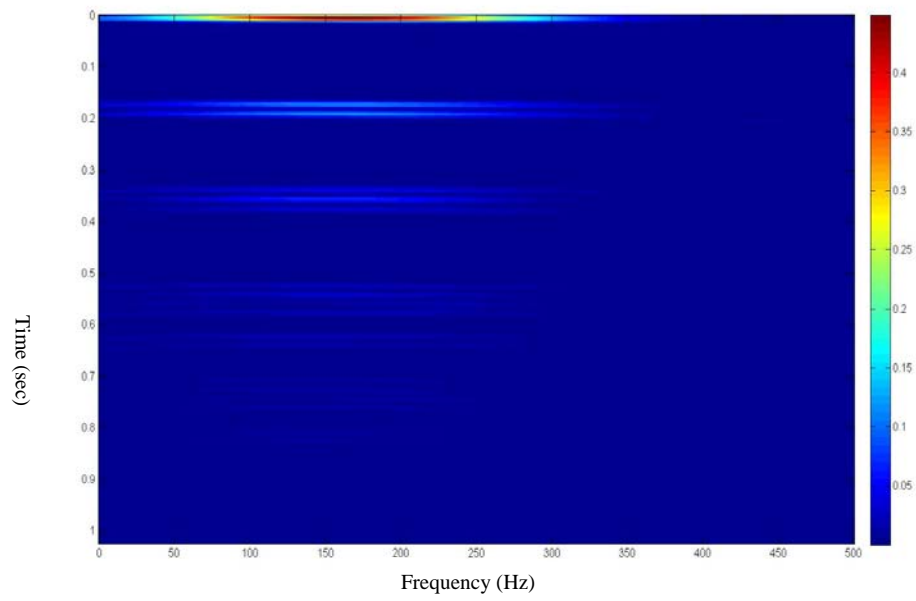


Figure 4-10 Gabor transform of MODEL1 monitor survey simulation

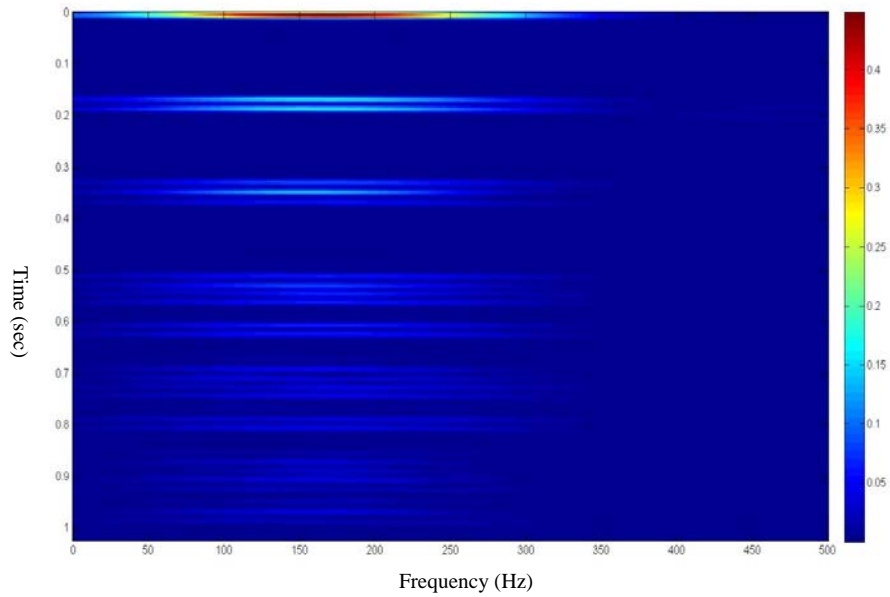


Figure 4-11 Gabor transform of MODEL2 initial survey simulation

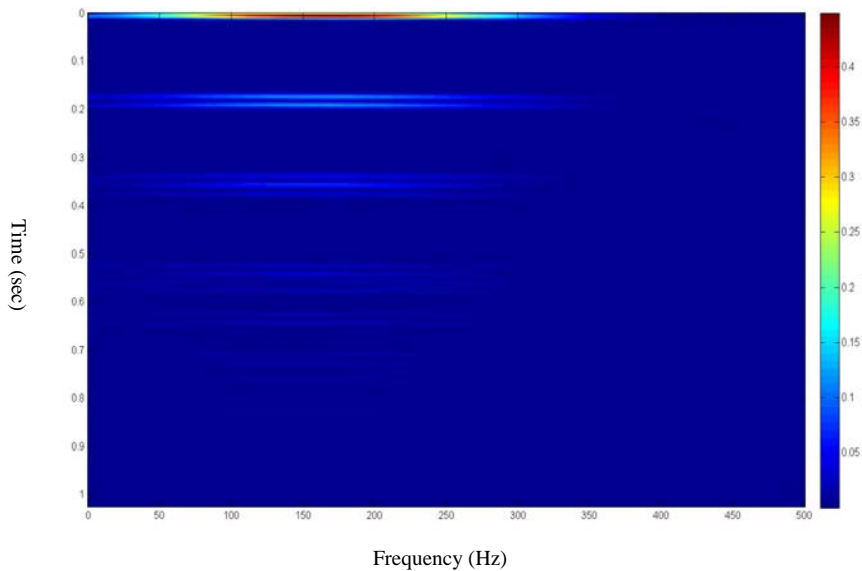


Figure 4-12 Gabor transform of MODEL2 monitor survey simulation

To illustrate the changes in a more clear way a second method was used. In this method the objective was to follow the wave front as it reaches each receiver in depth and quantify its amplitude response. Therefore the first arrival wave was picked using a 20

millisecond window. The Fast Fourier Transform (FFT) of this signal was then calculated and the results were plotted in depth.

The results of this analysis are presented in Figures 4-13 to 4-16. This method was found to be the most useful way in order to illustrate the results. This method seems to be the best way of illustrating the attenuation as the boundaries of the different layers are clearly imaged

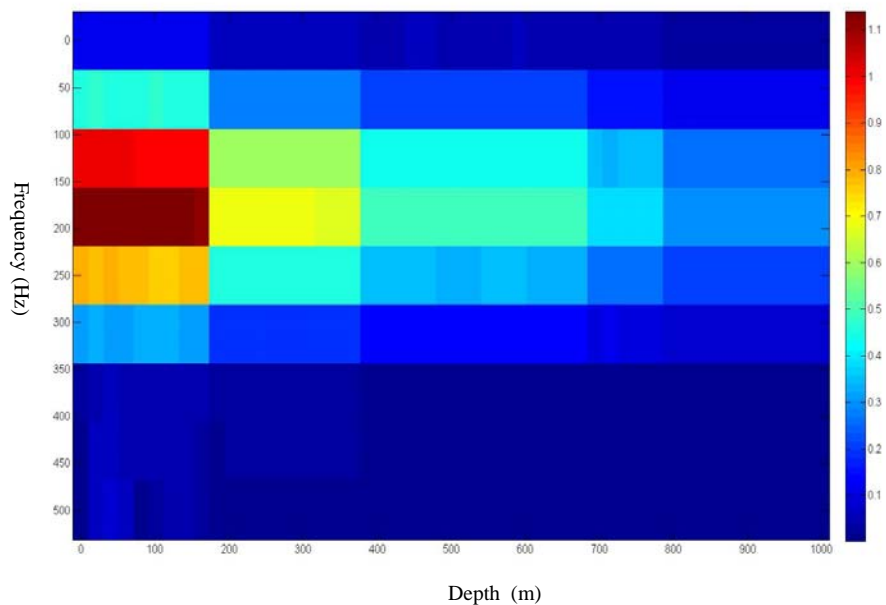


Figure 4-13 Frequency depth analysis of MODEL1 initial survey simulation

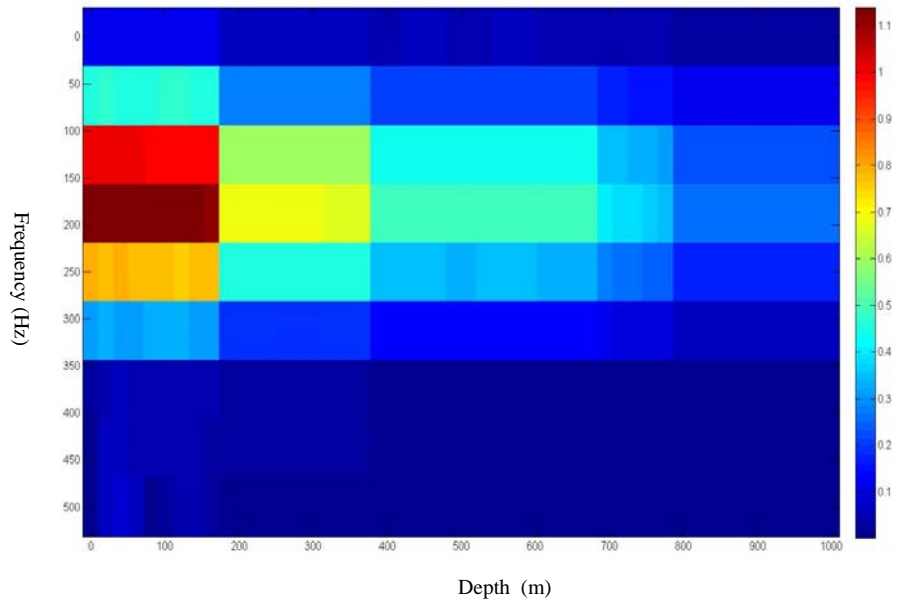


Figure 4-14 Frequency depth analysis of MODEL1 monitor survey simulation

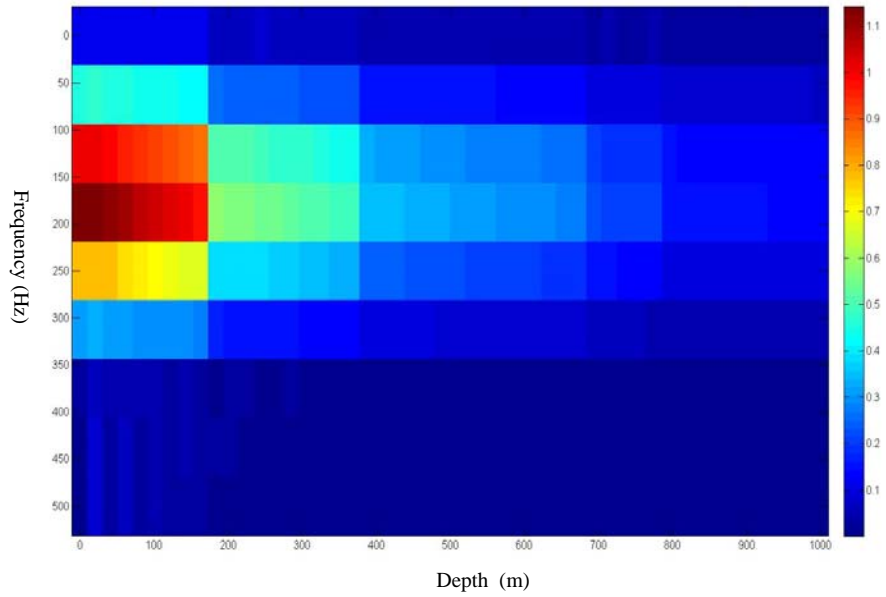


Figure 4-15 Frequency depth analysis of MODEL2 initial survey simulation

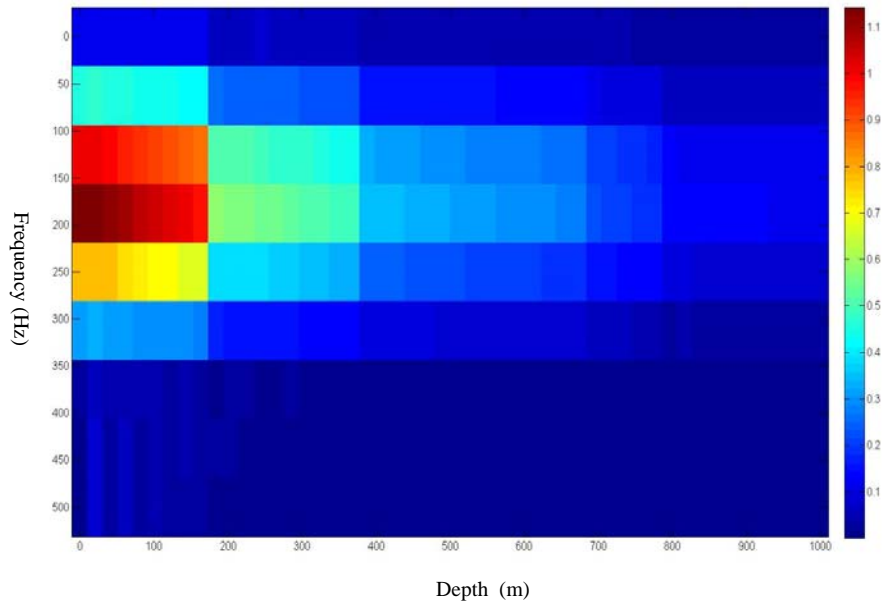


Figure 4-16 Frequency depth analysis of MODEL2 monitor survey

The difference of the seismic response of MODEL1 after production (Figures 4-13 and 4-14) is presented in Figure 4.16. Examination of this figure shows how the MODEL1 response is sensitive to the attenuation model changes. Note that the velocities and densities are the same between the two models and the only difference among them is the attenuation model.

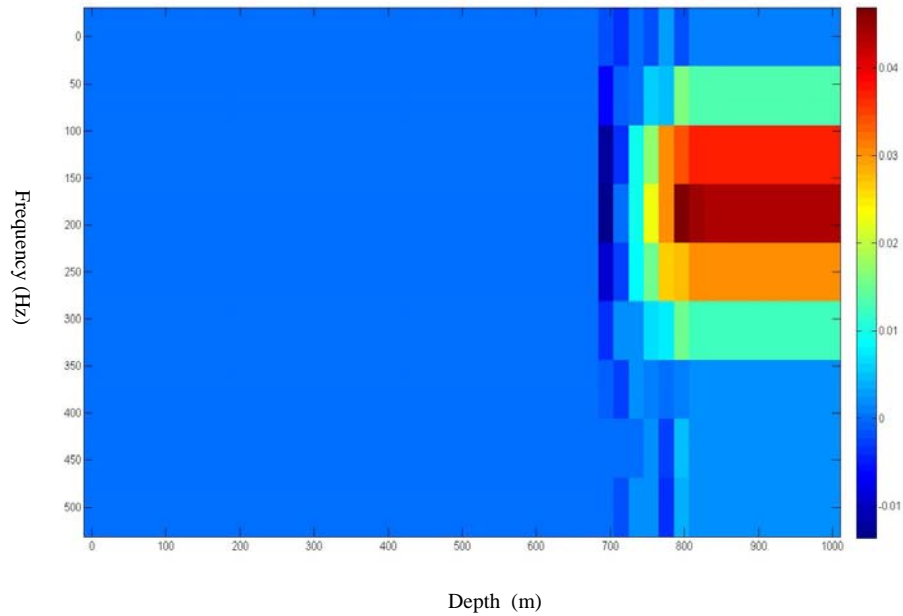


Figure 4-17 Difference due to the change in the attenuation (production related) in MODEL1

The difference of MODEL2 is presented in Figure 4.18. This figure illustrates that for a model with high attenuation differences one can still observe the differences. Above the reservoir layer the difference is zero which validates the model. A comparison between figures 4.17 and 4.18 suggests that the differences of MODEL 2 are roughly one order of magnitude less than the elastic case. This can be explained by considering the attenuation of MODEL2 which is about ten times more than that of the MODEL1.

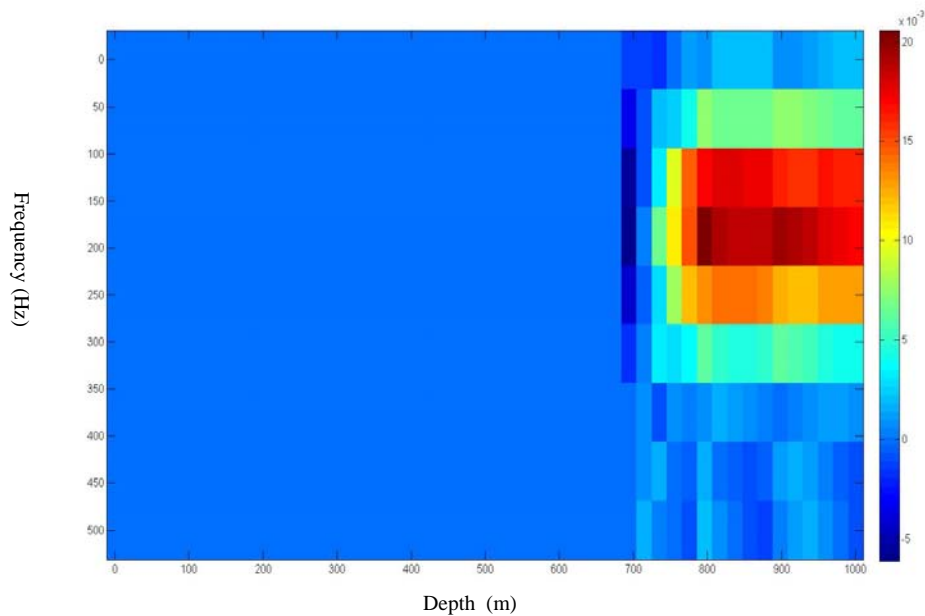


Figure 4-18 Difference due to the change in the attenuation (production related) in MODEL2

4.4.3 Discussion

The time-lapse seismic technique is a common method which has been attracting a lot of attention in the heavy oil production monitoring. Time-lapse seismic can help to monitor and evaluate the efficiency of the recovery process. As a result, the operator of the field will be able to identify the by pass portions of the reservoir and come up with better recovery techniques.

The response of time-lapse seismic processing is usually reported in terms of time delay maps. When dealing with cold heavy oil production the time-lapsed data does not show very significant time delays between the initial and monitor surveys. This is due to the fact that the velocity changes are not as significant as other production schemes such

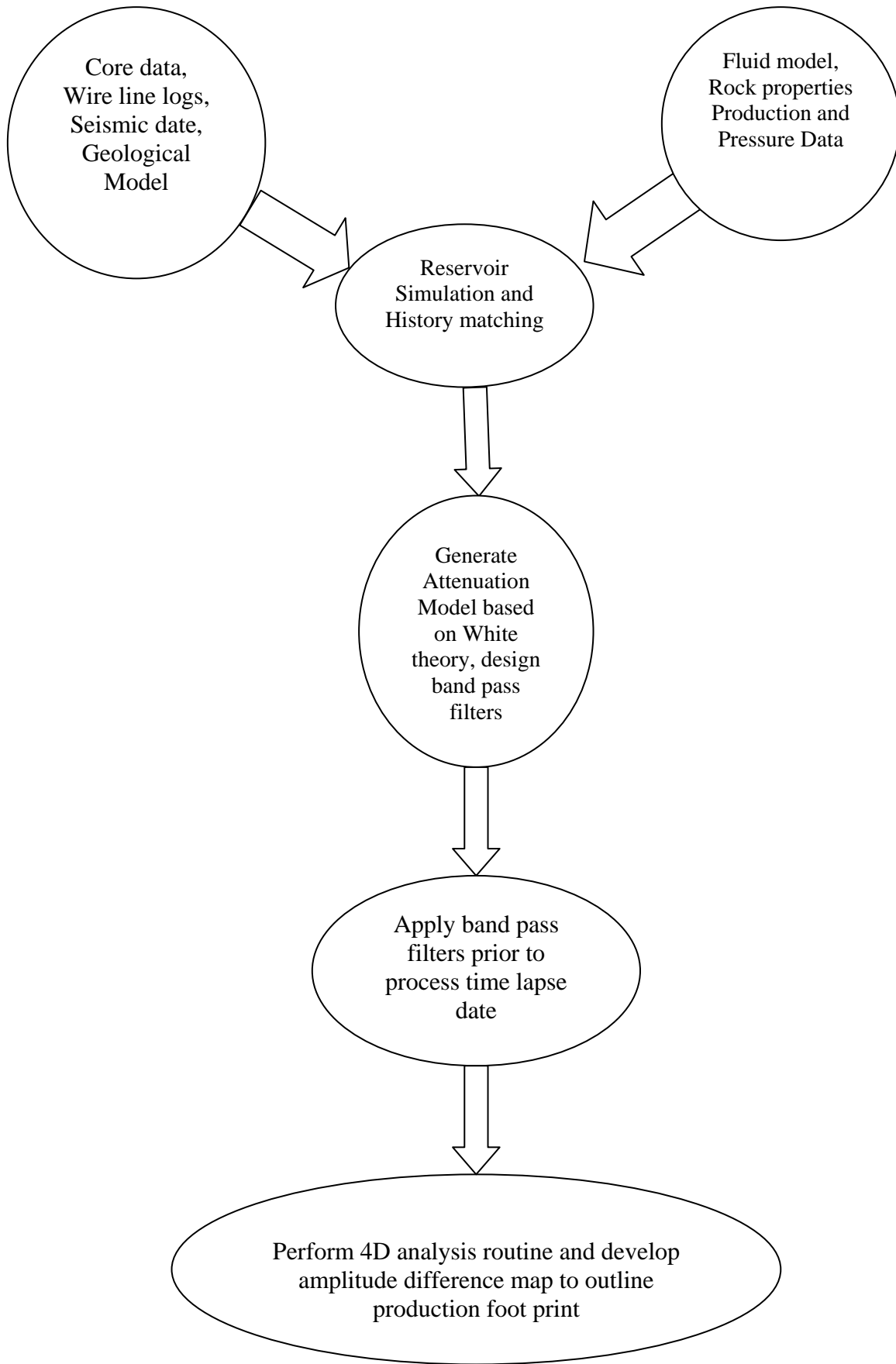
as thermal recovery methods. The results of this chapter lead to the conclusion that when dealing with patchy saturation it is important to understand the amplitude response with respect to attenuation model. This would improve the conclusions about the accuracy of seismic monitoring techniques.

CHAPTER FIVE: CASE STUDY OF INTERACTION BETWEEN RESERVOIR SIMULATION AND VISCOELASTIC SEISMIC

Based on the conclusions from Chapter 3 and 4 it was demonstrated that by applying White's theory in heavy oil one can quantify the result of patchy saturation (chapter 3) and see its impact on wave propagation through forward modeling (chapter 4). In this chapter the conclusions of the previous chapters are used to interpret a time-lapsed seismic data of a Canadian heavy oil reservoir.

At first a background about the field and production history is provided. The geological model of this field was created using the wireline logs and the initial seismic survey results (mapped horizons). The geological model was built using the Schlumberger Petrel software. Using the geological model and a commercial reservoir simulator (CMG STARS) the in-situ reservoir properties were calculated through a history matching process. The results of the reservoir simulation model are then used to develop the attenuation model.

The next step is to process the time-lapse seismic data. The processing is done using a new workflow to show the impact of attenuation on the conclusions driven from a 4D seismic study. Time lapse processing is done using the Pro4D package from Hampson Russell software. The flow chart below summarizes the workflow that was used in this chapter.



5.1 Case study of Primate Field

Primate is a heavy oil reservoir operated by Equal Energy. The field is located in Saskatchewan, Canada (Figure 5-1) and is a part of the heavy oil belt reservoirs in Western Canada. Equal Energy is operating this field using Cold Heavy Oil Production with Sand (CHOPS) technology. The main production zones in this field are the McLaren and Waseca formations. As shown by Figure 5-2 (Stratigraphy of Saskatchewan) these formations are parts of Mannville group in this area.

The thickness of the production zone of interest ranges from 5 m to 12 m and it is mainly perforated across the entire formation using high density deep penetration perforation scheme. No active bottom water or initial top gas has been reported based on the initial logs from this pool which is supported by the production history as well. Primate Field has an initial seismic survey done in 2004 and a repeat survey (monitor survey) after production done in 2009.



Figure 5-1 Primate Field (Equal Energy website)

Stratigraphic Correlation Chart

For updates, see
www.er.gov.sk.ca

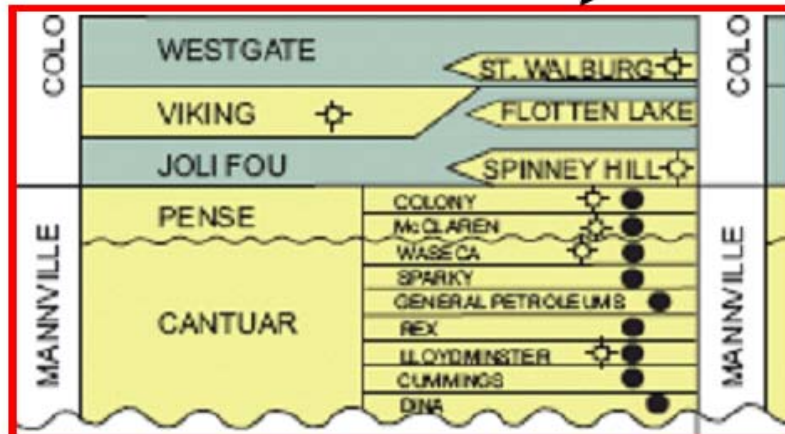
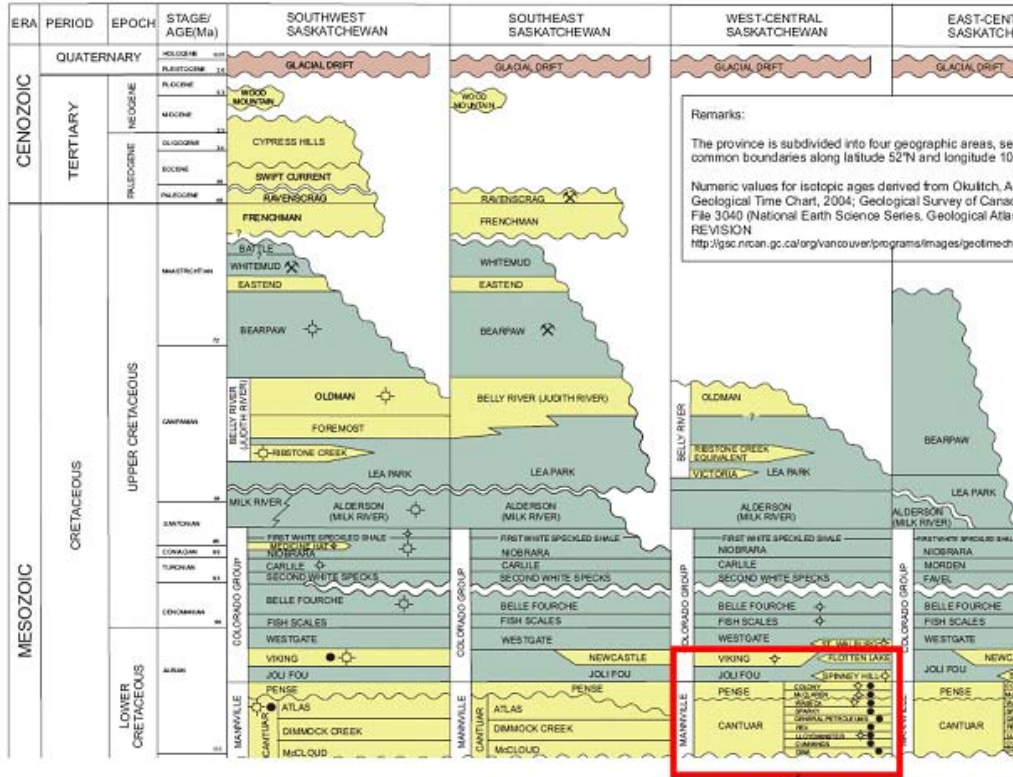


Figure 5-2 Stratigraphic correlation chart of Saskatchewan (Saskatchewan energy recourse website)

5.2 CHOPS Background

Cold heavy oil production with sand (CHOPS) is a non-thermal recovery method used in unconsolidated heavy oil reservoirs in Canada. In this process sand and reservoir fluid (oil/gas/water) are produced together in order to enhance the oil recovery. This process has proven to be more economically successful when vertical wells are used.

Although the process has been mostly developed in Western Canada, it was first applied in California. Vonde (1982) reported that with the application of specially designed pumping equipment Husky Oil Co. produced crude oil as low as 4 °API with sand cuts of up to 70%. The wells were located in the Brooks sand, in Cat Canyon field, California.

Application of the progressive cavity pumps was a major step in improving oil rate of CHOPS production. PCP pumps allowed primary production rates in excess of 150 bbl/d (24 m³/d) oil from wells that were previously restricted to less than 10 bbl/d (1.5 m³/d) when produced with conventional rod pumps and sand control completion methods. The main advantages of PCP pumps are higher drawdown and being able to produce sand with a reasonably low maintenance cost.

McCaffrey and Bowman (1991) examined the performance of Amoco's Elk Point and Lindbergh fields in Canada. The program was designed to investigate the communication between wells using tracer material. Surprisingly the results indicated

that wells were connected with a channel system exceeding 2 km in length that connected up to 12 wells.

There are two main mechanisms involved in unexpectedly high primary oil recovery observed in CHOPS operations. The first is the foamy oil associated with trapping gas evolving from within the heavy oil and the second is sand production. McCaffrey and Bowman concluded the high productivity of CHOPS operations is related to three main factors:

1. Sand production creates an area around the wellbore which provides a larger effective wellbore radius. This could be seen as a high negative skin effect in CHOPS wells.
2. Reduction in the in situ oil viscosity of the bitumen, as a result of foamy oil.
3. An increase in the porosity of the reservoir by producing sand which leads to creation of high permeability channels (wormholes). This improves the overall permeability of the reservoir; therefore access to the reservoir is improved.

From geomechanical points of view there are two main mechanisms which could lead to sand production:

1. Shear failure, basically related to aggressive drawdown. This means that some plane in the near wellbore region is subjected to a higher shear stress than it can

sustain. This may lead to a change of the near wellbore properties of the formation, and to a change in the near wellbore stresses.

2. Tensile failure, basically related to high production rate. The sand production is then related to fluid drag forces on the grains of the formation. Tensile failure could also be resulted by foamy oil exsolution.

5.3 Primate Field Geological Model

Petrel™ (Schlumberger 3D modeling software) was used to create the geological model. The wireline logs and initial seismic data provided the input used to build a geological model of Primate field. Figure 5-3 shows a sample suite of logs across the production zone. Well tops and seismic interpretations were used to create the top and base surface of the reservoir. A geological model was built using 100m by 100m blocks and 25 layers.

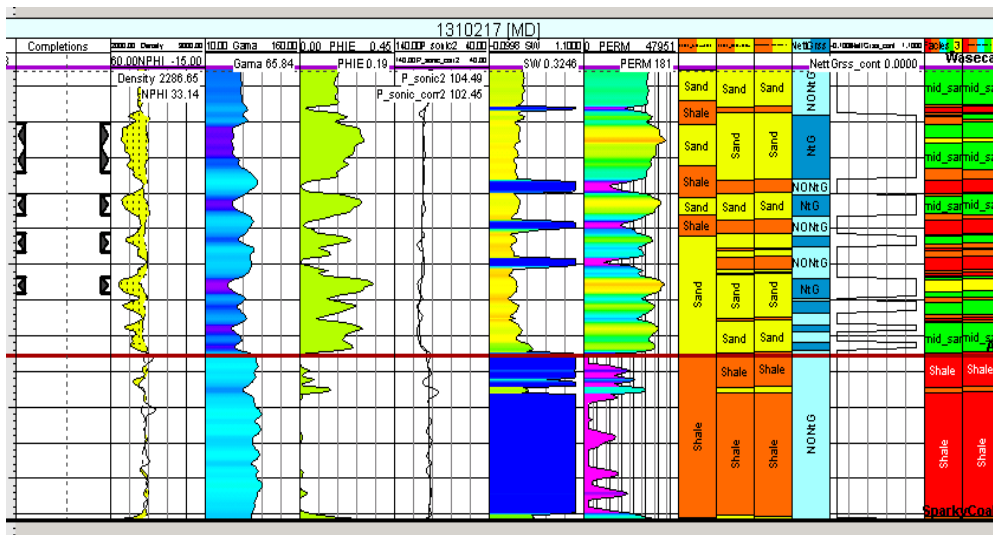


Figure 5-3 Well logs and facies model picked used to create the primate model

After discussion with the geological team of Equal Energy based on the gamma and the porosity log data, it was decided to use five facies to describe the reservoir as shale, shaly-sand, tight-sand, mid-sand and sand. Figure 5-4 is the cross plot of the facies distribution of the model after applying neural network analysis trained on the well log data. The predication of lithofacies was done using single-hidden layer neural network (Hastie et al., 2001).

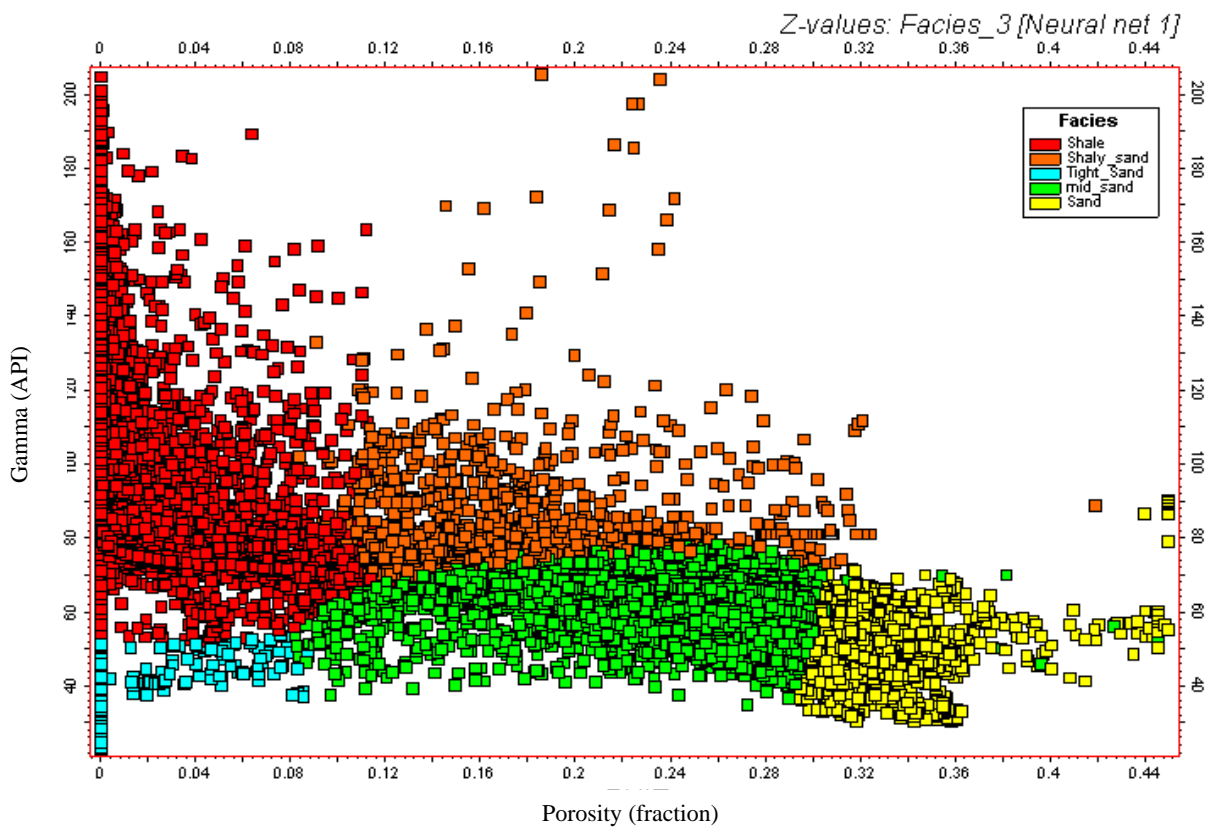


Figure 5-4 Cross plot of porosity versus gamma distribution after neural network analysis

The producing facies which contribute to the oil production are sand and mid-sand facies. The variogram analysis (Deutsch 1998), was performed for both the facies and properties such as porosity, permeability and water saturation. Using the well data

the variogram fitting was done for all the three directions. Figure 5-5 presents an example of the variogram that was used for sand facies. Then using Sequential Gaussian Simulation [SGS], Deutsch (1998), 50 realizations were created and ranked based on the oil in place. The P_{50} model was then used for the simulation.

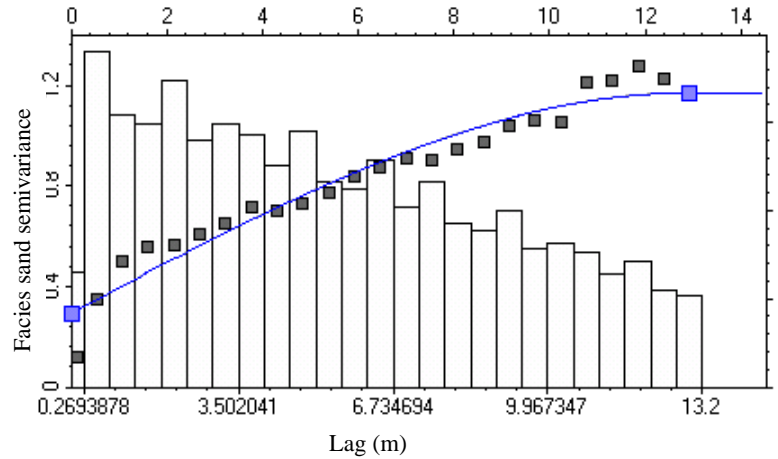


Figure 5-5 Variogram of the sand facies

The following figure shows the 3D view of the up scaled geological model which was used for history matching of Primate field.

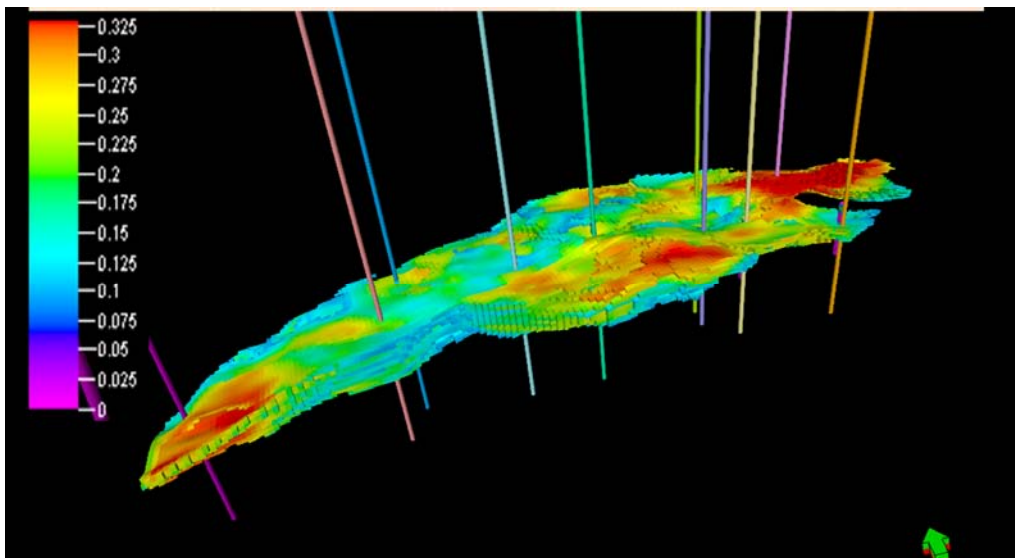


Figure 5-6 3D view of effective porosity map created using wireline logs and geological interpretations

5.4 Reservoir Simulation

Today, practically all aspects of reservoir engineering problems are solved with reservoir simulators, ranging from well testing to prediction of enhanced oil recovery. Every simulation study is a unique process, starting from the geological model and reservoir description to the final analysis of recovery factor optimizations. Reservoir simulation is the science of combining physics, mathematics, reservoir engineering, and computer programming to develop a tool for predicting hydrocarbon reservoir performance under various operating strategies (Aziz, K. and Settari, A. 1979). The finite-difference methods are extensively applied in the petroleum industry to simulate the fluid flow inside the porous medium. There are three main laws which govern the isothermal reservoir simulation:

1. Conservation of mass.
2. Darcy flow that is an expression of conservation of momentum.
3. Phase behaviour, that makes the connection between the fluid properties (such as density and compressibility) and the pressure and temperature of the system and phase changes.

By applying these three rather simple laws, the flow equation (diffusivity equation) is derived and discretized for the different phases that exist in the reservoir. Then by applying the initial and boundary conditions, flow equations are solved during each time step. A combination of a linear solver and a Newtonian solver is often used to solve the matrix of unknowns created at each time steps. The objective in this section of

this study is to illustrate how the reservoir simulation was used for history matching of production data. This knowledge provides a tool to estimate the in-situ properties of the reservoir for estimating the seismic response.

5.5 History Matching

This process starts by using a finite difference approach and a geocellular model to predict production rates for a time period for which the production information is available. If the computed rates of oil gas and water match the actual rates, the computation is assumed to be correct and can be then used to make future predictions. If the computed rates do not match the actual production data, some of the model parameters (e.g., geological data or operational data or fluid model). will be modified and the computation is repeated. The process of modifying these parameters to match the computed rates with the actual observed rates is called *history matching*.

The process of history matching is a time consuming and extremely difficult portion of simulation studies. The general approach in manual history matching is to modify the parameters that have the largest uncertainty and also the largest effect on the results. The quality and confidence in the simulation results are highly dependent on the inputs provided for the simulation. Therefore, it is very crucial to check and validate the input of simulation such as fluid and rock properties to reduce the number of simulation runs to obtain a decent history match.

In this study the fluid properties of the reservoir were modeled using the Peng – Robinson EOS model calibrated with the laboratory measurements. The rock properties such as relative permeability curves were modified as part of history matching process.

5.5.1 Fluid Modeling

The hydrocarbon part of the Primate field was modeled using three components and Peng Robinson EOS (Chapter 3) . The mole fraction of the reservoir was estimated based on the compositional analysis of the produced reservoir fluid:

Component	Mole fraction
Heavy	0.75
Intermediate	0.1
C ₁	0.15

C₁ is the methane which the major component of gas composition of the reservoir (up to 95%). Heavy and intermediate are the two pseudo components which were used to capture the physics of the Primate oil. The Heavy component was representing the high carbon number of the Primate oil (C₁₀⁺) and the Intermediate component was used for carbon numbers up to C₁₀.

The viscosity of the oil, produced GOR and the oil density were available to tune the equation of state model. EOS tuning was done using commercial PVT package (CMG WINPROP) through a regression analysis with the equation of state. In this method the predicted values from EOS are compared to the lab measurements. When there was a

mismatch the components properties such as molecular weight, critical pressure and temperature and acentric factor were modified then the predicted values from the equation of state are compared with the lab data. The process is done iteratively until a desired match is achieved. The following Table 5-1 summarized the thermodynamic properties of the components after the regression analysis. Figure 5-7 presents the dead oil viscosity data and the match obtained from equation of state model.

Properties		Components		
		Heavy	Intermediate	C1
Critical Pressure	atmp	18.4	19.4	45.4
Critical temperature	K	787.8	384.0	190.6
Accentric factor	N/A	0.8	0.8	0.0
Molecular Weight	gr/mol	359.6	96.0	16.0
Volume shift	N/A	-0.3	0.2	0.0
Critical Volume	l/mol	1.6	0.5	0.1
Boiling Point	K	719.3	409.7	112

Table 5-1 Properties of the pseudo components used for fluid modeling of Primate field

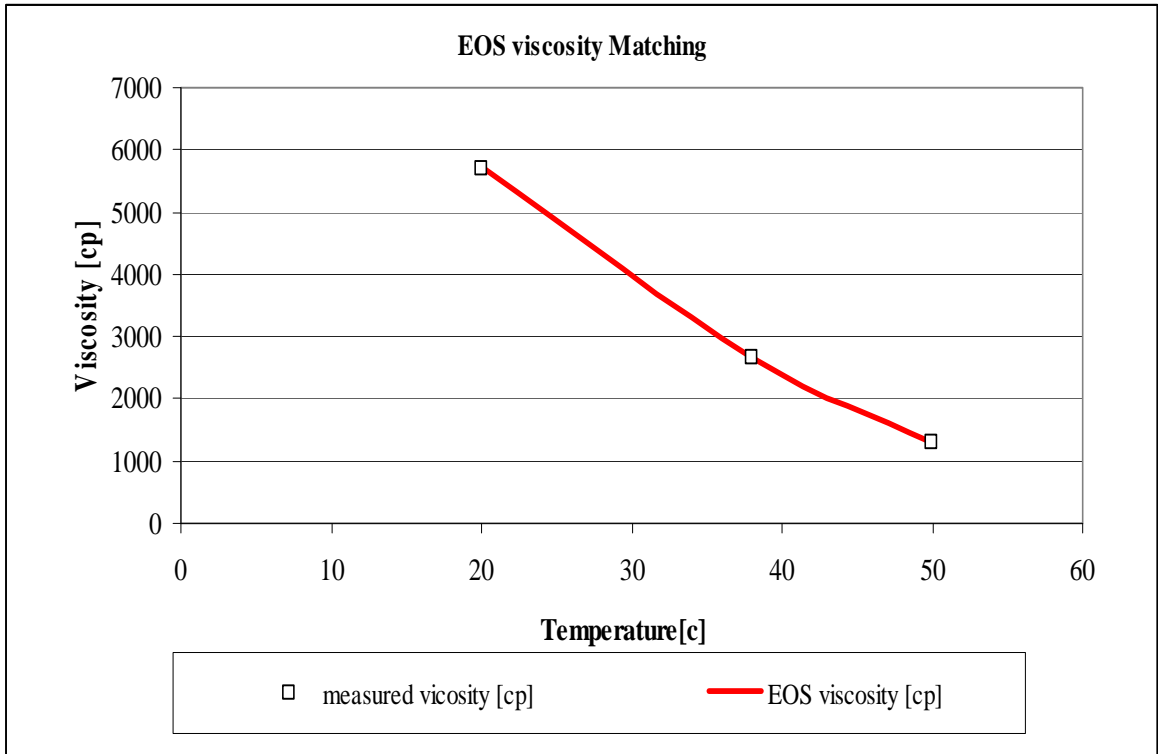


Figure 5-7 Equation of State Match to the dead oil viscosity data

In addition to the dead oil viscosity the oil bubble point pressure, oil API gravity and gas oil ratio were also used in the regression analysis. Tables 5-2 present the results of the regression analysis. Tuning the Equation of State (EOS) model has provided decent match to the lab measurements and deemed to be suitable for creating the PVT tables required for the simulation.

Property	Measured	EOS predicted	Error (%)
Bubble point (kPaa)*	7.00E+03	6.83E+03	2.48%
API gravity	12	11.99	0.08%
Gas Oil Ratio (m3/m3)	15	14.9	0.67%
Viscosity at 20 C	5.70E+03	5.73E+03	-0.67%
Viscosity at 38 C	2.65E+03	2.65E+03	0.17%
Viscosity at 50 C	1.31E+03	1.30E+03	0.50%
* At reservoir temperature of 35 C			

Table 5-2 Comparison between modeled and measured data of Primate oil field

The following figures present the EOS model prediction of oil and gas density and viscosity. Solubility of gas is modeled by K value tables which were generated by performing flash calculation using EOS. The fluid model was then imported to a commercial reservoir simulator (CMG STARS).

Unfortunately the lab measurements did not include the live oil viscosity values. The live oil viscosity (μ_l) is therefore calculated based on the following viscosity mixing rule from each components viscosity (μ_i) and its mole fraction (x_i):

$$\ln(\mu_l) = \sum_{i=1}^n x_i \ln(\mu_i) \quad (5.1)$$

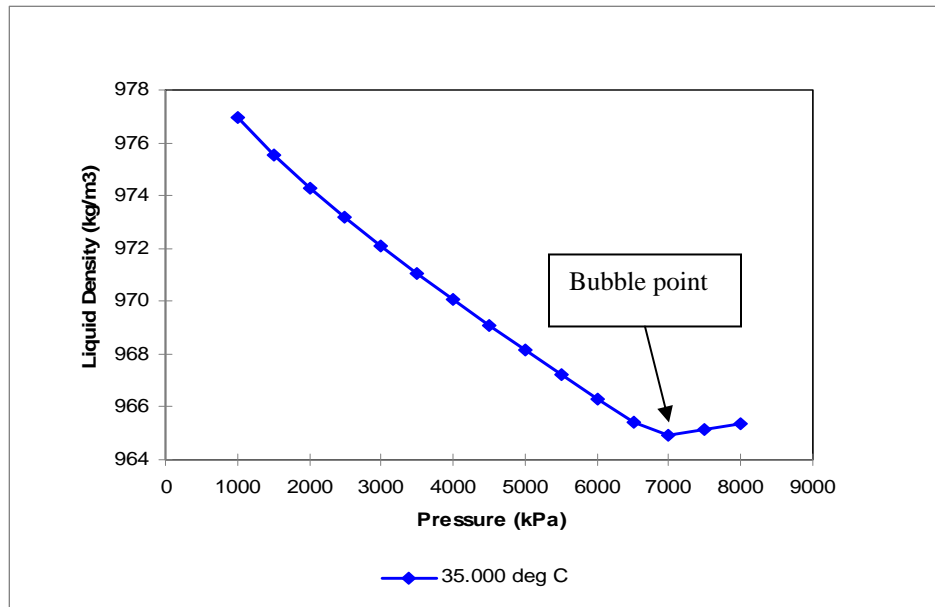


Figure 5-8 Liquid density of Primate Oil

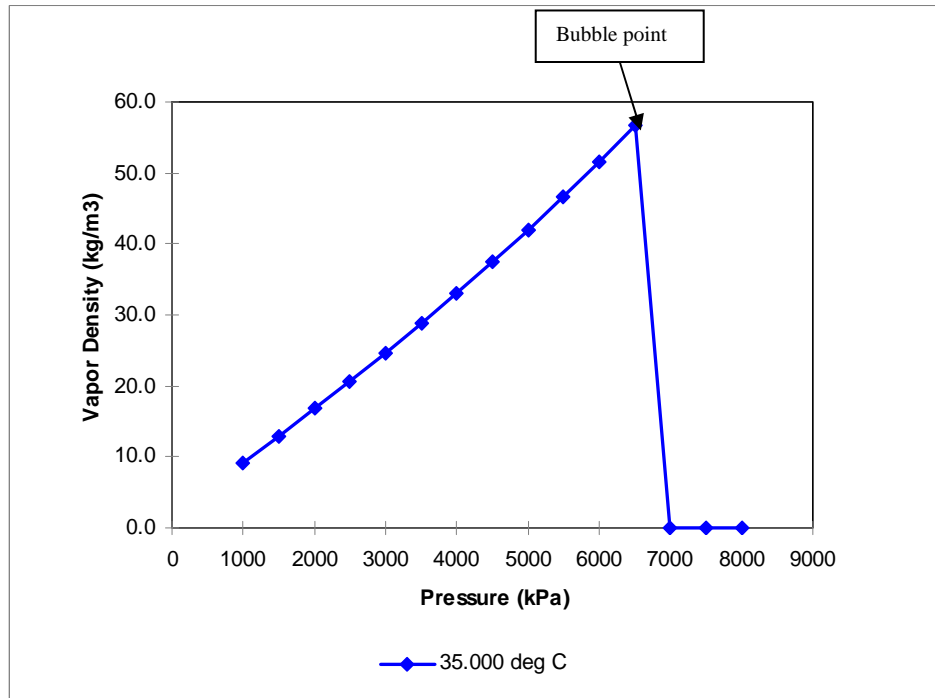


Figure 5-9 Vapour (gas) density of primate oil

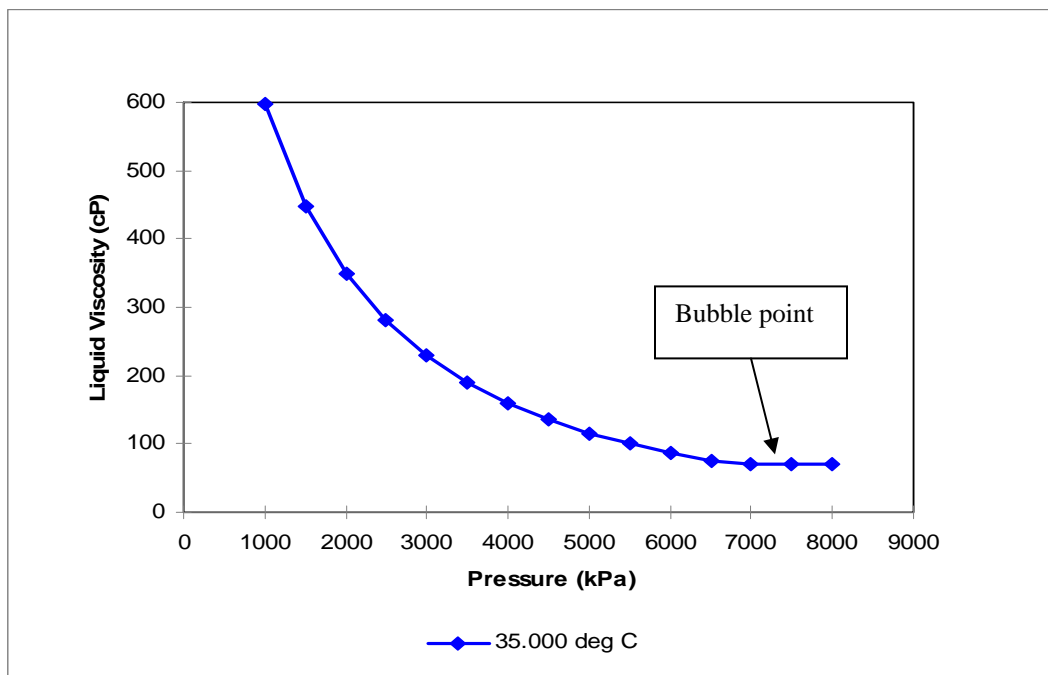


Figure 5-10 Liquid viscosity of Primate oil

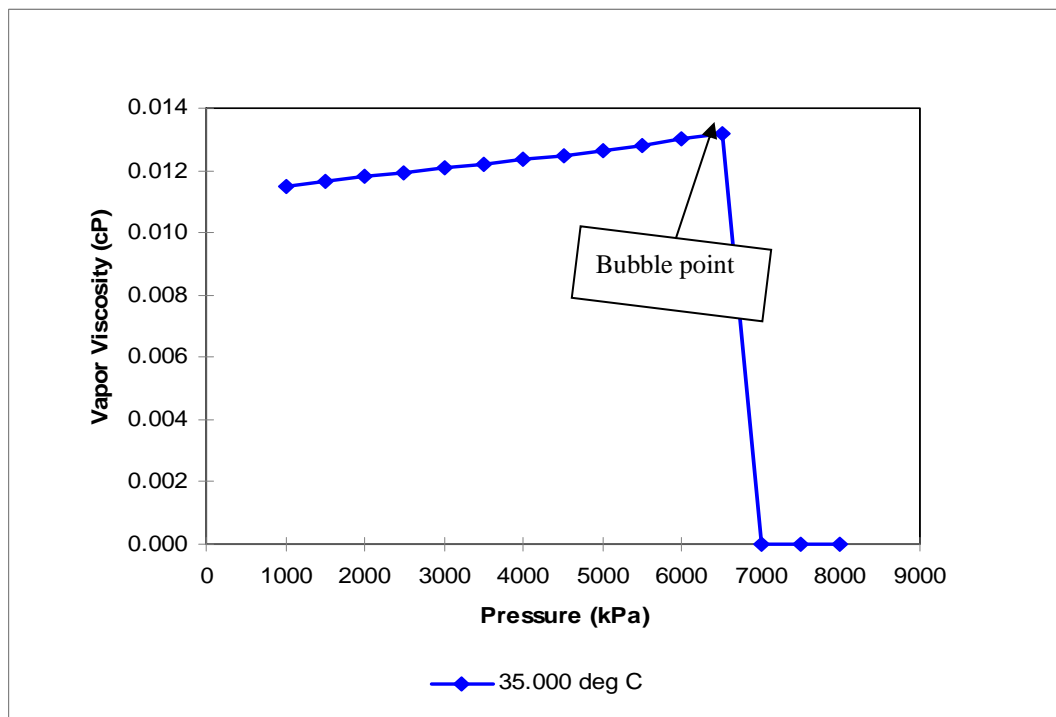


Figure 5-11 Vapour viscosity of Primate Oil

5.5.2 Rock Properties

Using Newman (1973) correlation and the average porosity of the reservoir (33%) the compressibility of reservoir rock is estimated to be $1E-5$ kPa⁻¹. The reservoir porosity, permeability, and oil / water saturation of the simulation blocks were directly imported from the geological model that was explained above.

The relative permeability curves for the oil-water system are presented in Figure 5-12. This curve was the main matching parameter to match the water and oil production history. The critical water saturation was selected low enough that the amount of mobile water at initial condition is controlled and it prevented a massive water production initially.

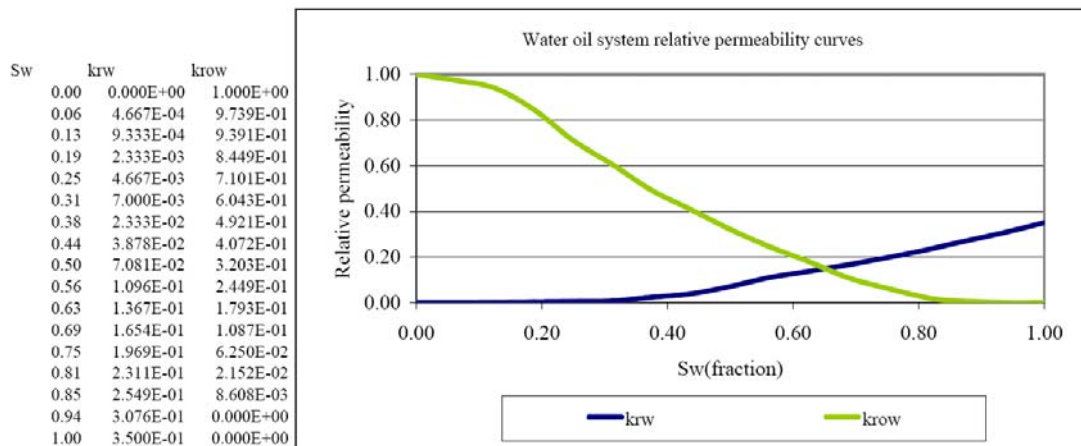


Figure 5-12 relative permeability of oil water system

A major matching parameter was the gas-liquid relative permeability curves. As it was explained above about the CHOPS production an important parameter in CHOPS production is the foamy oil. In this modeling the foamy oil was modeled by considering

low enough gas mobility. This technique helped to keep the gas in reservoir and provided a good match to the gas production history. Figure 5-13 presents the gas-liquid relative permeability curves.

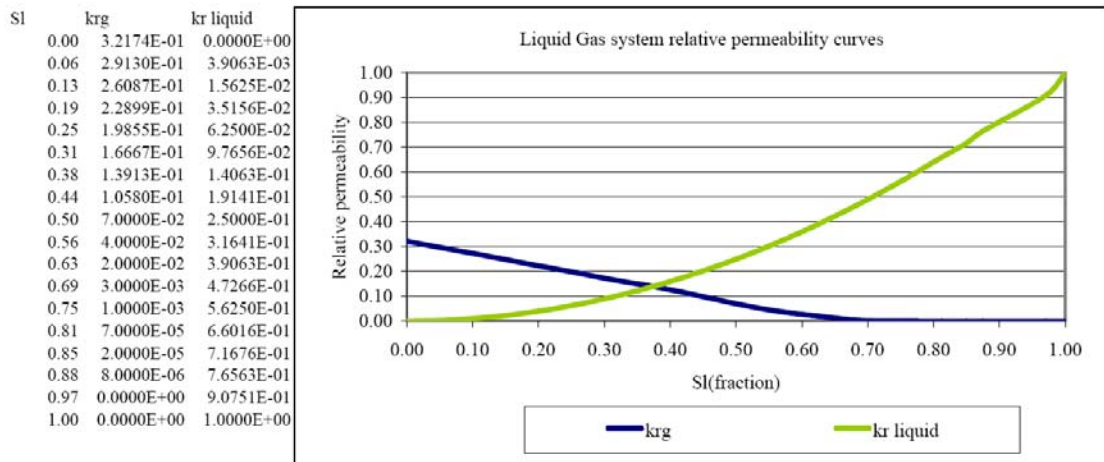


Figure 5-13 relative permeability of liquid gas system

5.6 History Match Results:

The production history and model predicted results of the Primate field are shown in Figures 5-14 to 5-17. Examination of this figure suggests that a very close match was obtained with the production history. The daily production rate of gas from this field does not have a very accurate measurement as it has been mostly flared and used for heating oil for sand separation. However the cumulative match to gas production is still under 10 percent error.

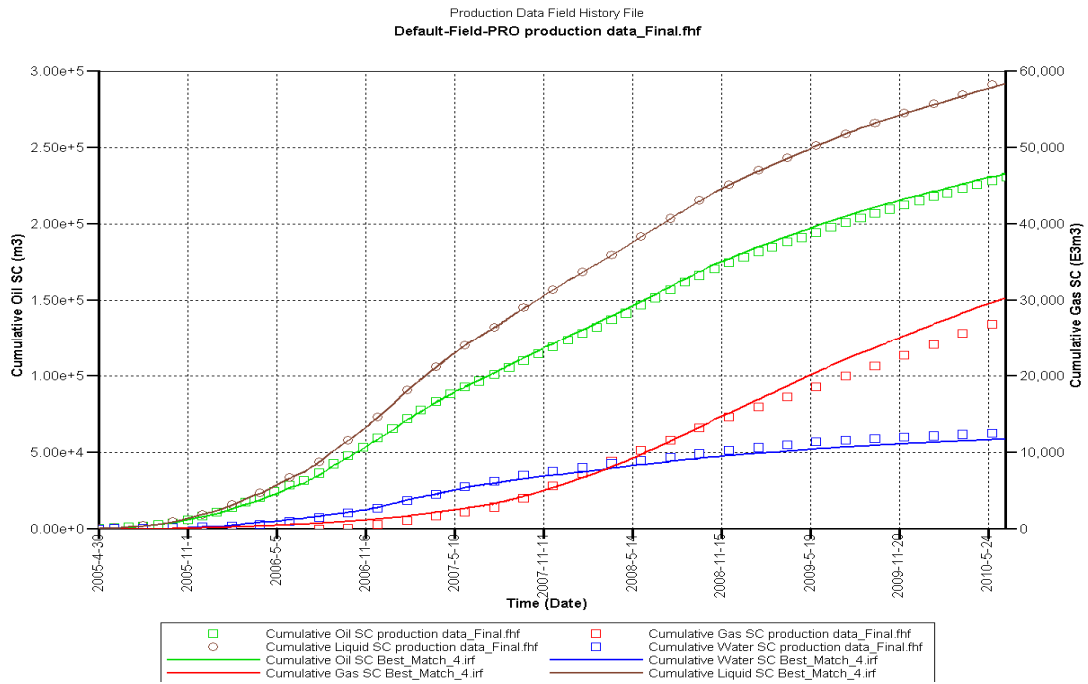


Figure 5-14 Results of history match of cumulative production of Primate field

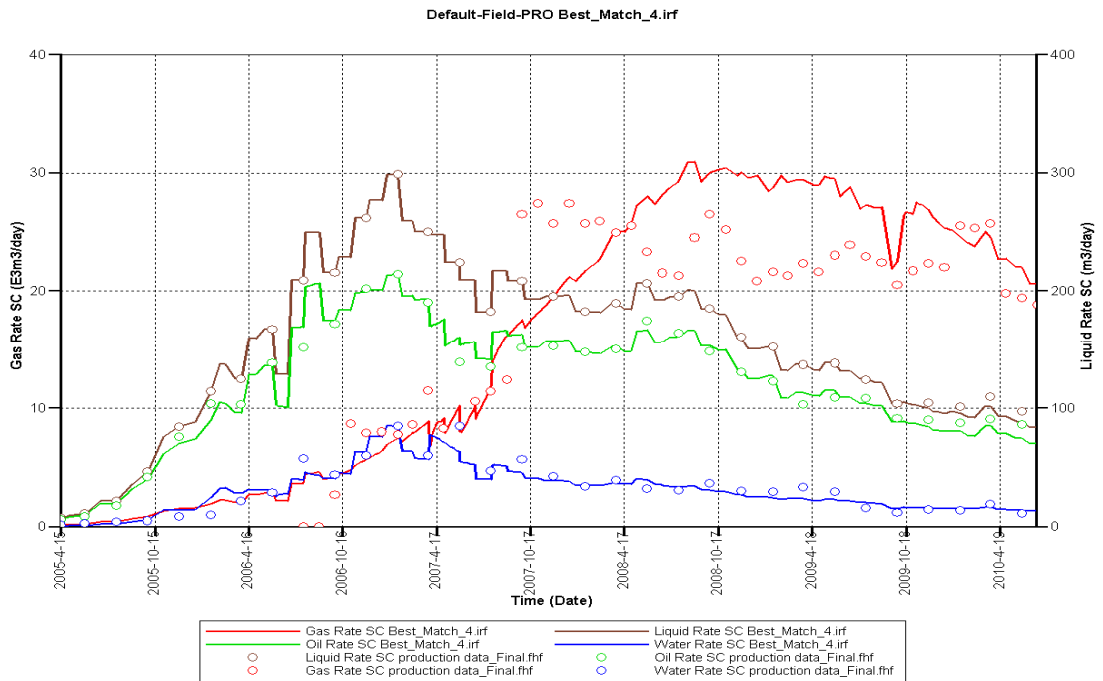


Figure 5-15 Results of history match of rates of Primate field

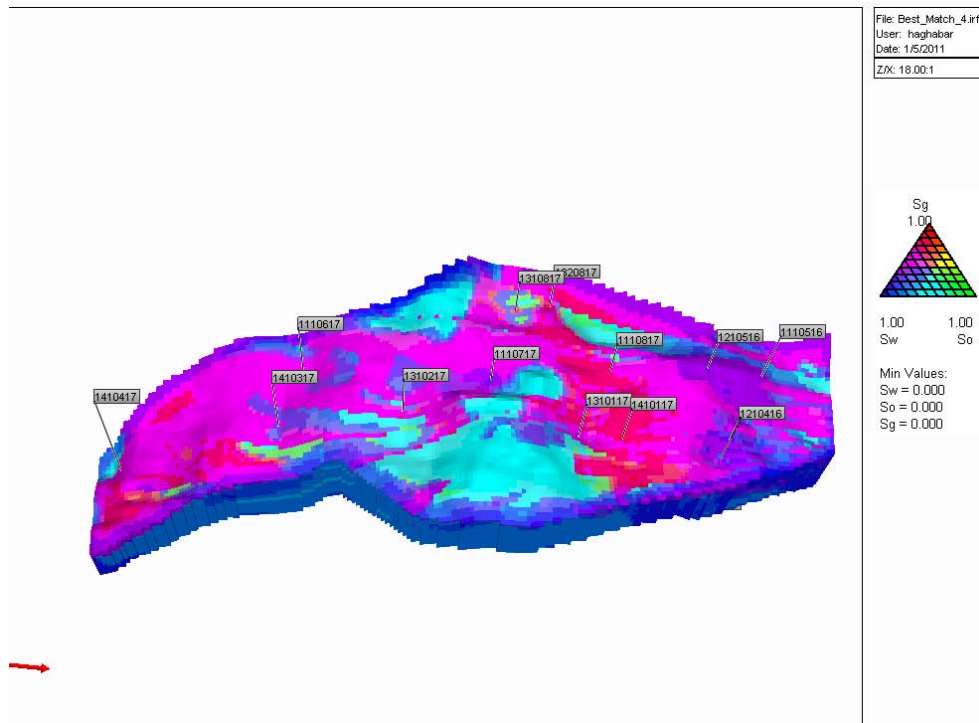


Figure 5-16 Ternary diagram of the saturations of different phases

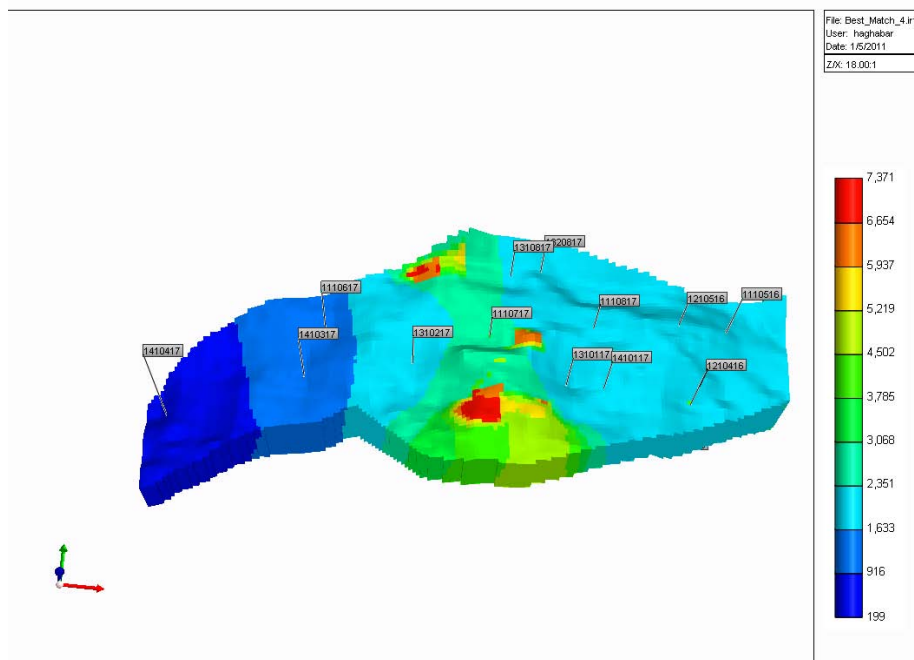


Figure 5-17 Pressure distribution of the model after production

5.7 White Attenuation Model

The next step of this work flow was to estimate the average properties of the reservoir for estimating the attenuation model. Below table presents the estimation of the reservoir properties to calculate this model.

Property	Initial condition	Dec 2009 (Time lapsed)
Oil saturation	0.65	0.57
Water saturation	0.35	0.32
Gas saturation	0.00	0.11
Pressure (kPa)	7,000.0	1,500.0
Oil density (kg/m ³)	964.9	975.5
water density (kg/m ³)	980.0	980.0
Gas density (kg/m ³)	N/A	13.0
Fluid density (kg/m ³)	960.4	872.4
Vapour viscosity (cp)	N/A	0.011
Liquid viscosity (cp)	100	400
Average oil permeability (mD)	1500	1350
Average gas permeability (mD)	0.0	0.01

Table 5-3 Summary of reservoir properties used as input for attenuation model

Using the above information the input of the White theory attenuation model was calculated and they are presented in Table 5-4. The attenuation model was then calculated for the 2009 seismic survey (time lapsed). The White theory attenuation response is presented in Figure 5-18. Examination of this figure shows that when a seismic wave passing through Primate filed the frequencies less than 40 Hz are significantly attenuated.

This conclusion was the basis for designing the band pass filters in section 5.10 of this chapter.

Parameter	Value
Dry bulk moduli of frame (Pascal)	6E9
Dry shear moduli of frame (Pascal)	5E9
Grain bulk moduli (quartz) (Pascal)	35E9
Grain shear moduli (quartz) (Pascal)	45E9
Grain density (kg/m ³)	2600
Porosity (fraction)	0.35
Gas Bulk Moduli (Pascal)	1E6
Liquid Bulk Moduli (Pascal)	2E9
Gas Density (kg/m ³)	13
Liquid Density (kg/m ³)	872
Gas Viscosity (Pascal.sec)	0.000011
Liquid Viscosity (Pascal.sec)	0.5
Gas effective permeability (m ²)	0.000001E-12
Liquid effective permeability (m ²)	1.35 1E-12
Gas saturation (fraction)	0.11
Gas bubble size (m)*	0.001

* Based on Wang & Maini (2005) please see Chapter 3 for more detail

Table 5-4 Input Parameters of White theory for Primate field

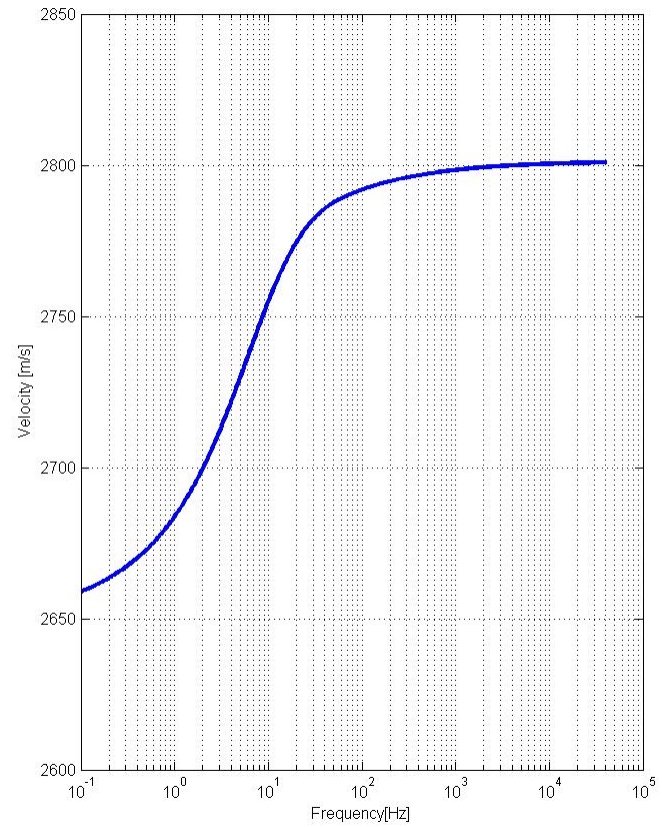
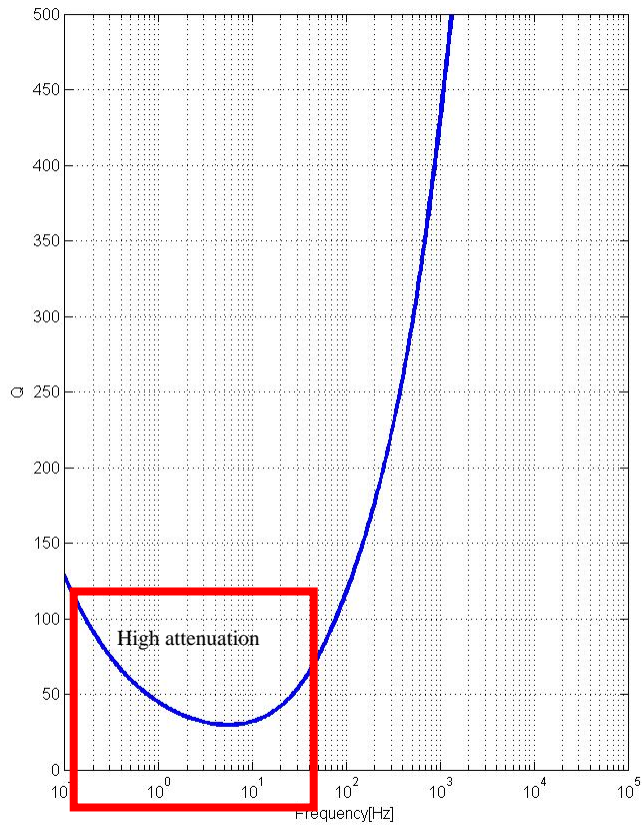


Figure 5-18 Attenuation model of Primate field for 2009 seismic survey

5.8 Time-Lapse Seismology

In the last two decades, the application of seismic monitoring of the reservoir's hydrocarbon production has gained significant momentum in the oil and gas industry (Vasco et.al 2004). The main concept behind the application of time-lapse seismology is the sensitivity of rock properties such as bulk, shear moduli, and density to changes in the reservoir pressure, temperature and geomechanical aspects such as compaction and dilation. 4D seismic is another alternative name used for time-lapse 3D seismic as time component adds another dimension to the 3D seismic survey.

For post stack data, the outcome of a 4D seismic analysis is usually a time delay map and amplitude difference map. The time delay maps usually get more attention as they can be used to estimate the velocity changes. By knowing the velocity changes one can estimate the recovery factor of heavy oil using a fluid replacement model.

In this thesis a new method was presented which puts more emphasis on understanding the change of the amplitude of the 4D seismic versus frequency. Based on the results of the White theory for patchy saturation (Chapter 3) it was concluded that when waves pass through this type of medium, the medium has a higher attenuation for a specific portion of the frequency content of the wave. This means that the different frequencies are attenuated with different attenuation coefficients. By using this concept and based on the knowledge from the reservoir rock and its state at time which time-lapse survey performed (through history matching) the band pass filters were developed. Through this method one is able to focus on part of the seismic frequency band which was affected most by production.

5.9 Seismic and Well Logs Tie

It is a common practice to first check the tie between the well logs depth and the seismic data to validate the seismic data and make sure that there is a good agreement between depth (logs) and time (seismic). This is done by convolving a representative wavelet obtained from the seismic input with a reflectivity model created by sonic data. The result is called synthetic seismogram and is compared with the seismic response at the location of the well. Figure 5-19 presents the statistic wavelet extracted from 2004 seismic survey. The time window for this wavelet extraction was from 200 ms to 800 ms which covers the production zone completely. This wavelet was then used for the convolution process.

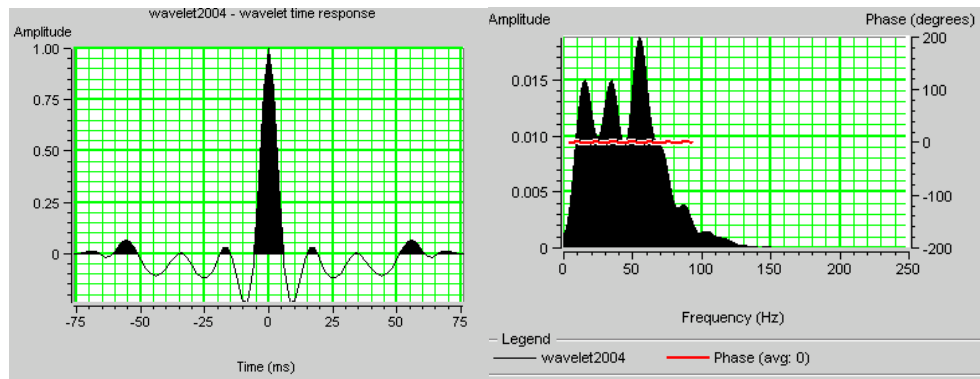


Figure 5-19 Wavelet extracted from 2004 seismic survey

Figure 5-20 presents a sample of synthetic seismogram comparison with the seismic survey. This process was done for all the wells with P-wave velocity and density data and the results are presented in Figure 5-21. The overall correlation of this tie between seismic and the synthetic seismogram is 0.61, which means a good agreement between them. It also validates a good tie between the seismic data and well depths.

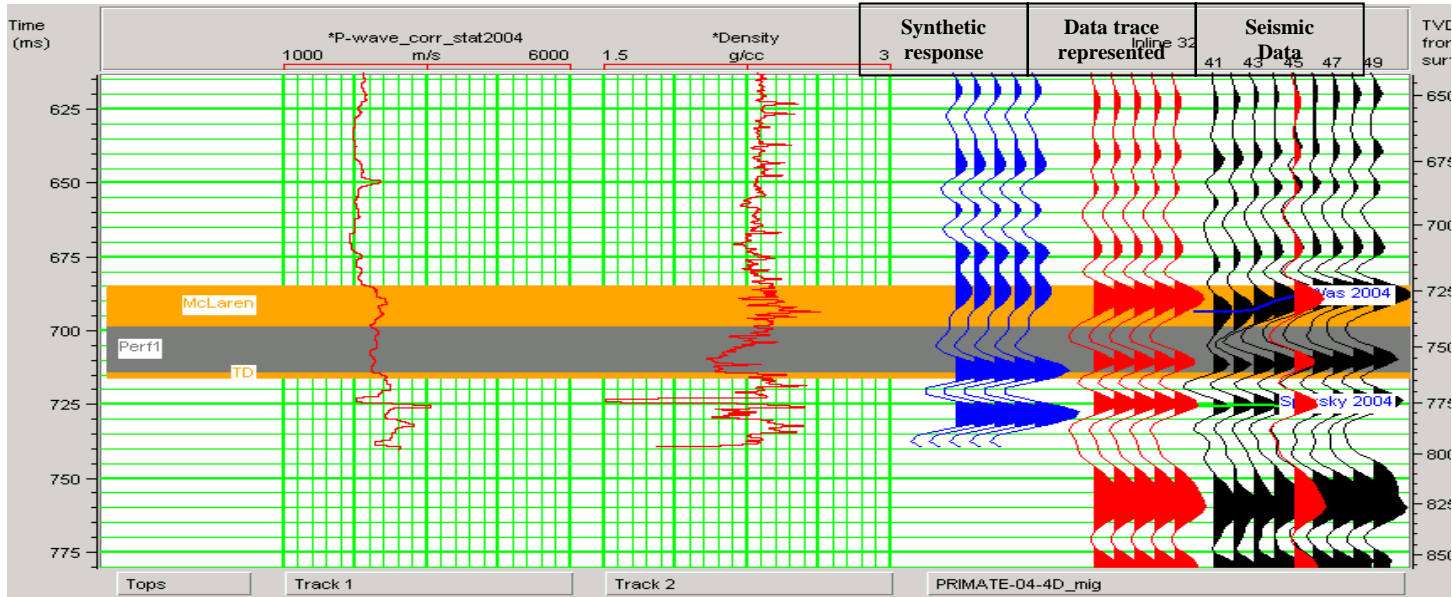


Figure 5-20 sample of synthetic seismogram and seismic tie

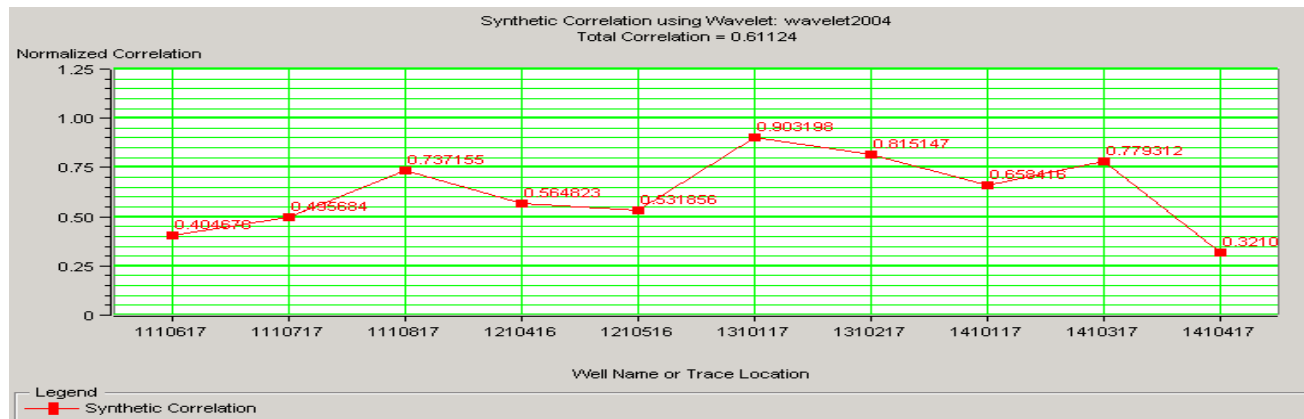


Figure 5-21 Correlation between synthetic seismogram and seismic data across the Primate field

5.10 Design of Band Pass Filters

When the attenuation created due to the patchy saturation is understood, the next step is to design the band pass filters. The goal of this filters is to investigate the changes that could be observed for different frequency band of time lapsed seismic data. Figure 5-22 presents the amplitude spectrum on the two seismic surveys of Primate field. Based on the conclusion from the White theory attenuation the following two band pass filters were applied on the initial and repeat seismic volumes.

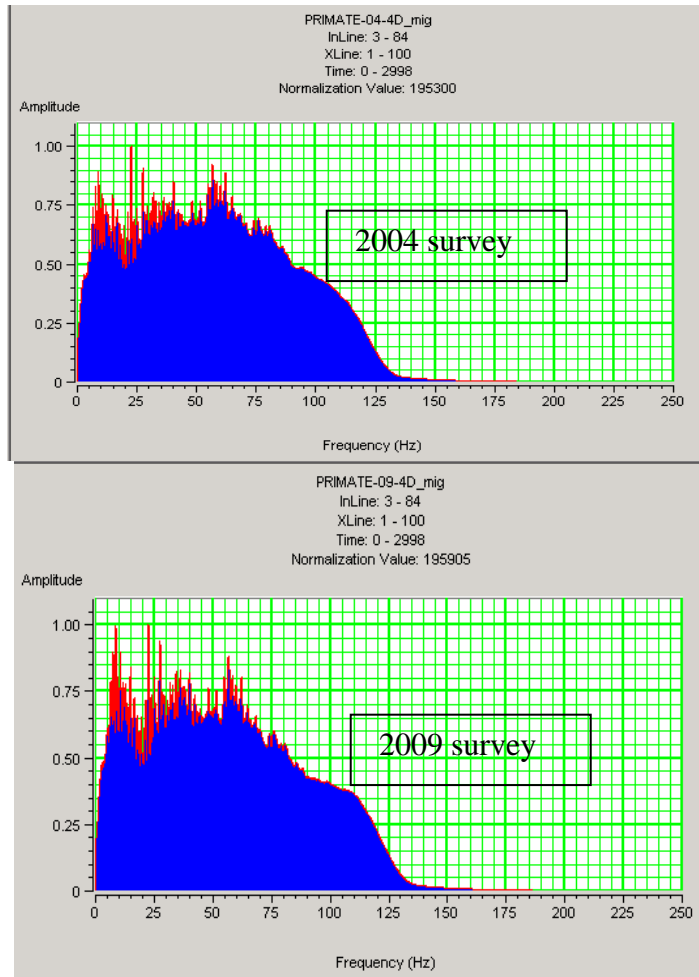


Figure 5-22 Amplitude spectrum of two seismic surveys of Primate field

As it is shown by Figure 5-18, the White attenuation model suggest that the band frequency less than 40Hz should be significantly attenuated due to the gas patchy saturation in Primate filed at the time of monitor survey (2009 survey).

Filter	Low cut (Hz)	Low pass (Hz)	High pass (Hz)	High cut (Hz)
Low frequency	2	10	35	45
High frequency	40	45	100	120

Table 5-5 Specifications of the band pass filters used to separate the low and high frequency data

As a result of applying this filter four seismic volumes were created for the 4D analysis. 4D workflow was carried out for a set of low frequency and set of high frequency pairs. Figure 5-23 is the amplitude spectrum of the low frequency pair. Figure 5-24 present the high frequency pair amplitude spectrum.

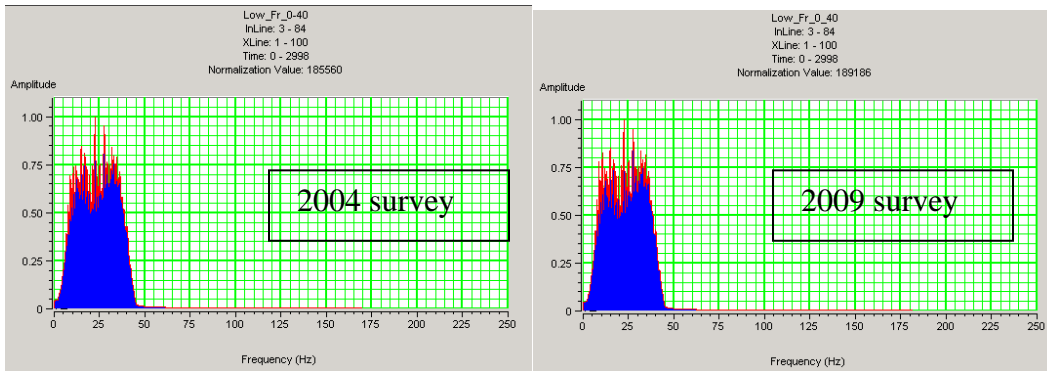


Figure 5-23 Amplitude spectrum of low frequency volumes

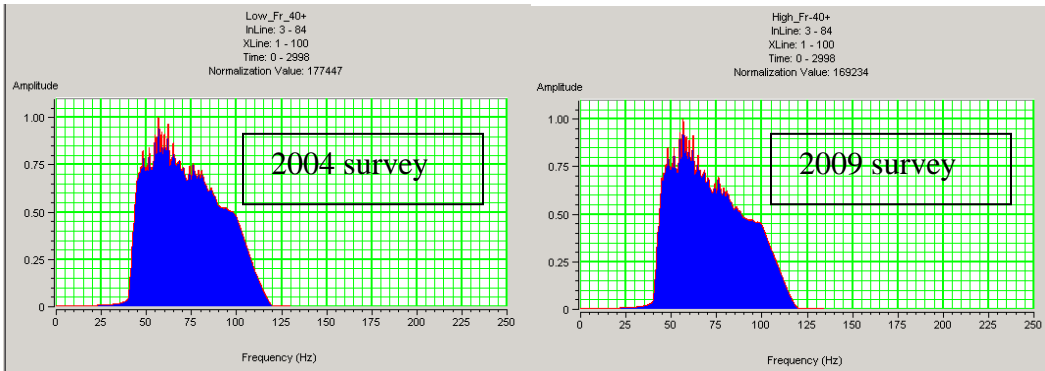


Figure 5-24 Amplitude spectrum of high frequency volumes

5.11 Discussion of Time-Lapse Results

Figures 5-25 and 5-26 present the amplitude difference between the 2009 and 2004 of Primate field for low and high frequency seismic volumes respectively. It is obvious the low frequency volumes show a clearer and more coherent image of the changes in the reservoir. This comparison is done without any corrections and it shows that the low frequency content of the seismic data have been altered most due to the production from the Primate field, as predicted by the attenuation model. This observation validates our theory that using White’s patchy saturation model and inputs obtained from reservoir simulation the low frequency up to 40Hz would get attenuated most at the time when seismic survey was repeated.

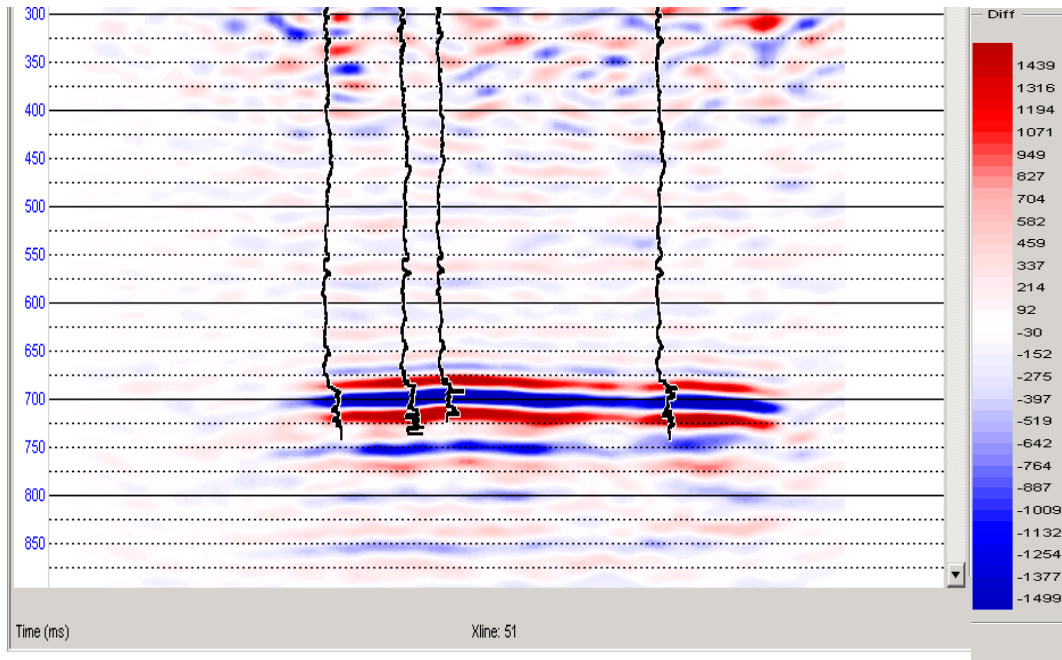


Figure 5-25 Amplitude difference of low frequency seismic volumes (2009 - 2004)

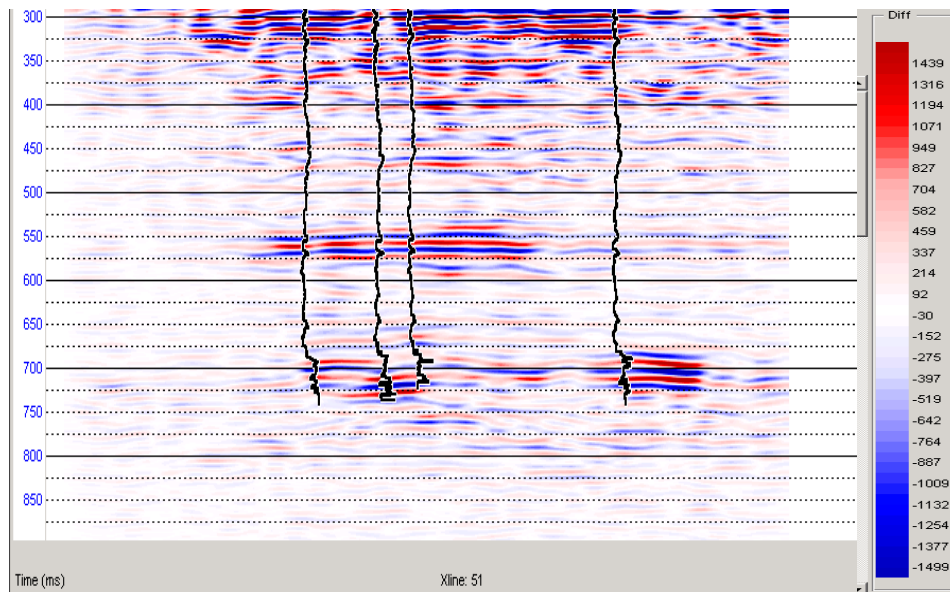


Figure 5-26 Amplitude difference of high frequency seismic volumes (2009 - 2004)

The next check was to compare the frequency content of the low frequency data in a time window of the reservoir between the initial and monitor surveys. This process is usually referred as estimating “*shaping filter*”. Figure 5-27 presents the results of the shaping filter in time and its amplitude spectrum. The results validate the previous estimation from White’s attenuation model. As shown on Figure 5-27 maximum attenuation happens at frequencies close to 10Hz to 30Hz similar to what was predicted by White’s attenuation model in the previous section.

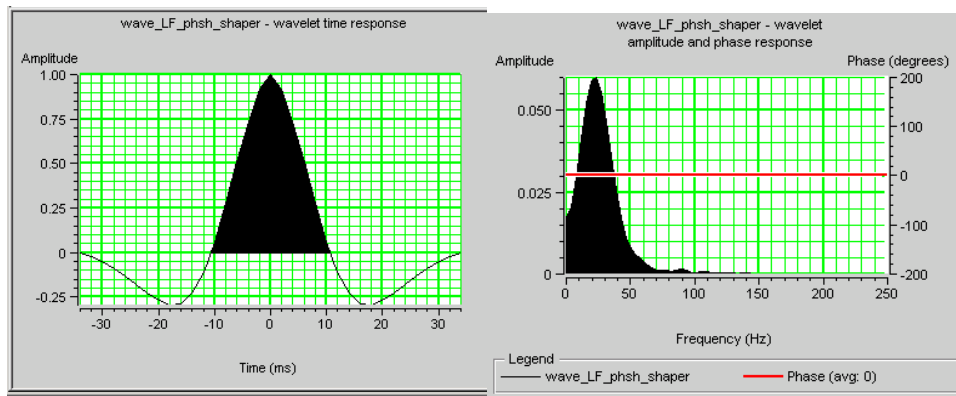


Figure 5-27 Shaping filter used in the workflow of low frequency seismic

4D analyses were completed for the low and high frequency seismic volumes by going through the following steps:

1. Phase and time shift correction
2. Shaping filter application
3. Amplitude normalization

After applying these calibrations the amplitude envelopes of the difference of the low and high frequency are presented in figure 5-28 and 5-29 for low and high frequency

volume respectively. Examination of figure 5-28 shows a good agreement with the production history of the field. The areas with highest production (highest foamy oil generation) have seen the most changes.

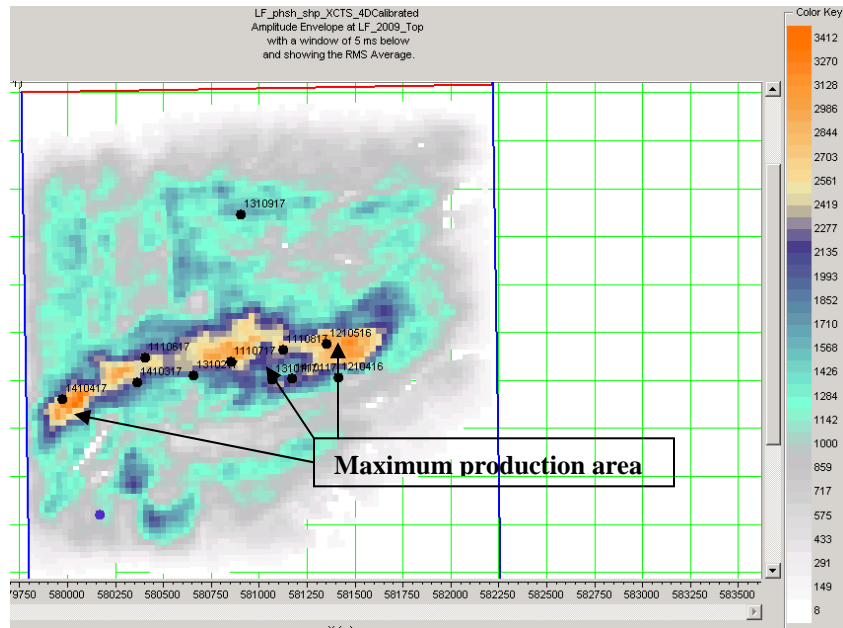


Figure 5-28 Amplitude envelope of difference between low frequency volumes after applying 4D corrections

As it is shown in figure 5-29 the results of the 4D analysis on the high frequency volumes are not conclusive and do not support the production data of the Primate field.

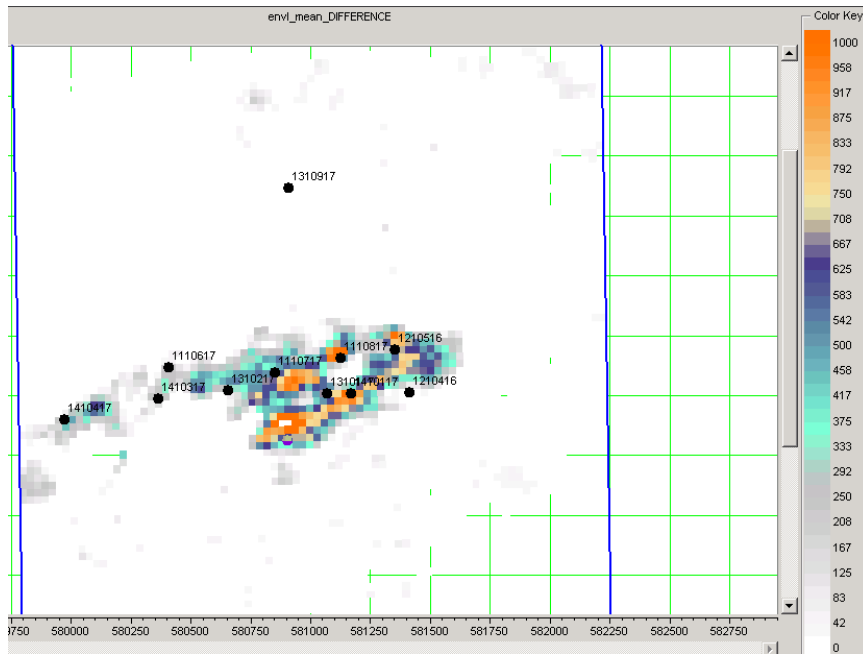


Figure 5-29 Amplitude envelope of difference between high frequency volumes after applying 4D corrections

CHAPTER SIX: CONCLUSIONS

Proposing a method for bridging the gap between the reservoir engineering and seismic modeling/inversion of heavy oil reservoir was the main goal and conclusion of this thesis. With advancements in the geomodeling and reservoir simulation in recent decades, now it is possible to have a better resolution of in situ reservoir heterogeneities. The goal of this thesis was to propose a method to leverage on this knowledge (reservoir simulation) and improve the imaging power of seismic data.

Providing a proper image from the state of reservoir depletion is a fundamental input to improve the recovery of the heavy oil field. The cost of performing a time lapse study is a small fraction of drilling new wells. Proper processing of time-lapse seismic considering the new method proposed in this study will help to improve the Net Present Value (NPV) of the asset.

The outcome of this research can be used to find the best time for shooting the monitor survey. It can also be used to better design the acquisition parameters to include and preserve the desired frequency band.

Solving the problem of wave propagation in the porous medium requires understanding of the scales of heterogeneities in the medium (micro, macro, or meso) with respect to the propagating wave frequency content.

After reviewing the Biot theory in Chapter two it was concluded that the heterogeneity of interest in this research (gas bubble surrounded by heavy oil) was not properly modeled using Biot Theory.

White's theory of patchy saturation was then investigated in chapter three. It was concluded that White's theory is capable of properly modeling the behaviour of heavy oil in the presence of gas bubbles. The processes involved in the creation of foamy oil are the main reason that validated the use of the White's theory. By reviewing the derivation of this theory, this thesis proposes the use of effective permeability of the gas and liquid phases in White's theory. The use of effective permeability rather than absolute permeability honours the physics behind the derivation of White's theory. It was also demonstrated through a comprehensive sensitivity analysis that the response of White's theory is mostly sensitive to gas saturation, bubble size, bulk moduli and mobility of the liquid phase. The sensitivity analysis showed how drastically the response of Whites theory is depending on the uncertainty of input data. Therefore it was proposed to calculate the inputs of White's model through equation of state modeling and reservoir simulation. The review of current models available for foamy oil suggests the importance of time and diffusion process in establishing the proper size of bubbles in the reservoir. Average gas saturation and in situ effective permeability of liquid phase could be established through a proper flow modeling by obtaining reasonable history matching to the pressure and production history of the field.

Application of White's theory of attenuation leads to velocity dispersion, which requires using viscoelastic constitutive models. In chapter four through a feasibility analysis it was concluded that with only varying the attenuation component of viscoelastic model one could observe sensible changes in seismic response. However the conclusions from comparing a high Q (low attenuation) and a low Q (high attenuation) suggest that amplitude response is directly impacted by the attenuation and application of this theory in real cases has its challenges.

In chapter five the application of the interactions between the reservoir simulation and seismic response was demonstrated using a time-lapse seismic dataset of a Canadian heavy oil field in Saskatchewan. There are three main steps involved in this process as per following:

1. Understanding the in situ properties of reservoir through building a geomodel and reservoir simulation (history matching).
2. Develop attenuation model by using the in situ properties following the White theory of patchy saturation. These properties are based on the average reservoir properties calculated from reservoir simulation.
3. Adding an additional step to time lapse processing flow (apply band pass filters based on frequency response of White's attenuation model) to identify and focus on the frequency band that contains information about reservoir depletion.

The result of chapter five validates the existence of an important link between in situ properties of heavy oil reservoir (foamy oil) and its attenuation response on seismic data.

6.1 Suggestions for Future Research on This Topic

Performing probabilistic reservoir simulation and taking into account the other equally possible geological realizations such as P_{10} and P_{90} cases would help to understand the uncertainty in the simulation results.

In this study the focus of history matching was on field level match. A good well level simulation would require more lab measurements on the rock properties such as relative permeability curves. Developing different sets of relative permeability for each facies will help to improve the quality of reservoir simulation. In addition Lab studies of foamy oil behaviour and using more advanced methods of modeling them such as considering reaction in the simulator will help to obtain a better match.

Modeling sand production history was not a part of this study, however in reality the creation of wormholes are a very important step in CHOPS. With recent improvement in the reservoir simulators it might be possible in future to incorporate sand production and permeability enhancement due to the creation of wormholes.

On the seismic front, moving toward a 3D viscoelastic modeling and using pre-stack data are the two major steps for future considerations. In this study the results were based on post stack data and 1D viscoelastic modeling.

Although currently there are robust codes developed for 3D viscoelastic modeling, the time required for this type of modeling is too long and not practical. With improvements in developing parallel codes and advancements on the hardware front this limitation would be eliminated in the near future. With application of 3D modeling, lateral changes in the attenuation and velocity dispersion model would be properly modeled.

Finally with the above mention advancements, in near future it might be possible to use the information from reservoir simulation and perform a joint viscoelastic inversion on seismic data of heavy oil reservoirs.

REFERENCES

- Aghabarati. H , Dumitrescu. C, Lines . L, Settari. A, 2008, Combined Reservoir Simulation And Seismic Technology, A New Approach For Modeling CHOPS, International Thermal Operations and Heavy Oil Symposium Calgary Canada
- Aki, K., and P. G. Richards, 2002, Quantitative Seismology, Second Edition, University Science Books.
- Aziz, K. and Settari, A. 1979, Petroleum Reservoir Simulation, Applied Science Publishers.
- Norris A.N. 1993, Low frequency dispersion and attenuation in partially saturated rocks: Journal Of Acoustical. Society. America. Volume **94**, 359-370
- Biot, M. A., 1962, Mechanics of deformation and acoustic propagation in porous media: Journal of Applied Physics, **33**, 1482-1498.
- Blanch J. O , Robertson .O. A., and Symes W. W., 1993 Viscoelastic finite difference modeling, Technical report, Rice University
- Blanch, J. O., Robertsson, J. O., Symes, W. W., 1995, Modeling of a constant Q: Methodology and algorithm for an efficient and optimally inexpensive viscoelastic technique, :Geophysics, **60** , 176-184
- Bourbon, ST., and Gonzalez-Serrano, A. 1983. Synthetic seismograms in attenuating media :Geophysics **48**, 1575-1587
- Cadoret , T., D. Marion, and B. Zinszner, 1995, Influence of frequency and fluid distribution on elastic wave velocities in partially saturated limestones : Journal of Geophysical Research, **100**, 9789–9803
- Carcione, J. M. Wave Fields in Real Media: Wave propagation in anisotropic, anelastic and

porous media (Handbook of Geophysical Exploration: Seismic Exploration)

Carcione, J. M., 1998, Viscoelastic effective rheologies for modeling wave propagation in porous media: *Geophysical Prospecting*, **46**, 249–270.

Carcione, J. M., and D. Gei, 2004, Gas hydrate concentration estimated from P- and S-wave velocities at the Mallik 2L-38 research well, Mackenzie Delta, Canada: *Journal of Applied Geophysics*, **56**, 73–78.

Carcione, J. M., H. B. Helle, and N. H. Pham, 2003, White's model for wave propagation in partially saturated rocks Comparison with poroelastic numerical experiments: *Geophysics*, **68**, 1389–1398.

Carcione, J. M., Kosloff, D., and Kosloff, R., 1988, Wave propagation simulation in a linear viscoelastic medium, *Geophysics. J. Roy. Astr. Soc.*, **93**, 393-407.

Carr, N., R. Kobayashi, and D. Burrows. 1954. Viscosity of Hydrocarbon Gases under Pressure: *Transactions of the AIME* **201** , 270–275

Cerjan C., D. Kosloff, R. Kosloff and M. Reshef, 1985 A non-reflecting boundary condition for discrete acoustic and elastic wave equations: *Geophysics* **50** 705–708.

Clayton R. W. and . Engquist B, 1977 Absorbing boundary conditions for elastic and acoustic wave equation *Bull. Seism. Soc. Am*, **67** ,1529–1540.

Deutsch, C.V., and A.G. Journal, 1998, *GSLIB: Geostatistical Software Library and User's Guide*, Second Edition, Oxford University Press, New York

Dutta, N. C., and H. Ode, 1979a, Attenuation and dispersion of compressional-waves in fluid filled rocks with partial gas saturation (White model):Part 1 Biot theory: *Geophysics*, **44**, 1777–1788:

- Dutta, N. C., and H. Ode, 1979b, Attenuation and dispersion of compressional-waves in fluid-filled rocks with partial gas saturation (White model): Part 2 Results:Geophysics, **44**, 1789–1805.
- Dutta, N. C., and A. J. Seriff, 1979, On White’s model of attenuation in rocks with partial gas saturation: Geophysics, **44**, 1806–1812.
- Helle, H. B., N. H. Pham, and J. M. Carcione, 2003, Velocity and attenuation in partially saturated rocks-Poroelastic numerical experiments: Geophysical Prospecting, **51**, 551–566.
- Hastie, T., R. Tibshirani, and J. Friedman, 2001, The Elements of Statistical Learning: Data Mining, Inference, and Prediction, Springer-Verlag, New York
- Hill, R., 1963. Elastic properties of reinforced solids some theoretical principles: J. Mech. Phys. Solids, **11**, 357–372.
- J. Kristek and P. Moczo, 2003, Seismic-Wave Propagation in Viscoelastic Media with Material Discontinuities: A 3D Fourth-Order Staggered-Grid Finite-Difference Modeling Bull: Seism. Soc. Am. **93**, 2273–2280.
- JafarGandomi, A., and H., Takenaka, 2007, Efficient FDTD algorithm for plane-wave simulation for vertically heterogeneous attenuative media: Geophysics, **72**, 43-53
- Johnson D. L. J. 2001. Theory of frequency dependent acoustics in patchy-saturated porous media: Journal Of Acoustical. Society. America, Volume **110**, 682-694
- Knopoff, L. 1964. ‘Q’. Rev. Geophysics, 2(4): 645–654. Publication 391: Institute of Geophysics and Planetary Physics, UCLA.
- Kristek, J., Moczo, P., Archuleta, R. J., 2002. Efficient methods to simulate planar free surface in the 3D 4th-order staggered-grid finite-difference schemes: Studia Geophys. Geod.,

46, 355-381

Kumar, R. and Pooladi-Darvish, M. 2001 , Effect of viscosity and diffusion coefficient on the kinetics of bubble growth in solution-gas drive in heavy oil: Journal of Canadian Petroleum Technology, **40**, pp. 30-37

Lamoureux P. Michael Adler H Daniel, 2004, CREWES Research Report — Volume 16
Lebedev, M., J. Toms, B. Clennell, M. Pervukhina, V. Shulakova, L. Paterson, T. M. Müller, B. Gurevich, and F. Wenzlau ,2009, Direct laboratory observation of patchy saturation and its effects on ultrasonic velocities : The Leading Edge **28** , 24–27.

Lee, A. L., M. H. Gonzalez, and B. E. Eakin, 1966, The Viscosity of Natural Gases: Journal of Petroleum Technology, **18**, 997–1000.

Liu, H. P., Anderson, D. L., Kanamori, H., 1976, Velocity dispersion due to anelasticity implications for seismology and mantle composition: Geophysics. J. R. astr. Soc., **47**, 41-58

Maini, B.B., 1996, Foamy Oil Flow in Heavy Oil Production,: Journal of Canadian Petroleum Technology **35**,21-24.

Mastmann, M., Moustakis, M. & Bennion, D.B. ,2001, Predicting foamy oil recovery ,SPE 68860, SPE Western Regional meeting held in Bakersfield, CA,

Mavko, G., Mukerji, T., and Dvorkin, J., 1998, The Rock Physics Handbook, Cambridge University Press, Cambridge, UK

McCaffrey, W. and Bowman, R. ,1991,Recent Successes in Primary Bitumen Production: 8th Annual Heavy Oil and Oil Sands Technical Symposium

Moczo, P., Kristek, J., Galis, M., 2004,Simulation of planar free surface with near-surface lateral discontinuities in the finite-difference modeling of seismic motion: Bull. Seism. Soc.

Am. **94**, 760 -768.

Moczo, P., Kristek, J., Galis, M., Pazak, P., Balazovjeh, M., 2007, The Finite-Difference and Finite-Element Modeling of Seismic Wave Propagation and Earthquake Motion: Acta Physica Slovaca **57**, 177-406.

Moczo, P., Kristek, J., Vavrycuk, V., Archuleta, R. J., Halada, L., 2002, 3D heterogeneous staggered-grid finite-difference modeling of seismic motion with volume harmonic and arithmetic averaging of elastic moduli and densities : Bull. Seism. Soc. Am. **92**, 3042-3066.

Müller, T. M., and B. Gurevich, 2004a, One-dimensional random patchy saturation model for velocity and attenuation in porous rocks: Geophysics, **69**, 1166–1172.

Müller, T. M., and B. Gurevich, 2004b, Seismic attenuation and dispersion due to wave-induced flow in 3-D inhomogeneous porous rocks: 74th Annual International Meeting, SEG, Expanded Abstracts.

Murphy W.F. 1982. Effects of partial water saturation on attenuation in Massilon sandstone and Vycor porous glass. Journal of the Acoustical Society of America **71**, 1458–1468.

Newman, G. H. 1973, Pore-Volume Compressibility of Consolidated, Friable, and Unconsolidated Reservoir Rocks Under Hydrostatic Loading: Journal Petroleum Technology. **25**, 129-134

Norris, A. N., 1993, Low-frequency dispersion and attenuation in partially saturated rocks: Journal of Acoustical Society of America, **94**, 359–370.

O’Connell, R., and B. Budiansky, 1974, Seismic velocities in dry and saturated cracked solids: Journal of Geophysical Research, **79**, 5412–5426

Pedersen S K, Fredenslund A.A , Christensen P. L and Thomason P ,1984, Viscosity of

Crude Oils: Chemical Engineering Science **39**, 1011-1016

Peng, D. Y., and Robinson, D. B. 1976. "A New Two-Constant Equation of State". Industrial and Engineering Chemistry: Fundamentals **15**, 59–64

Pitzer, K. S. 1955 "The Volumetric and Thermodynamics Properties of Fluids." Journal of the American Chemical Society **77**, no. 13 3427–3433.

Pooladi-Darvish M. & Firoozabadi, A. 1997, Solution gas drive in heavy oil reservoirs", presented at the 48th Annual Technical meeting of the Petroleum Society of CIM in Calgary

Pride, S. R., and J. G. Berryman, 2003a, Linear dynamics of double porosity and dual-permeability materials. I. Governing equations and acoustic attenuation: Physical Review E, **68**, 036603

Pride, S. R., and J. G. Berryman, 2003b, Linear dynamics of double porosity and dual-permeability materials. II. Fluid transport equations: Physical Review E, **68**, 036604

Robinson, D. B.; Peng, D. Y., 1978, "The Characterization of Heptanes and Heavier Fractions for the GPA Peng-Robinson Programs". Gas Processors Association (GPA) Research Report, Tulsa, OK,;

Sams, M.S., Neep, J.P., Worthington, M.H. & King, M.S.,1997, The measurement of velocity dispersion and frequency-dependent intrinsic attenuation in sedimentary rocks: Geophysics, **62**, 1456–1464.

Stoll, R.D., 1977. Acoustic waves in ocean sediments. Geophysics, **42**, 715–725.

Tanaka, H. & Takenaka . H ,2005, An efficient FDTD solution for plane-wave response of vertically heterogeneous median : Journal of Seismological Society of Japan, **57** 343-354

Vasco D.W., Datta-Gupta A., Behrens R., Condon P. and Rickett J. 2004. Seismic imaging of reservoir flow properties: time-lapse amplitude changes. *Geophysics* **69**, 1425–1442.

Vasheghani F , 2011, Estimating Heavy Oil Viscosity from Seismic Data, Thesis (Ph.D.) University of Calgary (Canada)

Vogelaar, B.B.S.A. & Smeulders, D.M.J. 2005. Low frequency attenuation in a saturated rock. Seismic Q–observation, mechanisms, and interpretation: Workshop at **67th** EAGE Conference, Madrid. Extended Abstract:

Vonde, T.R, 1982 Specialized Pumping Techniques Applied to a Very Low Gravity. Sand-Laden Crude-Cat Canyon Field, California: *Journal of Petroleum Technology*. **35**, 1951-1957.

White, J. E., 1975, Computed seismic speeds and attenuation in rocks with partial gas saturation: *Geophysics*, **40**, 224–232.

Wong, R. C. K, Maini. B, 2005, Estimation of Bubble Size in Heavy Oil Solution Drive Based on Kinetics of Gas Exsolution: Canadian International Petroleum Conference, Calgary